University of Kentucky
UKnowledge

University of Kentucky Doctoral Dissertations | Graduate School

2008

SURFACTANT AND METAL SORPTION STUDIES BY FUNCTIONALIZED MEMBRANES AND QUARTZ CRYSTAL MICROBALANCE

Abhay R. Ladhe
University of Kentucky, Abhay.Ladhe@uky.edu

Right click to open a feedback form in a new tab to let us know how this document benefits you.

Recommended Citation

Ladhe, Abhay R., "SURFACTANT AND METAL SORPTION STUDIES BY FUNCTIONALIZED MEMBRANES AND QUARTZ CRYSTAL MICROBALANCE" (2008). *University of Kentucky Doctoral Dissertations*. 671.
https://uknowledge.uky.edu/gradschool_diss/671

This Dissertation is brought to you for free and open access by the Graduate School at UKnowledge. It has been accepted for inclusion in University of Kentucky Doctoral Dissertations by an authorized administrator of UKnowledge. For more information, please contact UKnowledge@lsv.uky.edu.

ABSTRACT OF DISSERTATION

Abhay R. Ladhe

The Graduate School

University of Kentucky

2008

SURFACTANT AND METAL SORPTION STUDIES BY FUNCTIONALIZED MEMBRANES AND QUARTZ CRYSTAL MICROBALANCE

ABSTRACT OF DISSERTATION

A dissertation submitted in partial fulfillment of the
requirements for the degree of Doctor of Philosophy in the
College of Engineering
at the University of Kentucky

By
Abhay R Ladhe

Lexington, Kentucky

Director: Dr. Dibakar Bhattacharyya, Alumni Professor of Chemical Engineering

Lexington, Kentucky

2008
Copyright © Abhay R Ladhe 2008

ABSTRACT OF DISSERTATION

SURFACTANT AND METAL SORPTION STUDIES BY FUNCTIONALIZED MEMBRANES AND QUARTZ CRYSTAL MICROBALANCE

Functionalized membranes provide an elegant platform for selective separations and sorptions. In this dissertation, application of functionalized membranes for surfactant and metal sorption studies are discussed. Sorption behavior of surfactants is also studied using quartz crystal microbalance (QCM) and other techniques.

Adsorption of the ethoxylated surfactants on polymeric materials (cotton and polyester) and model gold surface was quantified from a non-aqueous siloxane based solvent (D5) and water. The role of ethylene oxide group and the effect of nature of polymeric materials on adsorption behavior was quantified and established. In the case of gold-water interface, the adsorption data was fitted to calculate adsorption/desorption rate constants. The study is important towards applications involving use of the surfactants in cleaning operations. PAA functionalized membranes were prepared and used for separation of the surfactants from the siloxane solvent. Finally the pH sensitivity of the PAA-surfactant complex was verified by successful regeneration of the membrane on permeation of slightly alkaline water.

The preparation and application of thiol and sulfonic acid functionalized silica mixed matrix membranes for aqueous phase metal ion sorption is also studied. The functionalized particles were used as the dispersed phase in the polysulfone or cellulose acetate polymer matrix. The effects of the silica properties such as particle size, specific surface area, and porous/nonporous morphology on the metal ion sorption capacity were studied. Silver and ferrous ions were studied for metal sorption capacities. The ferrous ions were further reduced to prepare membrane immobilized iron nanoparticles which are attractive for catalytic applications.

One dimensional unsteady state model with overall volumetric mass transfer coefficient was developed to model the metal ion sorption using mixed matrix membrane. The study demonstrates successful application of the functionalized mixed matrix membranes for aqueous phase metal capture with high capacity at low transmembrane pressures. The technique can be easily extended to other applications by altering the functionalized groups on the silica particles. The study is important towards water treatment applications and preparation of membrane immobilized metal nanoparticles for catalytic applications.

KEYWORDS: Ethoxylated nonionic surfactants, quartz crystal microbalance, mixed-matrix membrane, surfactant adsorption, metal ion capture

ABHAY R LADHE

12/01/2008

SURFACTANT AND METAL SORPTION STUDIES BY FUNCTIONALIZED MEMBRANES AND QUARTZ CRYSTAL MICROBALANCE

By

Abhay R Ladhe

DR. D. BHATTACHARYYA

Director of Dissertation

DR. B. KNUTSON

Director of Graduate Studies

12/01/2008

Date

RULES FOR THE USE OF DISSERTATIONS

Unpublished dissertations submitted for the Doctor's degree and deposited in the University of Kentucky Library are as a rule open for inspection, but are to be used only with due regard to the rights of the authors. Bibliographical references may be noted, but quotations or summaries of parts may be published only with the permission of the author, and with the usual scholarly acknowledgements.

Extensive copying or publication of the dissertation in whole or in part also requires the consent of the Dean of the Graduate School of the University of Kentucky.

A library that borrows this dissertation for use by its patrons is expected to secure the signature of each user.

Name	Date

DISSERTATION

Abhay R Ladhe

The Graduate School

University of Kentucky

2008

SURFACTANT AND METAL SORPTION STUDIES BY FUNCTIONALIZED MEMBRANES AND QUARTZ CRYSTAL MICROBALANCE

DISSERTATION

A dissertation submitted in partial fulfillment of the
requirements for the degree of Doctor of Philosophy in the
College of Engineering
at the University of Kentucky

By
Abhay R Ladhe

Lexington, Kentucky

Director: Dr. Dibakar Bhattacharyya, Alumni Professor of Chemical Engineering

Lexington, Kentucky

2008

Copyright © Abhay R Ladhe 2008

ACKNOWLEDGEMENTS

I will like to express my heartiest gratitude to my advisor Prof. Dibakar Bhattacharyya for his guidance, critical comments, motivation and encouragement which made this dissertation possible. His innovativeness, deep passion and dedication to the research has impressed me and will keep inspiring me in future. I also thank to my PhD committee members Dr. Tate Tsang, Dr. Stephen Rankin, Dr. Michael Jay, Dr. Allan Butterfield and Dr. John Selegue for their inputs on the work.

I would also like to extend my gratitude to the entire faculty at University of Kentucky and at University of Mumbai, Institute of Chemical Technology, who prepared me and motivated me for graduate studies.

I would like to thank John May from Environmental Research Training Laboratory for teaching and assisting me in different analyses. I would also like to thank Bruce Cole and Jerome Vice for their help throughout this process.

I would like to thank my colleagues in Dr. Bhattacharyya's lab, Aaron, Saurav, Jian, Yangchao, Ajay, Andrew, Dave, Deepak, Morgan, Noah, Scott, Tee, Vasile and Abhijit for their support and maintaining nice working atmosphere. Thanks to Peter Frailie and Nathan Garrison for their respective experimental contributions as a part of NSF-REU program.

My special thanks to my friends Amod, Arundhati, Gauri, Jivan, Kaustav, Kunal, Nitin, Sarita and Shriram whose company was both relief and fun for me. I am also grateful to my parents and my brother for their unconditional love and support.

Finally, I will like to thank P&G Corporation, Cincinnati, OH; Huber Corporation, MD; Research Challenge Trust Fund (RCTF) Fellowship and National Institute of Environmental Health and Sciences (Grant # P42ES007380) for financial support to this work.

Table of Contents

List of Tables

List of Figures

List of Files

Abhay Dissertation.pdf	2 MB

Chapter 1 Introduction

The development of new membrane materials to extend the industrial applications of membrane processes demand novel support layer and surface properties with desired functional groups. This has lead to the development of functionalized membranes for applications ranging from water treatment to reactors to advanced bio-separations. In addition to the size and diffusion rate based separations by conventional membrane processes, the functionalized membranes allow separations based on other driving forces like charge and physical/chemical interactions. In this dissertation, the area of functionalized materials and membranes was studied with focus on preparation and characterization of the functionalized materials with applications for surfactant and metal sorption studies. This section describes the contents of the dissertation and the research objectives are also broadly summarized.

Chapter 2 provides background information about membranes and membrane processes with focus on functionalized membranes. A detailed summary of literature studies on surfactant adsorption behavior at various solid-liquid interfaces from both aqueous and non-aqueous environment is also provided. All the analytical techniques and experimental procedures are summarized in Chapter 3. Chapter 4 gives details for characterization of the functionalized materials used in this study. Chapter 5 includes results, discussions and important findings for the surfactant partitioning, their adsorption at polymeric and model gold surfaces, and surfactant sorption using functionalized membranes. Development of functionalized mixed-matrix membranes and subsequent applications for metal ion sorption are discussed in Chapter 6. In Chapter 7, the mixed-matrix membranes are modeled and the metal ion sorption data was used to test the validity of the model. Finally, all the important findings of this research work are summarized in Chapter 8.

1.1 Surfactant sorption studies: research objectives

Surfactants are widely used in a variety of applications like cleaning, pharmaceuticals, paper processing, cosmetics, emulsifiers in food industry, etc. In most

of these applications, the surfactants adsorb at various available interfaces. Understanding the adsorption behavior of the surfactants at various solid-liquid interfaces is the key for technological advancement of these processes. In addition, the surfactants need to be separated from their solutions to be able to recycle and reuse the solvents. The overall objectives of this research include application of polyacrylic acid functionalized membranes for separation of the surfactants and to understand the adsorption behavior of the surfactants on polymeric and model gold surfaces from aqueous and non-aqueous environment.

The specific research objectives are:

- To study the partitioning of ethoxylated nonionic surfactants between siloxane solvent and water.
- To study sorption behavior of the surfactants at polymeric surfaces like cotton and polyester.
- To establish surfactant adsorption/desorption behavior at gold-water and gold-siloxane solvent interfaces.
- To determine the adsorption-desorption rate constants for the surfactant sorption processes.
- To prepare and characterize the polyacrylic acid functionalized membranes.
- To study the functionalized membranes for surfactant separation from hydrophobic siloxane solvent.
- To study the role of ethylene oxide content of the surfactants on their sorption behavior.

1.2 Mixed-matrix membranes: research objectives

Incorporation of functionalized particles in the membrane matrix lead to the development of functionalized mixed-matrix membranes. Mixed-matrix membranes open new domain for novel materials with desired functional groups. Functionalized membranes with appropriate functional groups can provide applications ranging from tunable flux and separations, toxic metal capture, toxic organic dechlorination,

biocatalysis, etc. In this study, functionalized silica mixed-matrix membranes were developed for aqueous phase metal ion sorption applications.

The specific objectives of the study are

- To prepare and characterize functionalized silica materials
- To prepare and characterize functionalized silica-polymer mixed-matrix membrane
- To demonstrate the applicability of the functionalized mixed-matrix membranes for metal ion capture and study the effect of various parameters like particle loading and residence time (by membrane pressure variation) on the capture efficiency
- To model the mixed-matrix membranes and check the validity of the model using experimental metal sorption data

Copyright © Abhay R Ladhe 2008

Part of this dissertation is published in the following articles:

1. Ladhe, A. R. and Bhattacharyya, D., 2005. Ethoxylated nonionic surfactants in hydrophobic solvents: Separation using membrane immobilized polyacrylic acid. Proceedings of the Annual Meeting of American Institute of Chemical Engineers, Separations (General).

2. Ladhe, A.R., Radomyselski, A. and Bhattacharyya, D., 2006. Ethoxylated nonionic surfactants in hydrophobic solvent: Interaction with aqueous and membrane-Immobilized polyacrylic acid. Langmuir, 22(2): 615-621.

3. Ladhe, A.R. and Bhattacharyya, D., In Press 2008. Adsorption of ethoxylated nonionic surfactants from siloxane based solvent and aqueous systems: Use of QCM and model polymeric surfaces. Chemical Engineering Communications.

4. Ladhe, A.R., Frailie, P., Hua, D., Darsillo, M. and Bhattacharyya, D., In Press 2008. Thiol functionalized silica-mixed-matrix membranes for silver capture from aqueous solutions: Experimental results and modeling. Journal of Membrane Science.

5. Ladhe, A. R.; Xu, J.; Hollman, A.; Smuleac, V.; Bhattacharyya, D., Invited Book Chapter, Submitted. Functionalized membranes for sorption, separation and reaction. Comprehensive Membrane Handbook, Elsevier.

Chapter 2 Background

This chapter includes a detailed literature summary about the research areas related to this dissertation. The literature studies on polyacrylic acid-nonionic surfactant interactions and nonionic surfactant adsorption behavior at various interfaces are summarized. The quartz crystal microbalance technique is discussed along with its working principal and related studies for surfactant adsorption. A comprehensive introduction to membrane processes and functionalized membranes is provided. The history of mixed-matrix membranes (MMMs) and their applications for liquid phase separations are summarized. The literature studies related to application of functionalized materials for metal ion capture are also discussed.

2.1 PAA-surfactant interactions

Interaction between polyacrylic acid (PAA) and ethoxylated nonionic surfactants has been studied for the last few decades and is receiving increasing attention in recent studies due to its scientific and industrial importance (Anghel et al. 1999; Anghel et al. 1998; Berglund et al. 2003; Nagarajan 1989; Robb 2000; Saito 1994; Saito 1993). Ethoxylated nonionic surfactants contribute approximately 55% of world production of nonionic surfactants and are used in a variety of technological applications such as detergency, cosmetics, pharmacy (Giger et al. 1984; Marcomini and Zanette 1996). Commercially available ethoxylated nonionic surfactants are often a mixture of surfactants with varying alkyl chain length and varying degree of ethoxylation (Asmussen and Stan 1998; Crook et al. 1965) and hence most of the previous studies involve use of ethoxylated surfactants with normal distribution of the ethylene oxide chain length. Alkyl chain of the nonionic surfactants contributes for the hydrophobic nature of the surfactant molecule and ethylene oxide chain length determines hydrophilicity. General structure of these surfactants may be represented as follows:

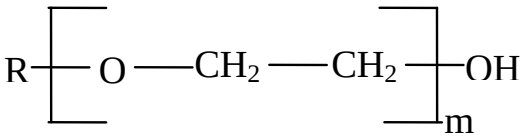

Where R= C_nH_{2n+1}

Typical value of m ranges from 3 to 12 and n varies between 9-18 (Asmussen and Stan 1998). An ethoxylated surfactant with *n* carbon alkyl chain and *m* number of ethylene oxide (EO) groups will be denoted as C_nE_m in the further discussions.

In the literature, the ethoxylated nonionic surfactants have been studied primarily in terms of their interaction with polyacrylic acid in aqueous phase and their adsorption behavior on various surfaces (mostly hydrophilic silica) in aqueous environment. Studies involving partitioning of the surfactants between aqueous and organic phases and adsorption of the nonionic surfactants from aqueous/nonaqueous solutions at different hydrophobic surfaces have also been conducted. Some of the main findings of these studies are discussed below.

2.1.1 Interaction between ethoxylated nonionic surfactants and polyacrylic acid in aqueous solutions

It is established in the literature that certain polyelectrolytes like polyacrylic acid and ethoxylated nonionic surfactant forms complex in aqueous solution due to hydrogen bonding (Figure 2.1) between carboxyl group of PAA and ethylene oxide group of the surfactant (Anghel et al. 1999; Anghel et al. 1998; Berglund et al. 2003; Nagarajan 1989; Robb 2000; Saito 1993; Saito and Taniguchi 1973). The hydrogen bonding phenomenon explains increase in pH of PAA solution on addition of ethoxylated nonionic surfactants. In addition to hydrogen bonding, the interaction is enhanced due to hydrophobic attraction between alkyl chain of the surfactants and PAA. The energy change in transferring one methylene unit from micellar to water environment is nearly the same for free micelles (-2.85 KJ/mol) and for PAA-bound micelles (-2.92 KJ/mol), indicating similar driving forces for the formation of the two types of micelles (Anghel et al. 1998).

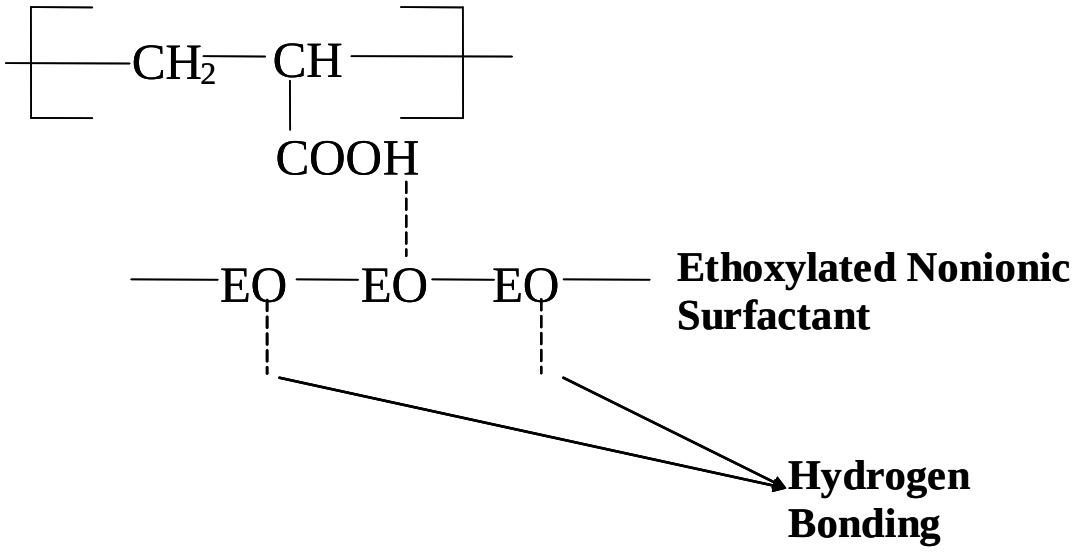

Figure 2.1 Schematics of hydrogen bonding interaction between carboxyl group of polyacrylic acid (PAA) and ethylene oxide groups (CH_2CH_2O i.e. EO) of the nonionic surfactants

The PAA-surfactant complex formation begins when the surfactant exceeds a particular concentration called the critical aggregation concentration (denoted by CAC). CAC depends on alkyl chain length of the surfactant and is independent of temperature and number of ethylene oxide groups in the surfactant molecule (Anghel et al. 1998). The micelles interacting with the polyelectrolyte are wrapped around by polyelectrolyte chain through hydrogen bonding with the ethylene oxide moieties and have about 15% lower aggregation numbers as compared to free micelles in bulk. The presence of polyelectrolyte segment at the micelle surface gives rise to two competing effects (Nagarajan 1989):

1. The wrapping of polyelectrolyte partially shields the hydrophobic core of micelle from being exposed to water. This reduces the core-water interfacial energy. This effect favors the formation of polyelectrolyte-bound micelle as compared to the free micelle.

2. The presence of polyelectrolyte chain at the surface of micelle increases steric interactions between hydrophilic groups of the surfactant and polyelectrolyte segment. This effect opposes formation of polymer-bound micelle.

Relative extent of the two effects dictates the preference between the formation of polyelectrolyte-bound micelles (CAC) and free micelles (Critical micelle concentration, i.e., CMC). In the case of PAA-$C_{12}E_8$ complex, shielding effect is more dominant than the effect of increase in steric interactions. Hence formation of polymer-bound micelle is favored which means CAC (0.7 mM) is less than CMC (1 mM). Polymethacrylic acid (PMA) is more hydrophobic in nature than PAA. The effect of steric repulsion at micelle surface becomes more important than the shielding effect in the case of PMA-$C_{12}E_{15}$ complex leading to higher CAC (0.4 mM) than CMC (0.11 mM).

The PAA-surfactant complex is pH sensitive and the complex formation is observed only in narrow pH range. Above pH 5 there is no complex formation and below pH 3 PAA forms a precipitate with the ethoxylated surfactants which redissolves in excess surfactant (Anghel et al. 1999). The composition of PAA-$C_{12}E_8$ complex (1.8 moles of EO per mole of carboxyl group) as determined by Anghel et al. (1998) suggests that not all the ethylene oxide units participate in the complex formation. The ethylene oxide units remain free or form loops or cross each other in the complex.

2.2 Adsorption of ethoxylated nonionic surfactants at solid-liquid interfaces in aqueous environment

In various applications like detergency, cosmetics, etc., ethoxylated surfactants adsorb at available solid-liquid interfaces. Studies have been conducted to understand the adsorption behavior of the surfactants at such interfaces in aqueous environment (Blom et al. 2005; Brinck et al. 1999; Cai et al. 2003; Caruso et al. 1995; Desbene et al. 1997; Geffroy et al. 2000; Gilchrist et al. 2000; Grant et al. 2000; Kharitonova et al. 2005; Kjellin et al. 2002; Kumar and Tilton 2004; Lindheimer et al. 1990; Portet et al. 1996; Somasundaran et al. 1991; Tahani et al. 1996; Thirtle et al. 1997; Torn et al. 2005). Parameters governing the adsorption behavior include morphology and chemistry of solid surface, functional groups involved in solute-solvent interactions, intermolecular forces between adsorbed molecules, pH, and temperature. Characteristics of the adsorption process were studied using variety of techniques like fluorescence decay (Levitz and Van Damme 1986), calorimetry (Denoyel and Rouquerol 1991; Lindheimer et al. 1990), neutron reflection (Lee et al. 1989; Thirtle et al. 1997), ellipsometry (Gilchrist et al. 2000; Kjellin et al. 2002; Stalgren et al. 2002; Tiberg et al. 1994), surface plasmon resonance (Caruso et al. 1995), quartz crystal microbalance (Caruso et al. 1995; Stalgren et al. 2002), HPLC (Desbene et al. 1997; Portet et al. 1996), and gravimetry (Rinia et al. 1996). Silica-water interface is the most studied surface for ethoxylated surfactant adsorption. The surfactant adsorption behaviors at various solid-liquid interfaces are summarized in this section.

2.2.1 Adsorption of ethoxylated nonionic surfactants on hydrophilic surfaces

Adsorption behavior of ethoxylated nonionic surfactants on hydrophilic surfaces is well established. Hydrophilic silica-water interface is the most studied surface for ethoxylated surfactant adsorption (Blom et al. 2005; Brinck et al. 1999; Desbene et al. 1997; Kharitonova et al. 2005; Kjellin et al. 2002; Portet et al. 1996; Thirtle et al. 1997; Stalgren et al. 2002). It is well established in the literature that the aqueous phase

surfactant adsorption on hydrophilic surface increases with increasing surfactant concentration and a plateau is observed just above the CMC. In most of the cases the adsorption isotherms follow the Langmuir model. The average area per ethylene oxide group calculated from the plateau value remains constant and is independent of the number of the ethylene oxide groups in the surfactant molecule. Increasing alkyl chain length of the surfactant molecule shifts the onset of the plateau towards lower concentration of the surfactant solution but has a negligible effect on the maximum adsorption.

There are two types of interactions involved in the surfactant adsorption process. Initially, the ethylene oxide groups of the surfactants interact with surface functionalities such as hydroxyl groups in the case of silica through hydrogen bonding. The surfactant molecules lay flat on the surface with both the ethylene oxide and alkyl chain parts of the molecule in contact with the surface. As the adsorption proceeds, the incoming ethylene oxide chains displace the flat lying alkyl chains from the surface and the alkyl chains get suspended in the solution away from the surface. This induces the lateral hydrophobic chain-chain interactions contributing for further adsorption of the surfactant molecules. The hydrogen bonding polar interactions are exothermic and hence the adsorption process is exothermic at low coverage. On the other hand, the chain-chain interactions being endothermic, the adsorption process becomes endothermic at higher coverage. In terms of enthalpy of adsorption, there is an endothermic minimum near surface coverage of 0.5 and as the coverage ratio approaches unity, the enthalpy of adsorption approaches zero (Lindheimer et al. 1990). Any more surfactant molecules added to the solution goes to form bulk micelles instead of adsorbing at the interface.

2.2.2 Adsorption of ethoxylated nonionic surfactants on hydrophobic surfaces

Systematic studies to understand the adsorption phenomenon of the ethoxylated surfactants at solid hydrophobic surfaces from their aqueous solutions have been reported in literature and some of the outcomes are discussed in this section (Geffroy et al. 2000; Grant et al. 2000; Kumar et al. 2004; Kumar and Tilton 2004; Lin et al. 1996; La Rosa et al. 2004).

The driving force for adsorption of ethoxylated nonionic surfactants on hydrophobic surfaces is the hydrophobic attraction between alkyl chain of the surfactants and the surface. The organization of $C_{12}E_8$ at the surface was observed to be strongly influenced by hydrophobicity of the surface (Grant et al. 2000) and the authors concluded that as the ratio of methyl to hydroxyl groups on the surface was increased from 0 to 1, the structure of adsorbed layer of $C_{12}E_8$ changed from micellar aggregates to bilayer to monolayer. The force required for expelling the surfactant between the surface and atomic force microscope (AFM) tip increased 4-5 times when the methyl to hydroxyl group ratio was increased from 0.5 to 1. This indicates increased adsorption energy of ethoxylated surfactants with increasing hydrophobicity of the surface and importance of the hydrophobic interaction between the surfactants and the surface.

Since the aggregation behavior of the ethoxylated surfactants at hydrophobic surfaces and in the bulk solution involves the same intermolecular interactions, a study was carried out (Kumar et al. 2004; Kumar and Tilton 2004) to relate the two phenomena. The adsorption isotherms of all the ethoxylated surfactants collapsed onto the same curve when the bulk and surface excess concentrations were rescaled by bulk critical aggregation concentration (CAC) and maximum surface excess concentration, respectively. This indicates strong relationship between self assembly of the surfactants in bulk and on hydrophobic surfaces. Surface excess concentration at air-water interface was observed to be higher than that at solid-water interface for the ethoxylated surfactants with more than three ethylene oxide groups in the molecule. The maximum surface excess concentration on solid hydrophobic surface was found to decrease with square root of number of ethylene oxide units in the surfactant molecules.

Most of the studies involving ethoxylated nonionic surfactants dealt with aqueous solutions of the surfactants as discussed earlier. Limited literature is available regarding the study of ethoxylated nonionic surfactants dissolved in hydrophobic solvents. Such studies primarily dealt with the effect of various parameters on reverse micelles, adsorption characteristics of the surfactants in non-aqueous environment, and their partitioning between aqueous and organic solvents. The key findings of the studies are discussed in the following part of the chapter.

2.3 Adsorption of the ethoxylated nonionic surfactants in non-aqueous environment

Many applications like lubricant coating, paint emulsions, and dry cleaning detergency, involve adsorption of the surfactants from hydrophobic solvents on solid-liquid interfaces. The knowledge of surfactant adsorption at liquid-solid interface is very limited in nonaqueous environment (Armisted et al. 1971; Rinia et al. 1996; Gregg and Sing 1967; Kipling and Wright 1964; Krishnakumar and Somasundaran 1994; Papke et al. 1995; Seguin et al. 2006; Soboleva et al. 2007). Initial studies dealt with adsorbed surfactant orientation on oxide adsorbents and estimation of their specific surface area from benzene and hexane (Armisted et al. 1971; Gregg and Sing 1967; Kipling and Wright 1964). In the case of benzene, adsorption isotherms of n-fatty acids were found to be independent of surfactant chain length as opposed to hexane where the adsorption varied with chain length (Armisted et al. 1971). In the case of ionic surfactant adsorption on silica from high polarity solvents, hydrocarbon chain interaction with solid surface plays an important role (Krishnakumar and Somasundaran 1994). Papke et al. (1995) developed a semi-quantitative technique to measure adsorption of surfactants onto colloidal dispersions in hydrocarbon solutions. Rinia et al. (1996) demonstrated for the first time the use of QCM technique to study adsorption of surfactants from nonaqueous solvents. They established the influence of bulk solution properties (Csurf > 2mM) on the QCM frequency shifts. They also proved that strong interaction between surfactant and solvent leads to increased sensitivity of the QCM shifts.

Seguin et al., (2006) studied adsorption and aggregation properties of C_nE_8 surfactant (n = 12, 14, 16) in ethylene and propylene glycol and concluded that the surfactant behavior (surface tension depression, etc.) is strongly dependent on the type of glycol. Soboleva et al. (2007) studied adsorption of Triton X-100 (a commercially available ethoxylated nonionic surfactant) from aqueous and non-aqueous (toluene) solvents at hydrophilic and hydrophobic quartz surface. Substantial differences in the extent of adsorption between water and toluene were explained in terms of aggregation behavior at the surface. In the case of adsorption from toluene, it was inferred that the TX-100 molecules orient themselves with the polar groups towards the surface regardless of its nature. Limited experimental data is available for CMC of the surfactants in

hydrophobic solvents. Studies have been carried out to predict the same (Flores et al. 2001; Voutsas et al. 2001) Flores et al. (2001) used phase separation model to predict the CMCs. The model assumes that the surfactant solution at a concentration above CMC is composed of two phases:

1. Solvent rich phase (whose surfactant concentration is CMC)
2. Surfactant rich phase approximating the reverse micelle.

Since these two phases remain in equilibrium, the activity of surfactant in phase 1 is equal to that in phase 2. Also activity of solvent in phase 1 is equal to its activity in phase 2. The concentrations satisfying this isoactivity criterion were determined for $C_{12}E_5$-Hexadecane system by Flores et al. 2001 using a program. These concentrations can also be determined graphically as shown in Figure 2.2 The activities of the surfactant and the solvent were predicted using UNIFAC. The agreement between predicted (0.0216 mole fraction of $C_{12}E_5$) and experimental (0.0191 mole fraction of $C_{12}E_5$) values of the CMC indicates feasibility of the approach towards predicting CMCs of ethoxylated surfactants in hydrophobic solvents. The details of the calculation are given in appendix A.

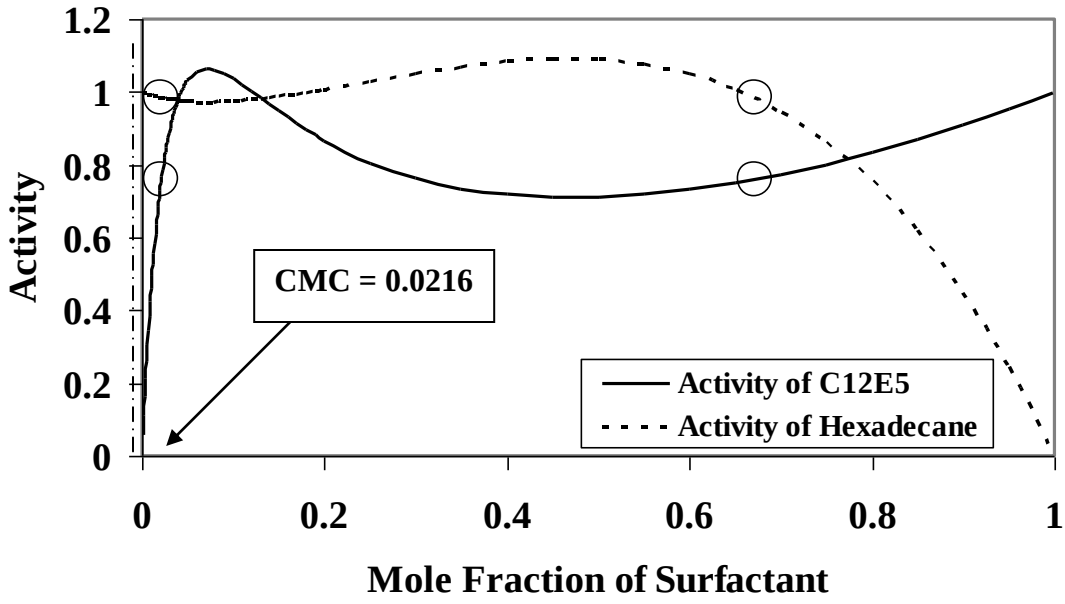

Figure 2.2 Prediction of Critical Micelle Concentration (CMC) of $C_{12}E_5$ in hexadecane by phase separation model (Graphical Method) (O Indicates points satisfying isoactivity criterion). Activities calculated using UNIFAC method. Calculated CMC = 0.0216 mole fraction of $C_{12}E_5$. Experimentally observed CMC = 0.0191 mole fraction of $C_{12}E_5$

2.4 Partitioning of ethoxylated nonionic surfactants

Ghoulam et al. (2002) studied partition coefficient of the ethoxylated surfactants between water and isooctane as a function of ethylene oxide chain length and temperature. The ethoxylated nonionic surfactants preferentially partition into the isooctane phase owing to their hydrophobic nature. The partition coefficient increases exponentially with increasing number of ethylene oxide groups per surfactant molecule and decreases by more than one-half an order of magnitude over a 20^0 C increase in temperature. It was also established that contribution of hydroxyl group of the surfactant to free energy of transfer from water to isooctane is more than that of ethylene oxide group and is more temperature sensitive. For a surfactant partitioning between organic and aqueous phase at a submicellar concentration, the partition coefficient can be expressed as follows:

$$K_p = \frac{V^o}{V^w} \exp\left(\frac{\Delta\mu_i^0}{RT}\right) \tag{2.1}$$

Where, K_p is the partition coefficient, V^o and V^w are the molar volumes of the organic phase and water respectively and $\Delta\mu_i^0$ is the energy corresponding to the transfer of 1 mole of surfactant from aqueous phase to organic phase. This type of approach was used by Ferrari et al. 1998 for determination of temperature dependence of standard chemical potential difference ($\Delta\mu_i^0$) for a surfactant partitioning between the water-hexane system. Since $\Delta\mu_i^0$ can be expressed as linear function of number of ethylene oxide groups (Ghoulam et al. 2002), equation (2.1) explains the exponential dependence of partition coefficient on ethylene oxide content of the surfactants.

2.5 Quartz crystal microbalance with dissipation monitoring (QCM-D) system

A quartz crystal microbalance (QCM) technique is useful for adsorption studies (Rinia et al. 1996; Caruso et al. 1995; Knag et al. 2004; Liu et al. 2005; Mokrani et al.

2005; Muller et al. 2005; Stalgren et al. 2002) due to its high sensitivity and simple relationship between frequency changes measured and adsorbed mass.

Quartz being piezoelectric by nature deforms under application of an electric field. The direction of deformation depends upon the direction of the applied electric field. On application of alternating electric field, the crystal starts oscillating at its fundamental frequency. Any addition or removal of mass to the gold surfaces by virtue of adsorption/desorption process will result in change in oscillation frequency of the crystal. The removal of applied electric field causes the exponentially damped sinusoidal decay of the crystal oscillations. The applied electric field is periodically disconnected in a controlled manner, and the decay time (τ_D) is measured each time. The dissipation factor (D) is defined as shown in following equation:

$$D=1/\pi f \tau_D \qquad (2.2)$$

Where f is the frequency of crystal oscillation.

The instrument allows simultaneous measurement of the changes in frequency of oscillation ($\Delta f/n$) of the crystal and also the dissipation factor (ΔD). Information pertaining to the mass, thickness and certain viscoelastic properties of the adsorbed layer can be derived from this data. If the adsorbed layer is sufficiently rigid and evenly distributed, the mass of adsorbed layer can be calculated using Saurbrey relation (Saurbrey 1959):

$$\Delta m = - C_m \Delta f / n \qquad (2.3)$$

Where C_m is Mass Sensitivity Constant (ng cm^{-2} Hz^{-1}) and n is the number of overtone. The fundamental frequency of oscillation for the crystals used in this study is 4.95 MHz and only one side of the crystal is in contact with the solution. The negative sign in equation (2.3) indicates that the oscillation frequency decreases with increasing adsorbed mass on the crystal. The adsorbed layer thickness is calculated by dividing the adsorbed mass by the density of the adsorbed layer.

Many studies report that the liquid phase QCM results deviate from the expected theoretical predictions and also differ from the findings of the studies using complimentary techniques (Rinia et al. 1996; Caruso et al. 1995; Stalgren et al. 2002). Overestimation of adsorbed mass has been reported for liquid phase QCM experiments.

The reason was attributed to the trapped or associated solvent with the adsorbed layer on the surface of QCM crystal.

QCM technique was used by Rinia et al. (1996) to study adsorption of surfactants from benzene. It is also widely used to study adsorption behavior of proteins on various surfaces (Jordan and Fernandez 2008; Moseke et al. 2008; Reimhult et al. 2008). The QCM gold surface can also be functionalized with self assembly of thiolated molecules to tailor the surface properties as desired.

The literature studies related to surfactant partitioning, adsorption-desorption behavior at various interfaces and the working principal and applicability of Quartz Crystal Microbalance for surfactant adsorption has been summarized in this chapter till now. The following part of this chapter will cover the background related to the functionalized membranes and related areas.

2.6 Functionalized membranes

Membrane applications in the separation area are being widely used in various industries for last few decades (Ho and Sirkar 1992). The current research in membrane science (Atwater and Akse 2007; Carter et al. 2008; Cuscito et al. 2007; Geismann et al. 2007; Kaur et al. 2006; Sing et al. 2008; Villalonga et al. 2008) is focusing more on development of new membrane materials with desired functional groups leading to development of functionalized membranes. Some of commonly studied functional groups are –OH, $-NH_2$, $-SO_3H$, −COOH, −SH, $-CONH_2$, etc. Functionalized membranes with appropriate functional groups can provide applications ranging from tunable water permeation and separations (Hollman and Bhattacharyya 2003; Majumder et al. 2007; Rao et al. 2002), toxic metal capture (Smuleac et al. 2005), environmental applications (Mauter and Elimelech 2008; Tee et al. 2005), biocatalysis (Hilal et al. 2006; Kasem et al. 1998; Kochkodan et al. 2007), etc. The functionalized membranes also provide opportunities for process integration by achieving separation and reaction in a single step (Gan et al. 2005; Onda et al. 1996). Membranes functionalized with polyelectrolytes are capable of charge based ion separations or toxic metal capture. These microporous membranes allow nanofiltration (NF) type separations at permeances much higher than

conventional membranes (Hollman and Bhattacharyya 2004; Malaisamy and Bruening 2005).

In the case of sorption, ion exchange or capture applications, the porous functionalized membranes can provide two significant advantages. Since membranes exhibit very high pore surface area which can be functionalized with desired groups, significantly higher capacity can be achieved as compared to conventional column applications. In addition to higher capacity, membranes offer minimum mass transfer resistance as the target molecules are transported to the active sites under convective flow conditions. The desired functional groups can be introduced in the membranes by either incorporating them during membrane preparation or by modifying the base membrane through surface chemistry.

The most common approach for preparation of functionalized membranes is by surface modification of the existing membranes. The desired functional groups can be introduced through either covalent or non-covalent attachment mechanism. Some of the commonly applied techniques for membrane functionalization include surface chemistry (Dai et al. 2005; Higuchi et al. 2002; Klein 1991; Kurakova et al. 2001; Yao et al. 2008), polymer deposition (Yoshimatsu et al. 1999), alternate adsorption of oppositely charged polyelectrolytes (Ariga et al. 2007; Decher 1997; Iler 1966; Sumleac et al. 2006) plasma or radiation induced grafting (Hautojarvi et al. 1996; Yamaguchi et al. 1991), gold-thiol chemistry (Chun and Stroeve 2001; Lee and Martin 2001; Smuleac et al. 2004), etc. The polymer deposition inside membrane pores can be achieved by cross-linking the desired macromolecules (Huang et al. 1998; Geismann et al. 2007) or by in-situ polymerization of corresponding monomers with simultaneous cross-linking (Gabriel and Gillberg, 1993; Li et al. 2006). Surface chemistry allows covalent attachment of the desired molecules on the membrane surface. Gold-thiol chemistry is studied for well defined, gold-coated, polycarbonate track etched (PCTE) membranes for fundamental studies and precise quantification of membrane performance (Wernette et al. 2006).

Based on the role of membranes, the applications of the functionalized membranes can be broadly classified into three categories: *separation*, *sorption* and *catalytic applications*.

2.6.1 Functionalized membranes for separations

Membranes containing immobilized functional polyelectrolytes have been developed for high capacity ion-exchange applications (Bhattacharyya et al. 1998; Ritchie et al. 1999 Bruening et al. 2008; Sata 1991) and tunable membrane separations (Ito et al. 2000; Nishizawa et al. 1995; Zhang and Nilsson 1993). Some of the commonly used polyelectrolytes (polypeptides) for such applications are poly(L-glutamic acid), polyacrylic acid, polycysteine, etc. The macromolecules can be incorporated within the membrane pore structure by single point covalent attachment through the reactive groups on the membrane surface. Once functionalized, the presence of these charged macromolecules inside the pores leads to the establishment of an electric potential field far removed from the pore wall. This allows ion exclusions in the highly open geometries at high membrane permeabilities as opposed to the low permeabilities encountered in the conventional nanofiltration (NF) applications. Thus one can obtain NF type separations at very low pressures. External stimulants like pH, ionic strength, and surfactants can cause change in the degree of ionization of the polyelectrolytes leading to the well-known helix-coil transitions (Zhang and Nilsson 1993), thus facilitating tunable separation applications. The concept of single layer polyelectrolyte immobilization can be easily extended to nonstoichiometric multilayer immobilization (layer-by-layer assembly), enhancing the density of the ionizable groups in the membrane phase.

Layer-by-layer (LbL) assembly offers easy and inexpensive way to create functionalized membranes with multilayers (using non-stoichiometric amounts) of charged polyelectrolytes. It was first suggested by Iler (1966) and established by Decher and coworkers (Decher 1997; Decher and Schmitt 1992). An excellent review from Ariga et al. (2007) summarizes various physicochemical fundamentals and possibilities for practical applications of the LbL assembly. Functionalization of the membranes using LbL technique allows flexibility in terms of number of layers and the layering sequence. Depending on the desired applications of the LbL modified membranes, the multilayers can be deposited either on the membrane surface (Hong et al. 2006; Krasemann and Tieke 1998; Liu and Bruening 2004) or inside the membrane pores by using convective

flow. By varying the deposition conditions like pH and supporting electrolyte concentration, the adsorbed layer properties can be optimized.

Hollman and Bhattacharyya (2004) prepared highly permeable ion selective membranes via immobilization of polyelectrolyte multilayer within the pores of microporous membranes. The polyelectrolytes used were poly(L-glutamic acid) (PLGA) and poly(L-lysine) (PLL). The first layer was covalently attached to the membrane support through surface chemistry and the rest of the layers were assembled through electrostatic interactions. The membranes showed As(V) rejection greater than 95% at membrane permeances (pressure < 2 bar) that exceed commercially available NF membranes. Smuleac et al. 2005 demonstrated high sorption capacity and rate for Hg^{2+} using polythiol-functionalized membranes.

2.6.2 Functionalized membranes for sorption applications

Membranes can be functionalized so as to have desired functional groups which can selectively interact and form a complex with target molecules as they pass through the membrane pores. This leads to the sorption of the target molecules by the membranes. The schematic of the process is shown in Figure 2.3. Such membranes have been used for applications like protein purification (Kubota and Shimoda 2005; Rao and Zydney 2006; Shi et al. 2008), metal ion sorptions (Ritchie et al. 2001; Warta et al. 2005), surfactant capture, etc.

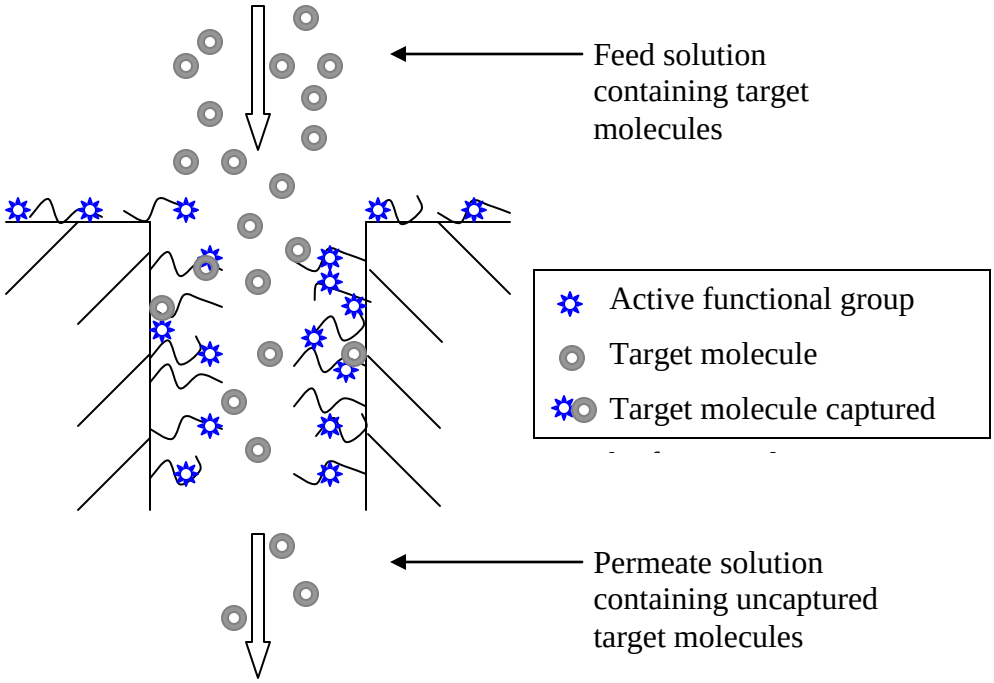

Figure 2.3 Schematic of a pore of functionalized membrane capturing target molecules as they permeate through the pore

Membranes functionalized with polyfunctional molecules exhibit very high capture capacities. It was demonstrated that membranes functionalized with covalently attached poly-glutamic acid (PLGA) (Bhattacharyya et al. 1998) or polycysteine (Ritchie et al. 2001) show sorption of heavy metal ions with high capacity. The applications of the functionalized materials and membranes for metal sorption are discussed in more detail in section 2.8

Another area for application of functionalized membranes for sorption applications is affinity membrane based separation of biomolecules. The area is especially attractive for the downstream processing in the biotechnological and pharmaceutical industries. (Brandt et al. 1988; Charcosset 1998; Datta et al. 2007; Datta et al. 2006; Hollman et al. 2005; Klein 2000; Roper and Lightfoot 1995; Thoemmes and Kula 1995; Zou et al. 2001). The most widely used affinity interaction in such applications is avidin-biotin interaction. (Datta et al. 2006). The affinity membranes were successfully applied for separation of BSA (Kugel et al. 1992), hormone 17-β-estradiol (Urmenyi et al. 2005), etc., from corresponding mixtures of biomolecules.

2.6.3 Functionalized membranes for catalytic applications

Functionalized membranes have the potential to contribute significantly towards the improvement of catalytic applications by providing alternative support for catalyst immobilization (Butterfield et al. 2001; Hilal et al. 2006; Konovalova et al. 2000). Membrane supported catalytic applications not only mitigate the need for dispersion of the catalyst and its subsequent removal from reaction mixture, but also provide highly favorable mass transport conditions.

Membrane immobilized enzymes act as biocatalysts in many bioreactions (Butterfield and Bhattacharyya 2003; Conrado et al. 2008; Giorno and Drioli 2000; Viswanath et al. 1998). The enzymes can be immobilized by either covalent or non-covalent attachment. Glucose oxidase is a commonly studied enzyme to evaluate immobilization techniques and effects of support matrices (Ozyilmaz et al. 2005; Rauf et al. 2006; Ying et al. 2002). It was observed that membranes can provide the highest

enzyme loading among the various supports studied with enhanced mass transfer conditions.

Another important area of catalytic applications involves use of metal nanoparticles. In addition to the large surface area to volume ratios, the different electronic properties of the nanoparticles (as compared to bulk materials) contribute towards the significant enhancements in catalytic activities. Zero valent iron based bimetallic nanoparticles are known for the degradation of toxic chlorinated organic compounds which is important for groundwater remediation (Feng and Lim 2005; Kim et al. 2008; Lowry et al. 2004; Tratnyek et al. 2000; Zhang et al. 1998). However, in the absence of polymers or surfactants, the nanoparticles can easily aggregate into large particles with wide size distribution. Xu (2007) reported a novel in-situ synthesis method of bimetallic nanoparticles embedded in polyacrylic acid (PAA) functionalized microfiltration membranes by chemical reduction of metal ions bound to the carboxylic acid groups. Along with high mass transfer rate, reduction of particle loss and prevention of particle aggregation are the added advantages of membrane based nanoparticle synthesis.

2.7 Mixed-matrix membranes (MMMs)

Mixed-matrix membranes consist of a continuous polymeric phase and a dispersed particulate phase. In such membranes, the dispersed phase can be functionalized with desired functional groups (Avramescu et al. 2003; Lin et al. 2007; Sambandam and Ramani 2007; Yen et al. 2007). This allows for a novel approach to introduce the functionalities in the membranes. Particulate silica is a good candidate for dispersed phase, as it can be easily functionalized with desired groups through well known silanization pathways.

MMMs were conceived for improving gas separation performances. Many studies have demonstrated higher gas permeability and/or selectivity for the MMMs when compared to the conventional homogeneous polymeric membranes with working principle based on the solution-diffusion mechanism (Kulprathipanja et al. 1988;

Mahajan and Koros 2002a; Mahajan and Koros 2002b). These membranes are shown to exceed Robeson's upper bound limit (Robeson 1991) for the performance of polymeric membranes in gas separation. Inorganic materials have shown performances well beyond the upper bound, but their applications are hindered due to the difficulty in preparing defect free and economical inorganic membranes. MMMs combine the performance benefit of the inorganic membranes with the easy applicability benefit of the polymeric membrane.

Apart from the gas separation applications, the concept of such composite membranes is successfully applied in the case of barrier membranes, which are useful for food packaging and corrosion resistive coatings (Lape et al. 2002; Liu and Cussler 2006; Shimotori et al. 2007). In this case the goal was to reduce the transport through the membranes, and it was accomplished either by adding impermeable flakes to the membrane polymer or by incorporating reactive groups within the membranes.

Although, the applications of the MMMs are well established in the area of gas separations, the development of their applications for liquid phase separations has been limited. Researchers have reported MMM applications for pervaporation to dehydrate organic mixtures (Adoor et al. 2006; Okumus et al. 1994; Vane 2008). Also the sulfonated silica-MMMs have been studied for fuel cell applications due to their improved proton conductivity, higher stability, and better performance (Lin et al. 2007; Sambandam and Ramani 2007; Yen et al. 2007) Avramescu et al. (2003) for the first time demonstrated the use of ion exchange-polymeric MMMs for adsorptive biomolecule separation. Saiful et al. (2006) have studied the MMM adsorbers for lysozyme capture and concentration. In order to change the membrane morphology from dense membrane (suitable in the case of gas separations) to more open micro-porous structure with high degree of pore interconnectivity (suitable for liquid phase applications), the MMMs were prepared via the well known phase inversion route with appropriate non-solvent addition. In this case it is desired to have a particle phase exhibiting rapid adsorption kinetics (for membrane adsorbers), high capacity and high selectivity towards target molecule, and easy regeneration.

The MMMs have significant advantages for separations over conventional column chromatography in terms of lower pressure drops, higher mass transfer rates (due

to convective flow) resulting in higher throughputs, and easier scale-ups. For conventional column adsorbers, throughput is inversely proportional to the bed height. An ideal case for maximum throughput will be very small bed height with very high bed diameter. Membranes actually have very low height (thickness) to diameter ratio, approaching the ideal case of packed beds for maximum throughput. This makes membrane applications attractive from industrial point of view. The mixed-matrix membranes for liquid phase applications can be easily prepared by Phase Inversion method.

2.7.1 Phase inversion method for membrane preparation

Phase Inversion method is a widely used method for membrane preparation. Polymeric ultrafiltration (UF) and majority of microfiltration (MF) membranes are prepared by phase inversion technique (Hwang and Jegal 2007; Kesting 1993; Pu et al. 2006; Strathmann 1986). A homogeneous polymer solution containing two or more components is phase separated into two distinct phases:

1. Polymer Rich Phase
2. Polymer Poor Phase.

The polymer rich phase forms the rigid membrane structure and the polymer poor phase forms the membrane pores. The phase separation can be achieved by three techniques:

1. Thermogelation of the mixture
2. Evaporation of volatile solvent
3. Addition of non-solvent

The required condition for phase inversion process is presence of miscibility gap over a certain composition and temperature range. Some of the important parameters governing the structure and properties of such membranes are type of polymer, concentration of polymer solution, type of solvent, type of non-solvent, temperature of non-solvent, evaporation time before addition of non-solvent, etc. Most commonly used polymers for preparation of phase inversion membranes are cellulose acetate, polysulfone and polyamide. Commonly used solvents include dimethylsulfoxide, dimethylacetamide, dimethylformamide, n-methylpyrrolidone, acetone, etc. Water, methanol, glycerol,

formic acid represent some of the commonly used non-solvents. In this study, polysulfone and cellulose acetate membranes were prepared by phase inversion method. Homogeneous solution of polysulfone in dimethylformamide (DMF) can be phase separated by addition of water (non-solvent) to form the membranes. Similarly, homogeneous solution of cellulose acetate and acetone can be phase separated by addition of water. The desired particles can be incorporated in the polymer solution during the preparation step to obtain mixed-matrix membranes.

2.8 Functionalized materials and membranes for metal ion sorptions

Among the various materials studied for metal ion sorptions, thiol-functionalized materials have been studied for sorption of heavy metal ions (Feng et al. 1997; Kang et al. 2004; Liu et al. 2003; Makkuni et al. 2007; Nakamura et al. 2007; Park et al. 2005; Vieira et al. 1999; Vieira et al. 1997; Zhang et al. 2003). Vieira et al. (1997) confirmed the preferential interaction of –SH groups with soft acids (Hg^{2+}>Ag^{+}>Cu^{2+}>Ni^{2+}>Zn^{2+}) in agreement with Pearson's concept (Pearson 1968) of hard and soft acids and bases. Kang et al. (2004) demonstrated highly selective adsorption capacity of the thiol-functionalized mesoporous silica materials for noble metal ions in the presence of other metal ions. Such a binding selectivity towards the target metal ions is important for many applications like waste treatment, which often involves metal ion mixtures.

Silver nitrate is a commonly used salt in many processes in the mirroring, photographic and electroplating industries (Atia at al. 2005). Compared to most metals, silver recovery from aqueous solutions is more profitable due to its high market value (Abasalan and Mehrdjardi 2003; Trochimczuk and Kolarz 2000). Also there is an increased interest in recovering silver found in trace amounts in the effluent of copper mining industry. Ritchie et al. (2001) studied polycysteine and other polyamino acid functionalized microfiltration membranes for Hg(II), Pb(II) and Cd(II) capture. Reactive barrier membranes for cesium ion containing silico-titanate as the sacrificial agent were studied by Warta et al. 2005. Some of the studies deal with the application of ion exchange-polymer composite sorbents for heavy metal separations (Paez et al. 2005; Khan and Alam 2004; Pan et al. 2007). The membrane systems are easier to operate and scale up as compared to the column adsorption techniques.

Functionalized membranes have been studied as adsorbents in the area of metal capture. It was demonstrated (Bhattacharyya et al. 1998) that membrane with covalently attached polyfunctional molecules exhibit very high metal capture capacities as compared to monomeric functional groups. The Pb capture with poly-L-glutamic acid (PLGA) functionalized membrane was 23 fold higher than that with equimolar quantity of glutamic acid. Ritchie and Bhattacharyya (2001) demonstrated up to 70% removal of Chromium (Cr III) from a stream containing multiple metal ions using 2 stage poly-L-glutamic acid (PLGA) functionalized membranes.

In this work, PAA-functionalized polyvimylidene fluoride (PVDF) membranes and thiol-functionalized silica polysulfone mixed-matrix membranes were studied for surfactant and metal ion sorption, respectively. The experimental details are given in next chapter.

2.9 Concluding remarks

Based on the detailed background study of the research areas, the following observations are made:

2.9.1 Surfactant sorption

Although surfactant adsorption behavior has been well studied for solid-water interface, the knowledge for the same in non-aqueous environment is very limited. Similarly, the polyacrylic acid-surfactant interaction has not been studied in hydrophobic siloxane solvent environment. In this research work, adsorption and partitioning behavior of the ethoxylated surfactants at solid-solvent interface is studied. Also the polyacrylic acid functionalized membrane was studied for surfactant sorption from hydrophobic siloxane solvent to quantify the PAA-surfactant interaction in hydrophobic domain.

2.9.2 Metal ion sorption

Functionalized membranes have been studied for separation applications in various fields but application of functionalized mixed-matrix membranes for liquid phase separations has not been exploited. This research work demonstrates applicability of functionalized mixed-matrix membranes for metal ion sorption applications from aqueous solutions.

Copyright © Abhay R Ladhe 2008

Chapter 3 Experimental and analytical procedures

3.1 Introduction

This chapter summarizes all the experimental procedures and chemicals, membranes, surfactants, polymers used for the research. The preparation of functionalized membranes, surfactant capture experiments, and metal ion capture experiments will be discussed in detail. This chapter will also summarize various analytical techniques used for this study.

3.2 Materials

3.2.1 Materials for surfactant sorption and partitioning studies

Surfactants: Pure surfactants used for fundamental studies are polyoxyethylene glycol n-dodecyl ether ($C_{12}E_n$) i.e. $C_{12}H_{25}(OCH_2CH_2)_nOH$, (n = 3, 5 and 8) and were obtained from Nikko Chemical Co. (Tokyo, Japan). Analysis by gas chromatography revealed single peak indicating high purity of the surfactants. Commercial nonionic surfactant 15-S-5 is purchased from the Dow Chemical Company. It is primarily a mixture of secondary alcohol ethoxylate with varying chain length and varying number of ethylene oxide groups per molecule.

Chemicals and Solvents: The hydrophobic siloxane based solvent D5, decamethylcyclopentasiloxane ($C_{10}H_{30}O_5Si_5$) (96+%) was obtained from Alfa Aesar. The nontoxic D5 solvent (MW = 371, density = 0.954) has a very low vapor pressure (0.24 mm Hg at 25 ºC) and high boiling point (211 ºC). The structure of D5 is given below.

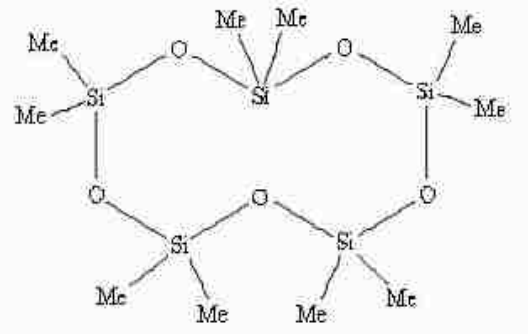

Polyacrylic acid was obtained from Polysciences Inc. as an aqueous solution with a concentration of 25 wt% and molecular weight of 50,000. Ethylene glycol (analytical reagent grade) was obtained from Mallinkrodt. HPLC grade isooctane and deionized ultrafiltered (DIUF) water was purchased from Fisher Scientific. Hydrogen peroxide (30% solution) was obtained from EMD Chemicals Inc. Ammonium hydroxide (50% V/V) was obtained from LabChem Inc.

Membranes: Hydrophilized Durapore Polyvinylidene Fluoride (PVDF) microfiltration membranes with an average pore size of 650 nm and membrane thickness of 125 μm were obtained from Millipore Corporation.

Adsorbent Materials: To study adsorption of surfactants at model gold surface, Q-sense QSX 301 Standard Gold crystals (surface area = 0.785 cm^2) were used. The polymeric surfaces used for the adsorption study were cotton and polyester and were obtained from P & G Corporation. The structure of the repeat unit of cotton (cellulose) and general structure for polyester is shown below.

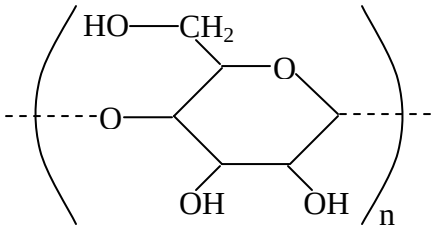

Cellulose repeat unit

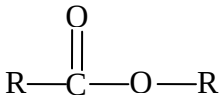

General Structure of Polyester

3.2.2 Materials for metal ion capture using MMMs

Polymers and solvents: Cellulose acetate (Mn = 50,000) and polysulfone (Mn = 16,000; MW = 35,000) were obtained from Aldrich. The solvents used were acetone and dimethylformamide (DMF) (extra dry, water < 50 mg/L), obtained from Acros Organics.

Chemicals: 3-Mercaptopropyltrimethoxysilane (MPTMS) (95%) and 3-(trihydroxysilyl)-1-propanesulfonic acid (35% in water) was obtained from Aldrich. Anhydrous ethanol was obtained from Sigma-Aldrich. Potassium hydrogen phthalate used to calibrate total organic carbon (TOC), was obtained from Nacalai Tesque Inc.

Dextran (482 kDa and 144 kDa) was obtained from Sigma. $AgNO_3$, NaCl, Na_2SO_4, and $FeCl_2.4H_2O$ were obtained from Fisher Scientific and $Ca(NO_3)_2.4H_2O$ was obtained from Mallinckrodt. Sodium borohydride ($NaBH_4$) in the form of granules was obtained from Sigma-Aldrich. Deoxygenated water was used for preparing solutions of $FeCl_2.4H_2O$. This precaution is necessary to prevent the oxidation of Fe^{2+} to Fe^{3+} and subsequent precipitation as the hydroxide. The ultra high purity nitrogen was purchased from Scott-Gross Co., Inc, Lexington.

Deoxygenated water: The DIUF water from Fisher Scientific was bubbled with ultra high purity nitrogen for at least 2 h and the water was stored in a closed vessel. The deoxygenated water was used in less than 1 h after the nitrogen bubbling is stopped.

Silica materials: The monodispersed Ludox TM-50 particles were obtained from Grace Davison and the silica gels (874-86-2 and 874-85-1) were provided by Huber Corporation. The average particle size, pore diameter and the BET surface area for the three types of silica are given in Table 3.1. Silica coated quartz crystal (QSX 303) obtained from Q-sense were functionalized with MPTMS to study silver-thiol interaction using QCM.

Table 3.1 Characteristics of various types of silica used in this study*

	Huber 874-86-2	**Huber 874-85-1**	**Ludox TM 50**
Average particle size (μm)	3.7	3.3	0.022
Pore diameter (nm)	11.8	3.54	N/A
BET surface area (m^2/g)	444	708	95

*** Data provided by Huber Corporation**

3.3 Analyses

The various types of analyses used in this study are summarized in this section.

3.3.1 Analysis of ethoxylated nonionic surfactants

The pure surfactant concentrations in the organic phase were measured with a Varian CP-3800 temperature programmable gas chromatograph equipped with a Chrompack capillary column of 15m length, 0.25mm internal diameter, and with Sil 8 CB as coating phase with a temperature program ranging from 70 ºC to 300 ºC at 10 ºC/min. The detector was an FID. Chrysene-d12 was used as an internal standard during the analysis. The relative standard deviation of the response factor for $C_{12}E_3$, $C_{12}E_5$ and $C_{12}E_8$ was 3.7%, 14.5% and 8.6%, respectively. The lowest limit used for calibration curves was 10 mg/L. The concentration difference between the feed and the permeate solution was used to determine the amount of surfactant captured by the functionalized membrane.

The analysis of aqueous solutions of the nonionic surfactants for concentration was not straightforward. The aqueous phase to be analyzed was partitioned with the pure organic phase (isooctane) and the partitioned organic phase was analyzed for surfactant concentration using GC-FID. Partition coefficients determined previously were used to back calculate aqueous phase concentrations in equilibrium with the determined organic phase concentrations. The original aqueous phase concentration was then calculated through mass balance. To be consistent, the pH of the aqueous solutions of the surfactants was adjusted to 3 before carrying out partitioning with the organic phase.

The solution of 15-S-5 in D5 was analyzed using super critical fluid-mass spectroscopy (SCF-MS) and its aqueous solution was analyzed by thin layer chromatography (TLC). These analyses were done by P&G Corporation, Cincinnati.

3.3.2 Analysis of polyacrylic acid (PAA) loading in membrane

The dry PVDF membrane was weighed before and after PAA functionalization and the weight difference was used as the PAA loading in the membrane. In order to calculate free carboxyl group, it was assumed that the ethylene glycol (cross-linker added in limited quantity) was completely reacted. Depending on the amount of PAA loading in the membrane and amount of ethylene glycol added, the number of free carboxyl groups available in the membrane was calculated.

3.3.3 Metal ion analysis

Varian SpectrAA-220 Atomic Absorption Spectrometer (AA) was used to measure concentration differences between the feed and permeate of aqueous metal ion solutions (Ag^{+}, Fe^{2+}, and Ca^{2+}). The wavelengths used for the analysis were 338.3 nm for Ag, 248.3 nm for Fe, and 239.9 nm for Ca. The analytical error for AA was less than 5% for Ag and Fe and was 15% for Ca analysis. The lowest calibration sample used was 1 mg/L of metal ion in the case of Ag and Fe. The lowest calibration point used for Ca was 5 mg/L. All the samples were diluted appropriately in order to use this concentration range. The upper limit for calibration was 15 mg/L to 30 mg/L.

3.3.4 Analysis of dextran solutions

Total organic Carbon (TOC-5000A) from Shimadzu was used to determine concentrations of the dextran solutions. The concentration difference between the feed and permeate was used to calculate dextran rejection. Based on known sample analysis, the analytical error was less than 5%.

3.3.5 Membrane imaging

Hitachi S-900 Scanning Electron Microscope (SEM) was used to obtain surface and cross-section images of the membranes. Hitachi S-3200 SEM equipped with energy

dispersive spectrometer (EDS) was used to detect presence of metal nanoparticles in the mixed-matrix membranes.

3.3.6 ATR-FTIR analysis of MPTMS functionalized silica

The MPTMS functionalized silica was characterized using Attenuated Total Reflectance – Fourier Transform Infrared (ATR-FTIR) spectroscopy using a Varian 7000e FT-IR spectrometer. The MPTMS functionalization causes a decrease in the silanol (Si−OH) peak intensity (Wavenumber 959 cm^{-1}). The peak intensity ratio Si−OH:Si−O−Si for functionalized and non-functionalized silica were compared to roughly quantify surface coverage

3.3.7 Analysis of surfactant adsorption at gold surface

Quartz Crystal Microbalance (QCM) E4 system from Q-sense was used to study adsorption of ethoxylated nonionic surfactants at gold-water and gold-D5 interfaces. Thiol- Ag^{+} interaction on MPTMS functionalized silica quartz crystal was also studied using the QCM system. The change in frequency was converted to adsorbed mass using Saurbrey relation. In this system, only one side of the crystal is in contact with the liquid solution.

3.4 Partitioning of 15-S-5

Partitioning study of 15-S-5 (a commercially available surfactant) between D5 and aqueous PAA solution was carried out to study the effect of partitioning on distribution of the surfactant. The solution of 15-S-5 in D5 (2 wt%) was mixed with equal volume (20 mL each) of aqueous solution of polyacrylic acid (15 wt%) using a wrist action mechanical shaker for 12 hours. After the mixture was allowed to settle for 24 hours, a three phase system was observed consisting of a top organic phase above the middle emulsion phase and bottom aqueous phase. The volume of emulsion phase varied from 2-8% of the total mixture volume. All samples were treated identically to maintain

consistency for agitation speed, temperature, pH of aqueous solutions and agitation time. The top organic phase was analyzed by SCF-Mass Spectra (analysis done by P & G Corporation) to study effect of partitioning on the distribution of surfactants between the two phases.

3.5 Adsorption of ethoxylated nonionic surfactants on cotton and polyester

The polymeric sample to be studied for ethoxylated nonionic surfactant adsorption was cut into pieces and heated in oven at 75 °C for 4 h. to remove any adsorbed moisture. The surfactant solutions of known concentrations were prepared in D5. 1 g of the dry polymer sample was added to 15 mL surfactant solution. The mixture was allowed to equilibrate for 12 h. in a mechanical shaker. The mixture was then allowed to settle and the clear D5 phase from top was sampled for analysis. This D5 phase was directly analyzed by GC-FID to measure the surfactant concentration. The difference between initial concentration and the concentration after equilibration with the polymeric samples was used to calculate amount of surfactant adsorbed. Because of the difficulty in analyzing water-based samples in GC-FID, the experiments with cotton and polyester were limited to D5 only.

3.6 Adsorption of ethoxylated surfactants at gold-water and gold-D5 interface

The gold-coated quartz crystal was chemically cleaned by heating it in a 1:1:5 mixture by volume of hydrogen peroxide (30% weight), ammonium hydroxide (50% V/V) and DIUF, respectively, for 20 minutes. Then the crystal was rinsed with DIUF water and dried using nitrogen. The crystal was then placed in the cell through which a solution of the surfactant was passed using a peristaltic pump. The solution was continuously passed over the gold surface for a certain amount of time. Most of the previous studies (Caruso et al. 1995; Stalgren et al. 2002; Rinia et al. 1996) used batch mode for adsorption experiments as opposed to the continuous peristaltic flow mode adopted in this study. This ensures constant surfactant concentration throughout the experiment. The flow rate was kept constant at 0.1 mL/min. The frequency ($\Delta f/n$) and

dissipation (*D*) data were measured and processed further to get the desired information about the adsorption process. In the case of gold-water interface, the experiments were carried out for surfactant concentrations of 250 mg/L. This concentration is higher than critical micelle concentration (CMC) of the surfactants (15 mg/L for $C_{12}E_3$, 26 mg/L for $C_{12}E_5$, and 56 mg/L for $C_{12}E_8$) in aqueous solutions. CMCs of the surfactants in D5 phase are not known.

3.7 Polyacrylic acid (PAA) functionalized membrane preparation

Partially cross-linked PAA-PVDF composite membranes were prepared to study polyelectrolyte-nonionic surfactant interactions. PAA-PVDF composite membranes were prepared previously by a dip coating method and were used for separation of aqueous organic solutions by reverse osmosis (Huang et al., 1998). Polyacrylic acid immobilized on such membranes was primarily on the surface and was highly crosslinked to achieve the dense layer required for reverse osmosis. In the present study, the goal was to immobilize the PAA inside membrane pores. The aqueous solution of polyacrylic acid (25 wt%, MW=50,000) containing ethylene glycol (4.3 wt%) as cross linking agent was passed through the membranes under application of vacuum. This approach allowed a thin coating of PAA layer on the surface of the membranes and membrane pores. Commercial low-pressure microfiltration PVDF membranes were used with nominal pore size rating of 650 nm. The membranes were then heated in oven at 110~120 ºC for 3 hours to allow partial cross-linking reaction to occur. The ether linkage formed between the carboxyl and hydroxyl groups generates the cross linked PAA network (Figure 3.1).

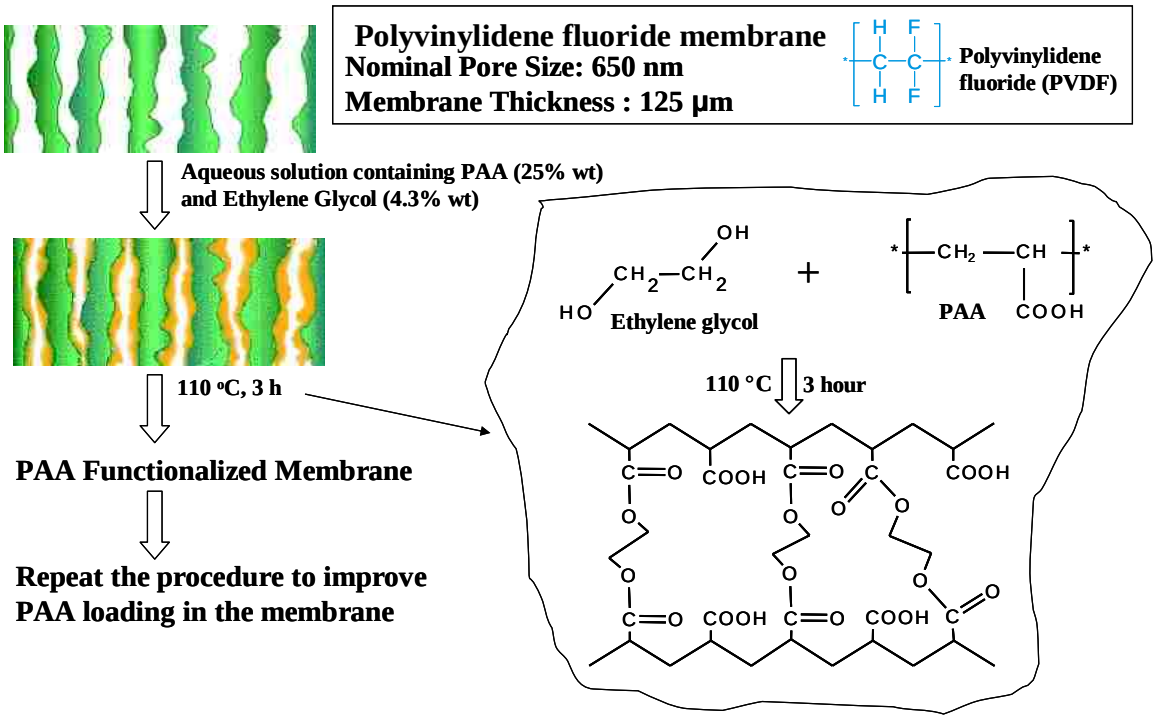

Figure 3.1 Schematics of membrane functionalization with polyacrylic acid (PAA)

The molar ratio of carboxyl to hydroxyl groups plays significant role in the cross-linking and surfactant capture studies. A specific amount of ethylene glycol was added to the aqueous PAA solutions such that the molar ratio of carboxyl to hydroxyl groups was 5:2, so that maximum of 40% of available carboxyl groups would be utilized for crosslinking. A higher degree of cross-linking allows better immobilization of the PAA but it is also important to have free carboxyl groups available for surfactant capture by interaction with ethylene oxide groups.

The process was repeated two more times to improve loading of PAA per unit area of the membranes. In the case of later two layers of the coating, the molar ratio of carboxyl to hydroxyl groups was maintained at 5:1, allowing 20% of available carboxyl groups to crosslink. The lower degree of cross-linking was maintained for the outer layers to allow more carboxyl groups to interact with the ethylene oxide groups. Dry membrane weights were measured before and after processing to determine quantity of PAA immobilized. The typical weight change of the membranes with addition of each layer of PAA was about 0.02 to 0.03 g. A typical weight gain data is given in Table 3.2. In general the PAA loading for a 15 cm^2 triple PAA-coated membrane was varied between 0.07 g to 0.1 g.

Table 3.2 Typical Weight gain data during PAA functionalization of PVDF membrane

Stage of PAA Coating	Weight of Membrane (g)	Weight Gain Per coating (g)	Total Weight Gain (g)
Bare Membrane	0.1240	-	**0.079**
Single Coated Membrane	0.1535	0.0295	
Double Coated Membrane	0.1836	0.0301	
Triple Coated Membrane	0.2030	0.0194	

3.8 Surfactant capture experiments with PAA-functionalized membranes

A Sepa ST membrane cell from Osmonics was used to carry out the permeation and surfactant capture studies. The solutions of desired concentrations (200 mg/L for $C_{12}E_8$ and 50 mg/L for $C_{12}E_5$ and $C_{12}E_3$) of the pure ethoxylated surfactants in water and D5 were prepared. To determine the PAA-surfactant interaction, a solution of the surfactant was permeated through the PAA-functionalized membrane at 2.04 bar transmembrane pressure. The permeate solution was again added to the feed side and re-permeated through the membrane. The process was repeated so as to permeate the surfactant solution through the membrane for four times. This was done to assure that the entire membrane capacity has been used for surfactant capture. In the case of surfactant capture from D5 solution, 0.1% water was added to the D5 solution. It was believed that the small amount of water is required to achieve better PAA-surfactant interaction. The membrane was wetted with water before the surfactant capture experiment was performed. The feed and the final permeate samples were analyzed by GC-FID for the surfactant concentrations. All of the experiments were conducted at 25 ºC.

3.9 Silica functionalization

The silica materials were functionalized to introduce free surface –SH or $–SO_3^-$ groups. The details for silica functionalization procedures are as follows:

3.9.1 Preparation of thiol (−SH) functionalized silica

The silica was first acid treated to activate the surface silanol (Si−OH) groups. 10 g of silica was added to 100 mL deionized ultra-filtered (DIUF) water and the solution pH was adjusted to 4.00 using 0.1 N nitric acid. The mixture was heated (50-60 ºC) with continuous stirring for 3 h. Silica was separated by filtering the mixture using a 0.22 μm PVDF filter. The silica cake was washed with 25 mL DIUF twice and then heated in an oven at 120 ºC for 8-12 h. The dried silica was used for further silanization. In the case of

Ludox TM 50, the silica was present in the form of aqueous emulsion. The silica solution was heated and water was evaporated to get the dry solid silica and the same procedure is used thereafter for functionalization.

A dry phase deposition method was used to functionalize the silica particles. The particles were dispersed in anhydrous ethanol (15 mL of ethanol per gram of silica) and MPTMS was added such that the ratio of the amount of silica (in g) to the amount of MPTMS (in mL) was 7:3. Ultra high purity grade nitrogen was bubbled through the mixture to evaporate the ethanol under fume hood, thus depositing MPTMS on the surface of the silica. For the silanization reaction, the silica was then placed in oven at 120 ^{o}C for 8-10 hrs. The material was allowed to cool and washed twice with 50 mL of anhydrous ethanol to remove any physically adsorbed MPTMS and dried again in an oven. The silica was analyzed using FTIR to verify the MPTMS deposition on the silica surface.

For regeneration studies, a batch of silica was functionalized using the above procedure with solution containing equimolar concentrations of MPTMS and 3-(trihydroxysilyl)-1-propane-sulfonic acid. The goal was to introduce both thiol and sulfonic acid groups on the silica surface, simultaneously and study the silica material for silver sorption and regeneration.

3.9.2 Preparation of sulfonic acid (SO_3^-) functionalized silica

The terminal thiol (−SH) groups of MPTMS were oxidized to sulfonic acid ($-SO_3^-$) groups by treating the thiol-functionalized silica with hydrogen peroxide (30 wt %) for 12 h under nitrogen atmosphere. The solution was filtered and the silica was washed with water. The silica was then dried and used for preparation of silica-polysulfone mixed-matrix membranes. The sulfonic acid functionalized silica was used to demonstrate preparation of membrane immobilized iron nanoparticles.

3.10 Silica-polymer mixed-matrix membrane preparation

Two types of membranes were prepared with the polymer backbone of either cellulose acetate or polysulfone. The silica particles were dispersed in the desired solvent (DMF for polysulfone membrane and acetone for cellulose acetate membrane). Polymer was added to this solution and allowed to dissolve. In the case of polysulfone membrane, the typical mixture consisted 2.5 g polysulfone in 14 mL DMF and 1.6 g silica. The mixture was continuously stirred for 8 h to ensure uniform distribution of the particles. The mixture was then briefly settled (30 minutes) to get rid of any trapped air bubbles which can cause membrane defects. The gel was then casted in the form of membrane on the glass plate using casting knife. The relative humidity of the room was approximately 45%. Deionized ultra-filtered (DIUF) water bath at 23 ^{o}C was used for phase inversion. The membrane casted on the glass plate was immediately immersed into this water bath to allow phase inversion process (no evaporation time). In the case of cellulose acetate membrane, the solvent was acetone-water mixture in a 7.2:1 ratio by volume. Figure 3.2 shows the schematics for the thiol-functionalized silica-polysulfone mixed-matrix membrane preparation procedure.

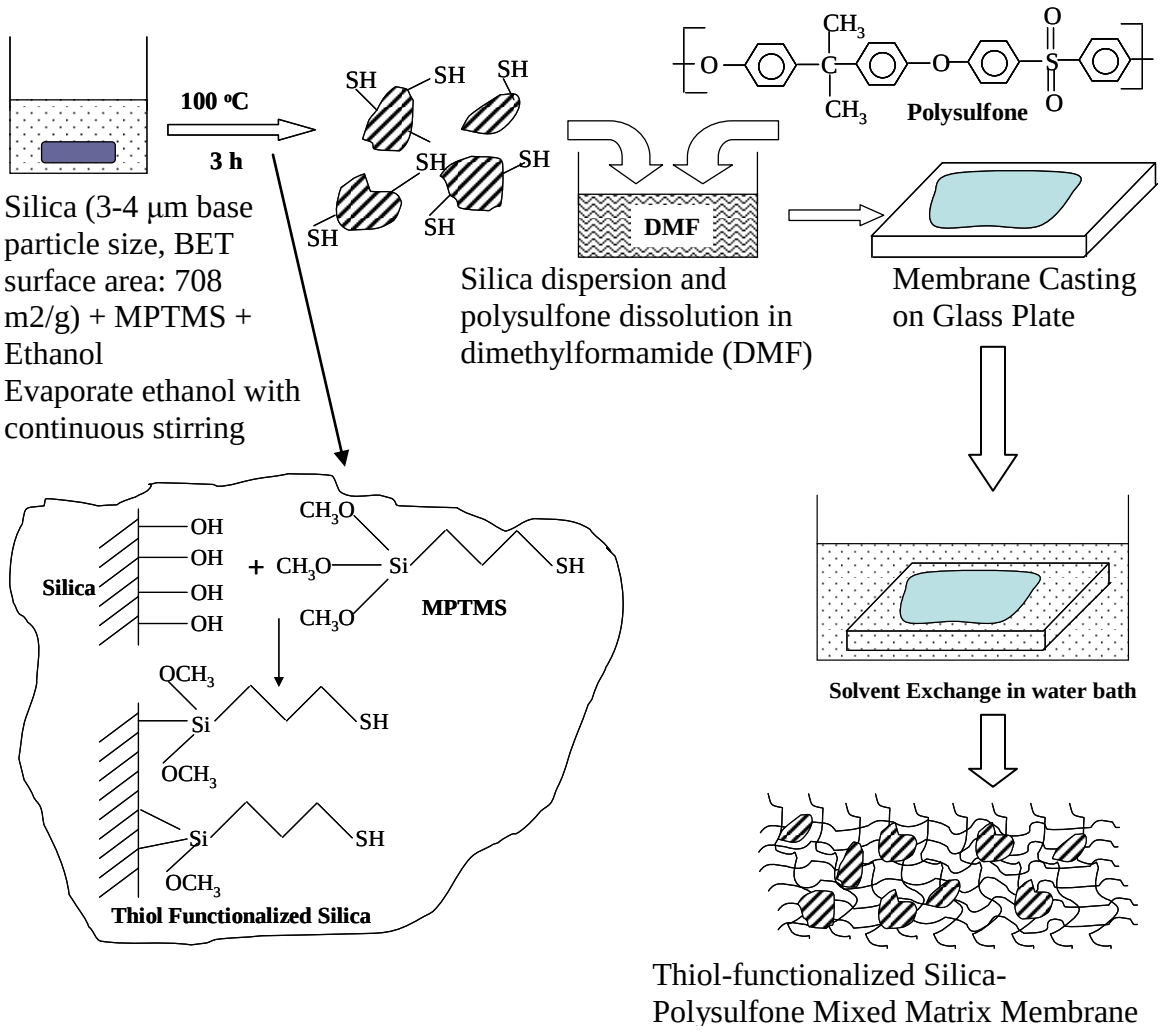

Figure 3.2 Schematics for synthesis of thiol-functionalized silica-polysulfone mixed-matrix membrane

The weight of the polymer and the silica was adjusted so as to get the silica loadings of 0, 10, 20 and 30 wt % in the final membranes. Except for 10 wt % silica loading, all other membranes were prepared with the silica type 874-85-1 only. Parameters like relative humidity, gelation bath temperature, and evaporation time strongly affect the membrane properties and even if these parameters were controlled, little fluctuations cause variations in membrane properties from batch to batch.

The water permeability of the silica-polymer composite membranes prepared as described above was determined by flux measurements. A Sepa ST membrane cell from Osmonics was used to carry out the permeance studies. The permeate coming out of the cell was collected at intermittent times to measure the membrane flux (J_W). The membrane flux was measured at various transmembrane pressures and the permeance was obtained as a slope of ΔP vs J_W graph. 100 mg/L solution of dextran (482kDa) was used to study dextran rejection of the polysulfone membranes. Dextran rejection data was used for the estimation of hydrodynamic pore size of the membranes.

3.11 Metal ion capture experiments

Desired concentrations of metal salts in deionized ultra filtered water were prepared. The solutions were permeated through the silica mixed-matrix membranes using the Osmonics Sepa ST stirred batch membrane cell. After placing the membrane inside the cell, metal ion solution was poured into it (feed solution). The cell was closed and connected to pressurized nitrogen tank and desired transmembrane pressure (ΔP) was applied by adjusting the regulator to pass the solution through the membrane. The solution was continuously stirred to maintain uniform concentration throughout the cell. The permeate coming out of the cell was collected at intermittent times to measure the metal ion concentration and the membrane flux (J_W). The feed and the permeate were analyzed by atomic absorption spectroscopy. Using the concentrations of the permeate samples and the membrane flux data, the total amount of metal salt permeated (mmoles) through the membrane was calculated. Total amount of metal ion captured (mmole per g of silica) was calculated by numerical integration over the filtration run.

The effect of the type of metal ion, type of functionalized silica, residence time, membrane flux, and adsorbent capacity was studied on the metal ion capture capacity of the membrane and the rate of capture. Ag^+ ions are photosensitive and need to be protected from direct light. Hence in all the experiments, the $AgNO_3$ solutions were prepared in amber bottles, and the bottles are covered with aluminum foil. Fe^{2+} ions can precipitate at higher pH and in presence of oxygen. To prevent this, all the Fe^{2+} solutions were prepared with deoxygenated water and the pH was adjusted to 5.

3.12 Preparation of membrane immobilized iron nanoparticles in mixed-matrix membranes

It was hypothesized that the sulfonic acid groups present on the silica surface in the membrane can capture the ferrous ions from ferrous chloride solution. In order to reduce pH changes during this process, the sulfonic acid groups were first converted to sodium form ($SO_3^-Na^+$) by passing 0.1 M sodium chloride solution through the membrane. The membrane was then washed with DIUF. In order to verify the presence of sulfonic acid groups, sodium sulfate rejection was studied for the membrane.

150 mg/L of $FeCl_2.4H_2O$ solution (48 mg/L Fe^{2+}) was passed through the sulfonic acid functionalized silica-polysulfone mixed-matrix membrane and permeate samples were collected for various time intervals. The permeate samples were analyzed by atomic absorption spectroscopy to determine the Fe^{2+} concentration and the data was used to construct the breakthrough curve for Fe^{2+}. Also based on volume of the samples and concentration difference between feed and permeate, the amount of Fe^{2+} captured by the membrane was calculated.

Sodium borohydride solution (0.1M) was passed through the membrane to reduce the Fe^{2+} ions to Fe^0 and in the process iron nanoparticles were formed inside membrane matrix. In order to confirm the existence of iron nanoparticles inside membrane matrix, SEM-EDS images of the membrane cross-section were obtained.

3.13 Quartz crystal microbalance (QCM) for metal ion-surface –SH interaction

Interaction of Ag^+ with surface −SH groups was studied using quartz crystal microbalance. The silica coated quartz crystal (Surface area = 0.785 cm^2) was functionalized with 3-mercaptopropyltrimethoxysilane by deposition from its alcohol based solution. A solution of 95% ethanol and 5% water was prepared and the pH was adjusted to 5 using acetic acid. The pH 5 environment is useful for hydrolysis of methoxy groups of MPTMS and to prevent the disulfide formation. MPTMS is added with continuous stirring to yield a 2% final concentration. After 10 minutes, allowing the time for hydrolysis and silanol formation, the silica coated quartz crystal was immersed into the solution for 2 minutes. After removing the crystal from solution, it was rinsed free of the excess MPTMS with pure ethanol. The MPTMS layer was cured for 15 min at 110 ^oC in oven. This introduced free –SH groups on the crystal surface.

The MPTMS functionalized silica crystal was mounted in the QCM cell and pH 5 water was circulated to obtain a steady baseline. It should be noted that only one side of the crystal is in contact with solution throughout the experiment. 100 mg/L Ag^+ solution (pH adjusted to 5 using acetic acid) was passed over the crystal and the interaction of Ag^+ ions with surface –SH was observed in terms of the mass adsorbed at the crystal surface.

Copyright © Abhay R Ladhe 2008

Chapter 4 Material characterization

Polymeric materials (cotton and polyester), thiol-functionalized silica, PAA-functionalized membranes, and silica-polymer MMMs were characterized by various techniques like SEM, FTIR and by water flux studies. The summary of the characterization results is given in this chapter.

4.1 Characterization of polymeric materials

In order to compare the amount of surfactant adsorbed per unit area, detailed characterization of the polymeric materials was required. The specific surface area of the samples was too low to perform a successful BET analysis. SEM images of the two types of samples were taken in order to get information about structure and accessible surface area of the material. The SEM images are shown in Figure 4.1. Figure 4.1a and 4.1b show the arrangement of fiber bundles for the two types of surfaces. In the case of polyester, the arrangement of the fiber bundles is very orderly as compared to that of cotton. In the case of cotton, the continuity of fibers is low. The average bundle diameter as seen from the SEM images is approximately 0.4 mm for the cotton sample and 0.6 mm for the polyester sample. Figure 4.1c and 4.1d show the detailed structure of cotton and polyester fibers, respectively. The polyester fibers are very smooth and have uniform diameter of about 25 μm. In the case of cotton, the fibers exhibit axial cracks or defects and deviate to a large extent from the cylindrical shape. The apparent fiber diameter varies from 10 μm to 20 μm. The smaller fiber diameter and axial defects in the case of cotton may result in higher specific surface area than that of polyester.

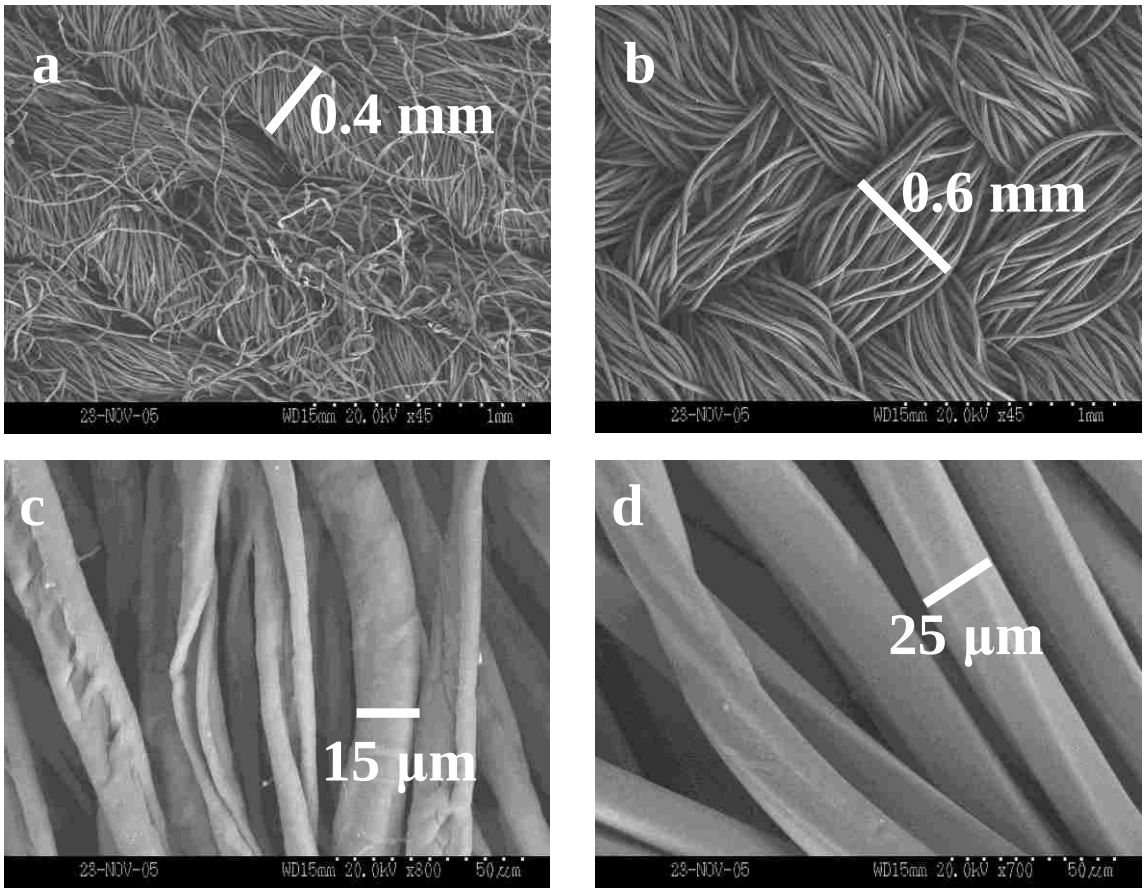

Figure 4.1 SEM images of the polymeric surfaces: a. Arrangement of fiber bundles for cotton b. Arrangement of fiber bundles for polyester c. Structure of fibers for cotton d. Structure of fibers for polyester

In order to calculate available surface area for surfactant adsorption, the average fiber diameter of 15 μm was used for the cotton and 25 μm was used for the polyester sample. The spacing between two adjacent fibers is in the order of few microns indicating almost all the surface area of the fiber is accessible by the surfactant molecules for adsorption. The density of the most of the polyester materials is around 1.4 g/cm^3 and density of cellulose (Pinto and Maaroufi 2005) is 1.36 g/cm^3. Assuming the density of polyester to be 1.4 g/cm^3 and density of cotton to be 1.36 g/cm^3, the calculated specific surface area were 0.20 m^2/g and 0.11 m^2/g for cotton and polyester, respectively.

4.2 Characterization of polyacrylic acid (PAA) functionalized membranes

In order to verify successful PAA functionalization, SEM images of the PVDF membrane were obtained before and after functionalization. The images are shown in Figure 4.2. It can be clearly observed that the PAA-functionalized membrane shows lesser and smaller pore morphology as compared to bare PVDF membrane, indicating PAA functionalization. In order to verify this further, permeance of PAA-functionalized membrane was determined by water flux measurement at varying pressures and compared with bare membrane permeance. The significant reduction in the water flux is a clear indication that PAA has been successfully functionalized inside the pores (Figure 4.3).

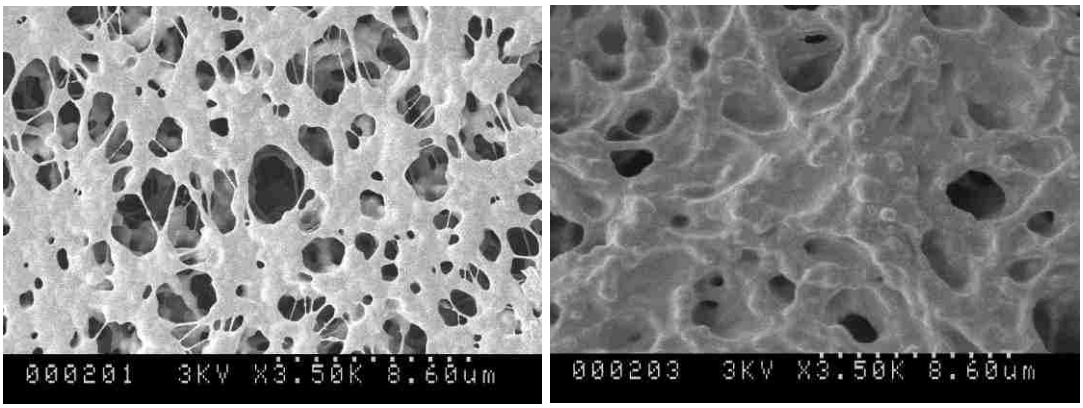

a. **b.**

Figure 4.2 Comparison of SEM images of surface of PVDF membrane (0.65 µm nominal pore size) before and after PAA functionalization a. Bare PVDF membrane b. PAA-functionalized PVDF membrane. Substantial PAA loading is observed in the case of PAA-functionalized membrane

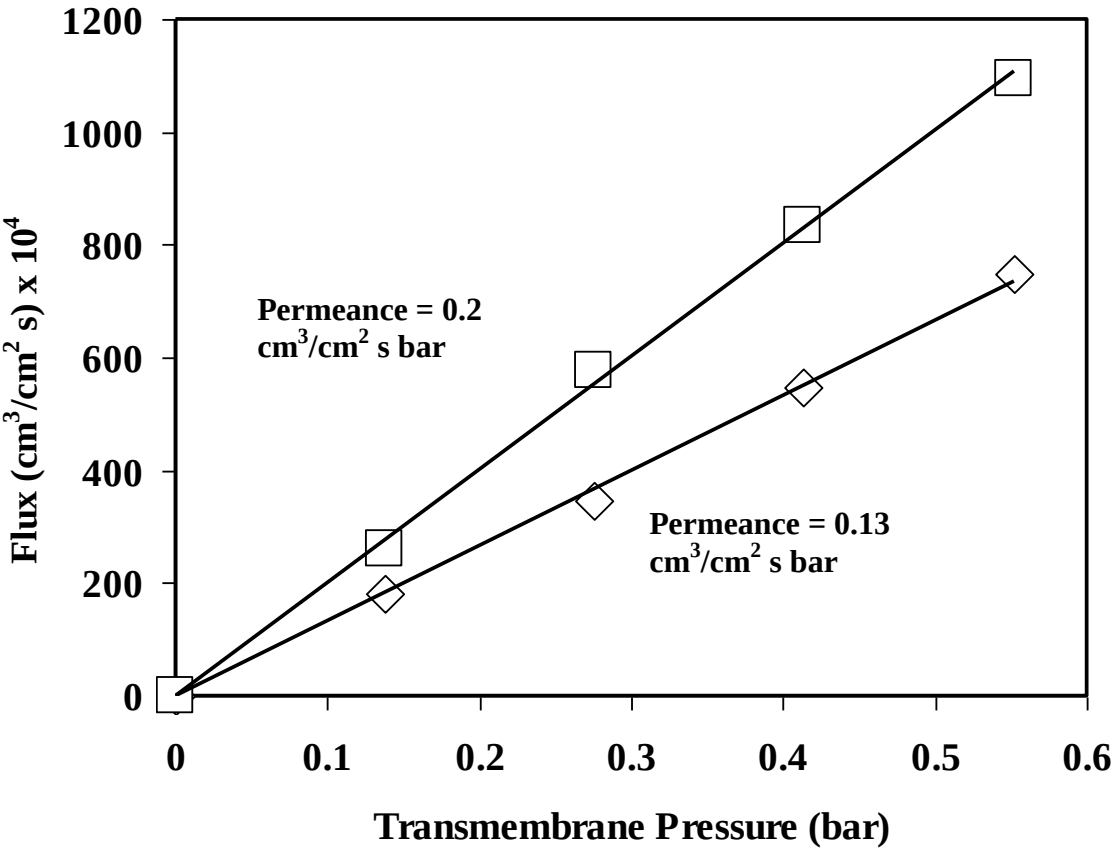

Figure 4.3 Effect of PAA functionalization (single layer coating) on water flux (pH = 5.8) through hydrophilized PVDF Membrane (0.65 µm). For three layer coating (not shown in figure) water permeance = 1 x 10^{-4} cm^3/cm^2 s bar

Under the assumption of uniform cylindrical pores (with tortuosity = τ), the permeability (A_i) (i = w for water and i = D5 for D5 solvent) can be represented using the Hagen-Poiseuille relation as follows:

$$A_i = \frac{J_i}{\Delta P} = \frac{\varepsilon_m r_p^2}{8\mu_i \tau L} \tag{4.1}$$

Where

J_i: Permeate flux, ε_m: Membrane porosity, r_p: Pore radius, μ: Viscosity,

L: Thickness of membrane, τ: Tortuosity of the membrane pore and ΔP: Applied transmembrane pressure

From the definition of ε_m one can write,

$$\varepsilon_m / \tau = \frac{N_p \pi r_p^2}{A_m} \tag{4.2}$$

Here N_p is number of pores in the membrane sheet of area A_m.

For the bare membrane water permeability experiment, the values of the parameters are:

$\frac{J_w}{\Delta P} = 2\times10^{-8} m^3/m^2 s\ Pa$, $r_p = 3.25\times10^{-7} m$, $\mu = 1\times10^{-3} Pa\ s$, $L = 1.25\times10^{-4} m$

and $A_m = 1.5\times10^{-3} m^2$. The values of r_p and L are specified by Millipore.

Substituting this data in Equation (4.1) yields $\varepsilon_m / \tau = 0.189$

And subsequent use of equation (4.2) yields $N_p = 8.543\times10^8$

The PAA-functionalized membrane was further characterized for its flux behavior at varying feed solution pH. The effect of PAA functionalization on pure water transport at varying pH levels is shown in Figure 4.4. The water permeability of 1.01 x 10^{-4} cm^3/cm^2 s bar measured at pH 6 is an order of magnitude smaller than the permeability measured at pH 2. The pH sensitivity of the flux in the case of membranes functionalized with macromolecules such as polypeptides is reported in the literature (Hollman and Bhattacharyya 2002). It is established in the literature that at lower pH levels (pH < pKa), the polyelectrolyte is unionized and remains in the compact form (Zhang and Nilsson 1993). In the case of PAA-functionalized membranes, higher pH levels result in

ionization of carboxyl groups to form negatively charged carboxyl ions. The electrostatic repulsion between the adjacent carboxyl ions results in extended conformation of PAA chains, which poses increased resistance for water flow through the pores. The PAA chains may not be able to extend to the fullest extent due to cross-linking at various points throughout the chains but from Figure 4.4 it is evident that the extension is sufficient to cause the flux drop at higher pH levels.

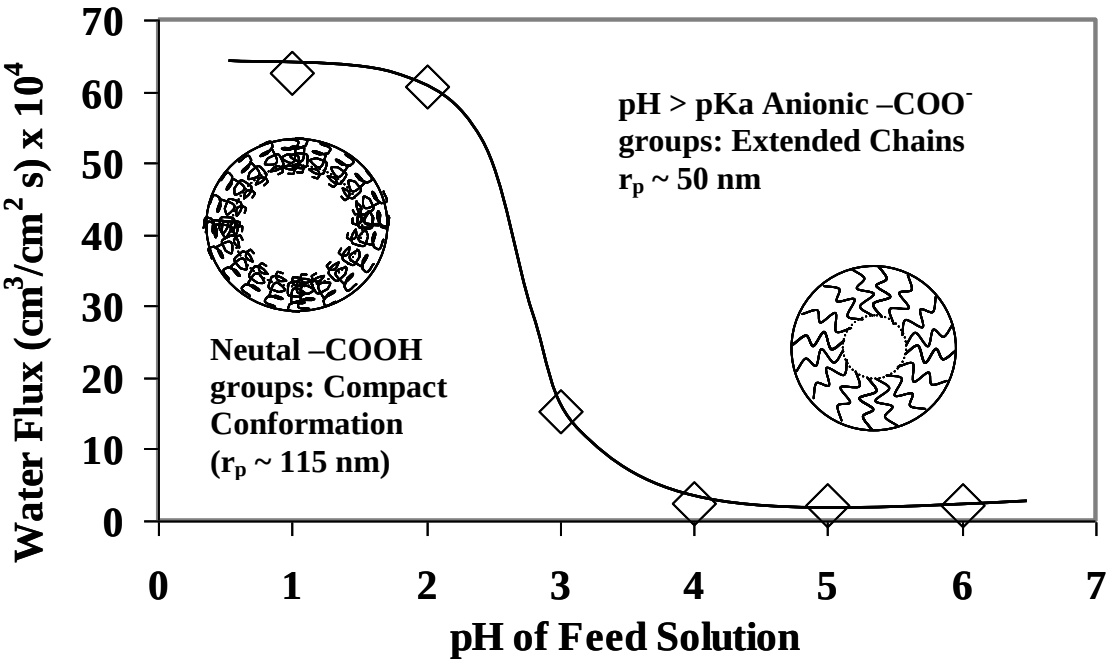

Figure 4.4 Permeate water flux as a function of pH for PAA-functionalized PVDF membrane (0.65 µm, three-layer PAA coating; transmembrane pressure = 2.04 bar)

The reduction in pore radius due to functionalization can be quantified by comparing permeate flux of bare membrane with that of a functionalized membrane. Combining equations (4.1) and (4.2) and rearranging we obtain

$$r_{eff} = r_p \left(\frac{J_{w \quad functional ized \quad membrane}}{J_{w \quad bare \quad membrane}} \right)^{0.25} \tag{4.3}$$

Effective pore radius (r_{eff}) was calculated for different pH levels and the results are shown in Table 4.1 The hydrodynamic pore radius decreased from 325 nm to 120 nm due to functionalization and it further decreased to 50 nm due extension of PAA chains at higher pH.

Table 4.1 Calculation of hydrodynamic pore radius of PAA-functionalized membrane

Bare Membrane Flux at 2.04 bar Transmembrane Pressure = 0.408 cm^3/cm^2 s			
Bare Membrane Pore Radius = 325 nm			
For PAA-functionalized Membrane			
pH	**Flux x 10^4 (cm^3/cm^2 s)**	**Hydrodynamic Pore Radius (nm)**	**PAA Layer Thickness (nm)**
1	62.7	114	211
2	60.7	113	212
3	15.3	80	245
4	2.50	51	274
5	2.3	50	275
6	2.1	49	276

4.3 Characterization of thiol-functionalized silica

In order to verify the successful functionalization of the silica (874-85-1) particles with MPTMS, ART-FTIR spectra for the non-functionalized silica and the MPTMS functionalized silica were obtained and compared as shown in Figure 4.5. The silica material exhibits associated water even after drying. It starts losing the water only after 250 ^{o}C. In addition, the non-functionalized silica exhibits silanol groups (Si−OH) at surface. These groups correspond to the absorbance band around 980 cm^{-1} (Boccuzzi et al. 1978). The corresponding peak is observed at 959 cm^{-1} in the case of non-functionalized silica. During MPTMS functionalization of the silica surface through the silane chemistry, these free Si−OH groups are consumed. This should cause a decrease in the peak intensity for functionalized silica which indeed was observed as represented by diminished peak at 952 cm^{-1}. The strongest peak represents stretching of Si−O−Si bonds of the silica network. In order to roughly quantify the MPTMS surface coverage, the ratio Si−OH: Si−O−Si peak intensities in both the cases are compared. The ratio is 0.054 for non-functionalized silica and 0.011 for functionalized silica. This represents an 80% decrease in Si−OH group concentration indicating 80% surface coverage in the case of functionalized silica. This value is in good agreement with the maximum coverage of 76% observed (Feng et al. 1997) for an MPTMS monolayer on mesoporous silica.

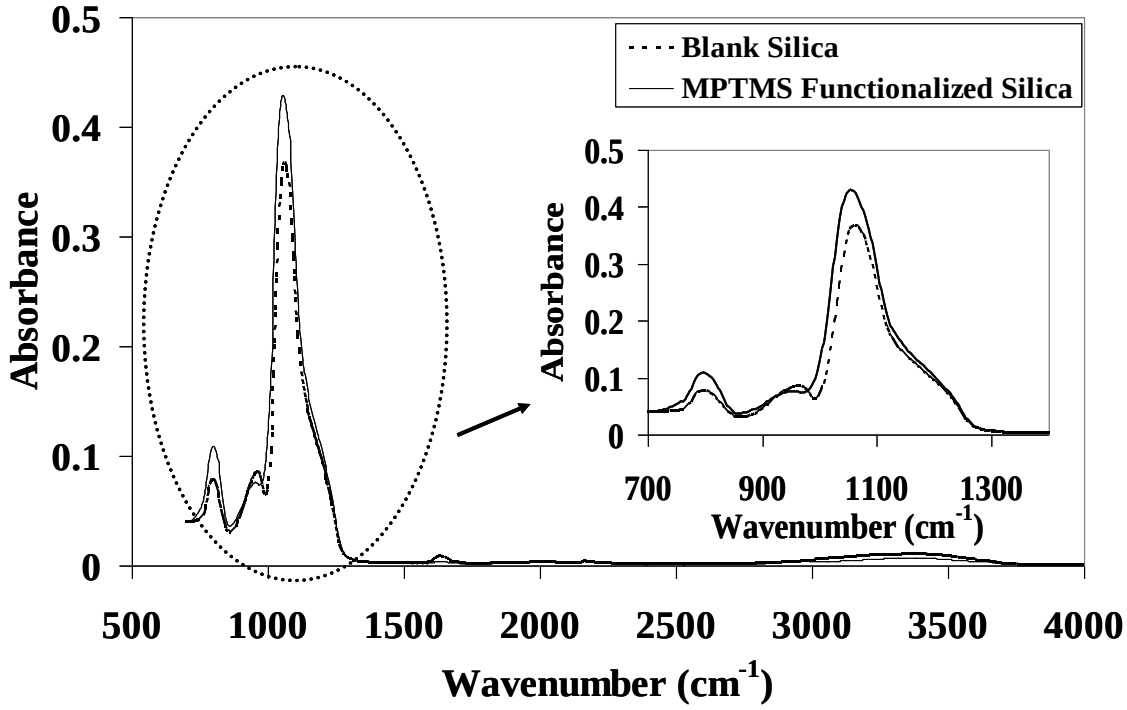

Figure 4.5 FTIR-ATR spectra for blank and MPTMS functionalized silica (874-85-1). The peak representing free Si−OH groups on silica surface (959 cm^{-1}) diminishes in the case of MPTMS functionalized silica

In order to characterize the MPTMS functionalized silica for the maximum silver capture capacity, aqueous phase batch experiments were carried out. A known mass of silica was added to known volume of Ag^+ solution (pH = 5.8-6.0) of known concentration and the mixture was equilibrated overnight with vigorous shaking. A portion of the mixture was filtered (using 0.22 μm polyvinylidene fluoride membrane) to remove any suspended silica particles and then analyzed for Ag^+ concentration by Atomic Absorption spectroscopy. The difference between the initial concentration and the sample concentration was used to calculate the silver capture capacity for that batch of functionalized silica. The typical silver capture capacity was in the range of 1.5-2.1 mmole of Ag/g of silica. In the case of limited availability of silver in the aqueous phase, the amount of silver captured increased linearly with the amount of silver present in the aqueous solutions. Most of the experiments reported in this study involved silica with a capture capacity of 2.1 mmole/g. If we assume 1:1 stoichiometry between thiol group and silver ion, the silver capture capacity of 2.1 mmole/g leads to 1.8 thiol groups per nm^2 of silica (Based on BET surface area of 708 m^2/g for silica type 874-85-1).

4.4 Characterizations of silica-polysulfone mixed-matrix membranes

In order to get an idea about the membrane morphology and the silica particle distribution, the MMMs were characterized by SEM imaging. Figure 4.6 shows the SEM image of a cross-section of a 40% silica-polysulfone MMM. The cross section clearly displays two regions, a dense top layer over a more open structured layer. Silica particles in the dense region are not directly visible, but their impressions can be observed in the image. Some of the Silica particles in the open structure are indicated by the arrows and it can be observed that the silica particles are evenly distributed along the entire membrane thickness. According to the particles size analysis of 874-85-1 silica, performed by Huber Corporation, less than 10% particles are below 2 micron in size and less than 10% particles are greater than 5.1 micron. This is important for high separation capacity as particle agglomeration may render some sites inaccessible. Additional SEM images of mixed-matrix membranes are provided in Appendix B.

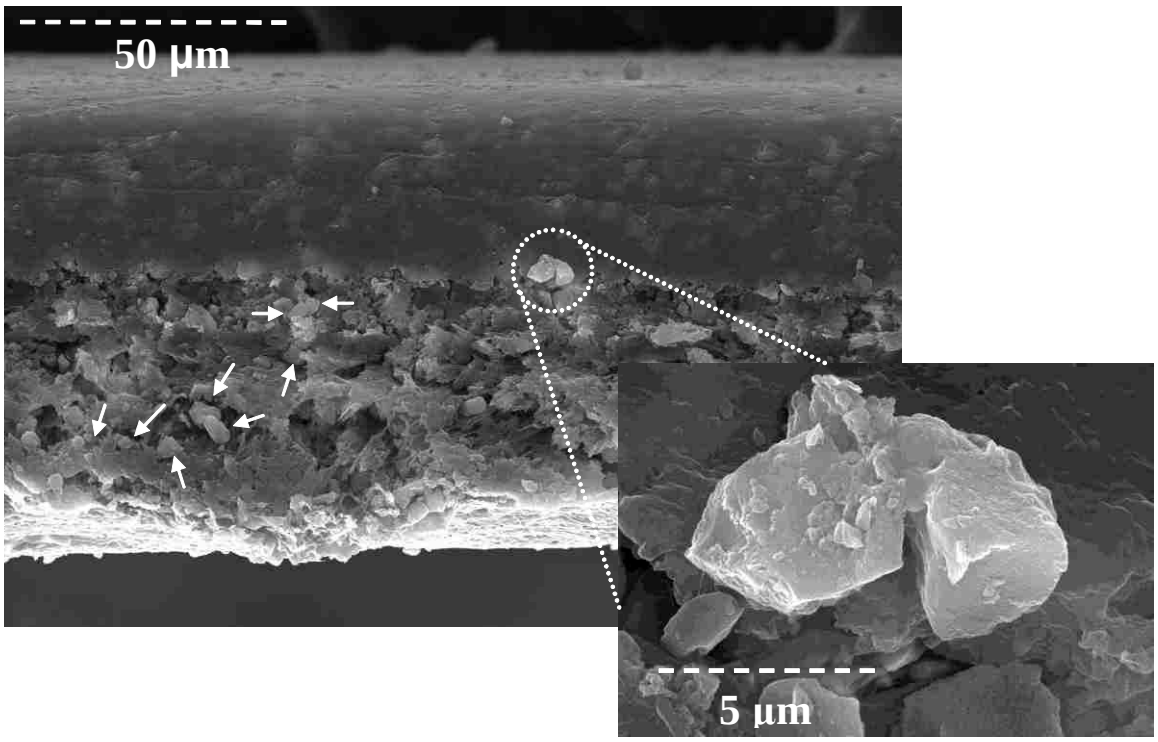

Figure 4.6 SEM image of cross-section of 874-85-1 MPTMS functionalized silica-polysulfone MMM (40% loading). Arrows point to some of the silica particles in membrane matrix indicating their uniform distribution along the membrane thickness

4.5 Membrane flux behavior for silica-polymer MMMs

The effect of silica loading on water permeance of mixed-matrix membranes was studied and the results are shown in Figure 4.7 The error bar corresponds to the standard error of triplicate permeance values measured for membranes prepared from same batch. As the silica loading increased from 10% to 40%, the water permeance of the membranes also increased. Increase in membrane permeance with increasing particle loading was also observed by Zhang et al. (2006) in the case of zirconium oxide MMM. Their study concluded that increasing particle loading improves pore interconnectivity but does not change skin layer pore size resulting in higher permeance with little effect on retention properties. In our study, membrane water permeance was studied for both functionalized and non-functionalized silica MMMs and there was no significant difference in the two cases. For the studied silica loading range (0.1 to 0.4), the permeance data can be represented by following linear correlation:

$$A = 1.4 \times 10^{-4} \psi \qquad (4.4)$$

Where A is membrane water permeance in $m^3/(m^2$ s. bar) and ψ is silica weight fraction in membrane (for 10% silica loading ψ = 0.1). Equation (4.4) can be extended to express membrane flux as a function of silica loading as follows:

$$J_W = 1.4 \times 10^{-4} \psi \ \Delta P \qquad (4.5)$$

Where J_W is membrane flux in $m^3/(m^2$ s) and ΔP is applied transmembrane pressure in bar.

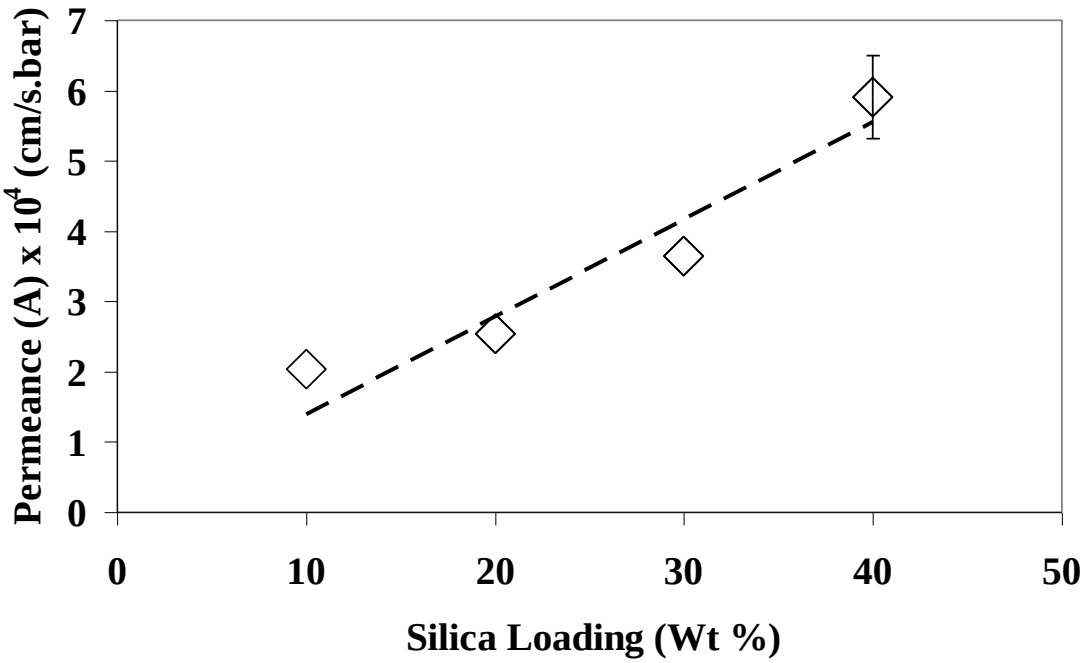

Figure 4.7 Effect of silica loading on membrane water permeance for non-functionalized 874-85-1 silica-polysulfone mixed-matrix membrane. Dotted line indicates fitted linear correlation for the data (R^2 = 0.91)

4.6 Free volume fraction (ϕ) estimation for silica-polysulfone MMMs

Free volume fraction (ϕ) of the membranes was calculated by the membrane water uptake measurements. Silica mixed-matrix membrane was soaked in water overnight. The membrane was then removed and lingering water was allowed to drip. The membrane was dabbed lightly with tissue paper to remove any remaining water from the membrane surfaces. The wet membrane was weighed (W_1, kg). The wet membrane was then dried in oven at 110 ^{o}C for 8-10 h and the dried membrane was weighed again (W_2, kg). The difference between the weights represents weight of water inside membrane pores. Free volume fraction was calculated using following expression:

$$\phi = \frac{W_1 - W_2}{A_m L \rho_W} \tag{4.6}$$

Where, A_m is membrane area (m^2), L is membrane thickness (m) and ρ_W (kg/m^3) is density of water.

Typical value of ϕ for a MPTMS functionalized 874-85-1 MMM (ψ = 0.4) was around 0.6. For the two membranes from same batch the values obtained were 0.58 and 0.63. In order to get an idea about effective pore size of the membrane, dextran rejection was studied. For 10% silica-polysulfone MMM, observed dextran rejection was 51% and 88% using 144kDa and 482 kDa MW dextran, respectively. Hydrodynamic pore radius (r_1) for the membrane was estimated using Ferry-Faxen equation (Ferry 1936; Lindau 1998) which is given below.

$$(1-R) = \left(1 - \frac{r_s}{r_1}\right)^2 \cdot \left(1 - 0.104\frac{r_s}{r_1} - 5.21\left(\frac{r_s}{r_1}\right)^2 + 4.19\left(\frac{r_s}{r_1}\right)^3 + 4.18\left(\frac{r_s}{r_1}\right)^4 - 3.04\left(\frac{r_s}{r_1}\right)^5\right) \tag{4.7}$$

R is the rejection of dextran. r_s is the hydraulic radius of the dextran molecule in nm, which can be determined from the following correlation (Richie et al. 2001):

$r_s = 0.027\ M^{0.498}$

M is the molecular weight of dextran in Da.

Based on 482 kDa dextran rejection data (R = 0.88), calculated value for hydrodynamic pore radius was about 39 nm.

4.7 Characterization of sulfonic acid functionalized silica-polysulfone membranes

Membrane flux data was measured for the silica-polysulfone mixed-matrix membrane. Figure 4.8 shows the membrane flux behavior and the permeance for the membrane is 4.15 x 10^{-4} cm^3/cm^2 bar s The permeance is in the same range as that observed for typical silver capture experiments with 40% silica loading (6 x 10^{-4} cm^3/cm^2 bar s)

In order to verify the presence of sulfonic acid groups, sodium sulfate rejection was studied for the membrane. If the thiol groups were not oxidized to sulfonic acid groups, the membrane is expected to show negligible salt rejection. 100 mg/L sodium sulfate ($Na_2SO_4.10H_2O$) solution was used as a feed solution and permeate was collected for 10 min time intervals. The conductivity of the feed and permeate samples were measured using conductivity meter, to get an idea about salt rejection by the membrane. The salt rejection data is summarized in Table 4.2

It can be observed from the salt rejection data, that initially the salt rejection was 32 % and then it decreased and stabilized in the range of 11-17 %. The fact that the membrane is rejecting salt solution indicates presence of negatively charged sulfonic acid groups in the membrane. The presence of the negatively charged groups inside membranes is known to reject negatively charged ions by means of Donnan exclusion effect.

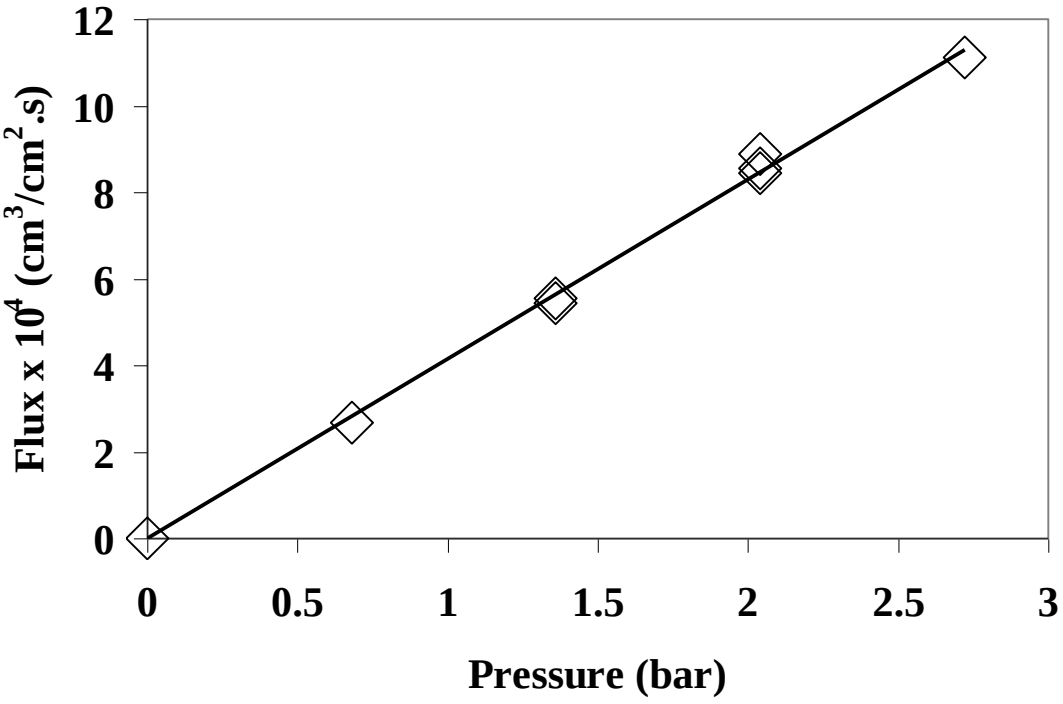

Figure 4.8 Membrane flux behavior for sulfonic acid-functionalized silica-polysulfone MMMs. (Membrane Permeance = 4.15 x 10^{-4} cm^3/cm^2 s bar)

Table 4.2 Sodium sulfate salt rejection data for sulfonic acid functionalized silica-polysulfone membrane (Transmembrane pressure = 3.4 bar)

Time	Permeate	Concentration of Na_2SO_4	% Rejection
(min)	Volume (mL)	mg/L	
10	5.5	66.2	32.7
20	5.6	84.6	13.9
30	5.5	87	11.5
40	5.4	82.2	16.4
Concentration of Feed Solution		98.3	
Concentration of Retentate		101.5	

4.7.1 Quantification of iron capture by sulfonic acid functionalized silica-polysulfone mixed-matrix membranes

The sulfonic acid-functionalized silica polysulfone mixed-matrix membrane was studied for iron ion capture. The concentration of the permeate was measured continuously. The breakthrough curve for Fe^{2+} in the case of sulfonic acid functionalized silica-polysulfone membrane is shown in Figure 4.9. As shown in the figure, the membrane is saturated with respect to iron pick up in about 1 h. The total amount of Fe^{2+} captured was calculated by numerically integrating the breakthrough curve data. The iron capture capacity of the membrane was 0.62 mg (For 15 cm^2 membrane area, 100 μm membrane thickness, 40% silica loading).

Based on membrane weight and 40% silica loading, the amount of silica in the membrane was approximately 0.022 g. Based on the measured silver capture capacity i.e. 2 mmole Ag/g of silica, and complete oxidation of –SH groups to sulfonic acid groups, maximum amount of sulfonic acid groups in the membrane = 0.044 mmoles. Assuming one ferrous ion captured per 2 sulfonic acic groups, maximum iron capture possible = 0.022 mmole i.e. 1.23 mg. The observed iron capture is 0.62 mg which is 50.4 % of theoretical maximum possible. This indicates 50% overall yield for Fe^{2+} capture using the sulfonic acid functionalized silica-polysulfone membrane.

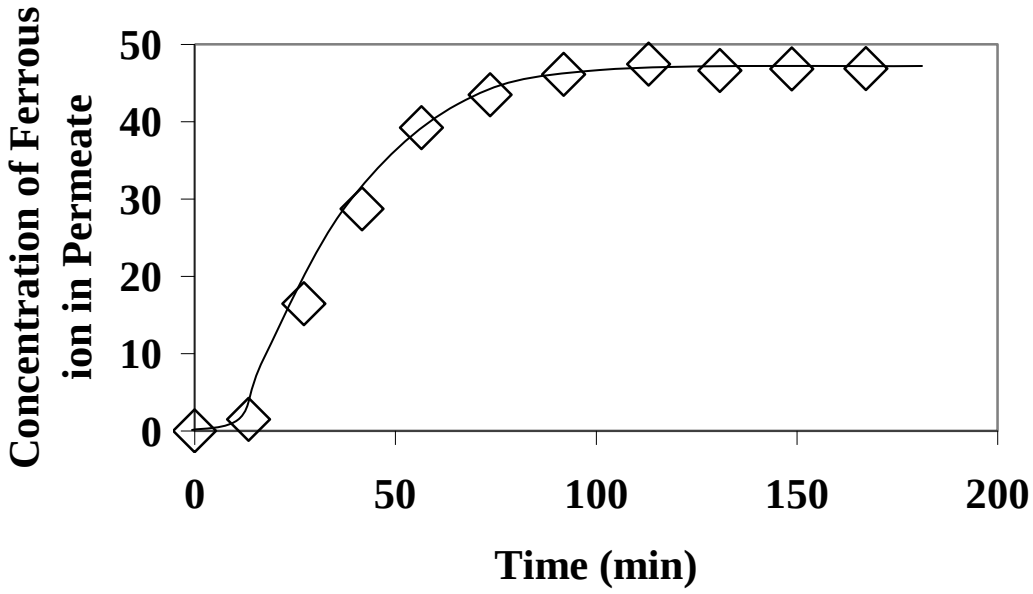

Figure 4.9 Breakthrough curve for Fe^{2+} capture using sulfonic acid functionalized silica – polysulfone mixed-matrix membrane. Solution of $FeCl_2$ in deoxygenated DIUF water at pH 5.2 with Fe^{2+} concentration of 48 mg/L was used for the study

The Fe^{2+} ions were reduced by sodium borohydride to form iron nanoparticles inside the membrane matrix. The nanoparticles are immobilized and hence do not agglomerate which is usually the case in bulk solutions. In order to confirm the existence of iron nanoparticles inside membrane matrix, SEM-EDS images of the membrane cross-section were obtained. Figure 4.10 shows the SEM image of the cross-section of the membrane (4.10 a) and the corresponding spectrum with elemental analysis (4.10 b).

The presence of Fe peak in the SEM-EDS analysis strongly supports the presence of iron nanoparticles in the membrane matrix. It must be noted that, the amount of iron present in the membrane is very small so as to obtain an iron peak over a large area. Iron peaks are observed only at the silica particle surface.

It has been previously demonstrated that the membrane immobilized iron nanoparticles can be successfully applied for chloro organic degradation. The procedure provides an alternative way for preparation of such membrane materials.

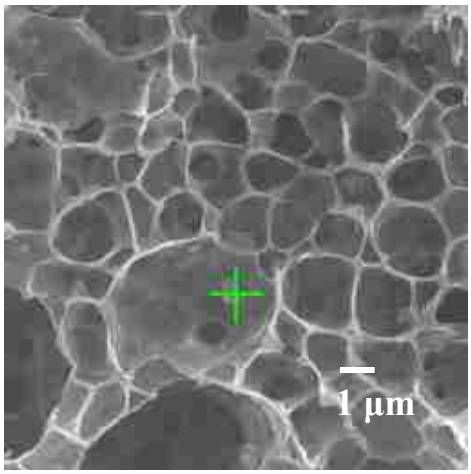

(a.)

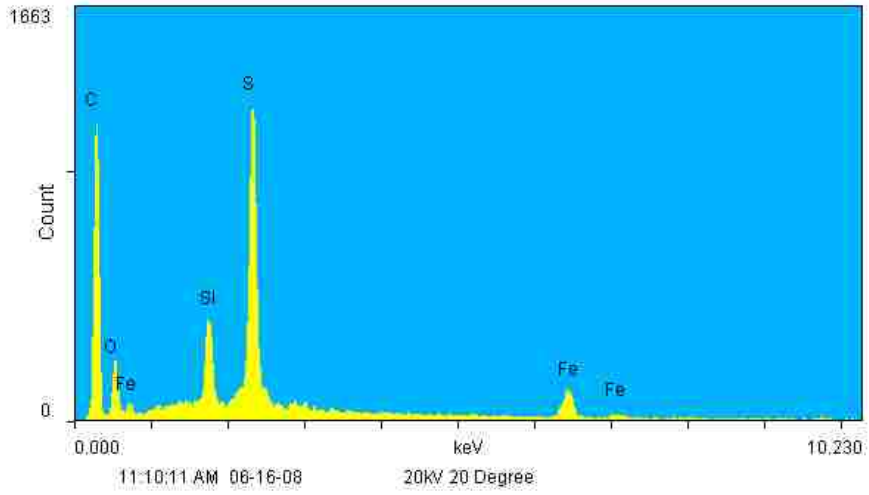

(b.)

Figure 4.10 a. SEM image of cross sections of sulfonic acid functionalized 874-85-1 silica-polysulfone mixed-matrix membrane after it has been used for Fe^{2+} capture treated with 0.1 M sodium borohydride. The + sign indicates the location of the spot for which the elemental analysis spectrum was obtained. b. Elemental analysis spectrum for the spot indicated in Figure 4.10 a. The presence of Fe peak in the elemental analysis indicates presence of iron nanoparticles in the membrane matrix

4.8 Summary of findings

Polymeric materials (cotton and polyester) were characterized by SEM imaging and it was observed that polyester exhibits smoother, uniform fibers than cotton. The apparent fiber diameter is 25 μm for polyester and approximately 15 μm for cotton material. The calculated specific surface area for cotton is 0.2 m^2/g, as compared to 0.11 m^2/g for polyester.

PVDF membranes were successfully functionalized with PAA as indicated by the SEM images and the decreased membrane permeance for PAA-functionalized membranes. Applying Hagen-Poiseuille equation to the membrane permeance data, the calculated porosity (ε_m / τ) was 0.19. It was also demonstrated that even though the PAA chains are partially cross-linked inside PVDF matrix, they are capable of undergoing charge transition with changing pH of feed solution. The PAA-functionalized membrane flux decreased from 65 x 10^{-4} cm^3/cm^2 s to less than 5 x 10^{-4} cm^3/cm^2 s as the feed solution pH increased from 2 to 4. The corresponding decrease in the effective pore radius was from 114 nm to 50 nm.

The ATR-FTIR analysis of MPTMS functionalized silica indicates that approximately 80% surface coverage is achieved during the functionalization. The silver ion capture capacity of the silica material was in the range of 2 mmole Ag^+/g of silica material.

Silica-polysulfone mixed-matrix membranes were successfully prepared with uniform distribution of the silica particles through the entire cross-section of the membrane. The SEM image also shows no agglomeration of silica particles during membrane preparation.

In the case of silica-polysulfone MMMs, it was observed that membrane permeance increases with increasing silica loading. The porosity of the membranes, determined by water uptake measurements was in the range of 0.6, indicating highly porous open membrane structure. The estimated value of effective pore radius from dextran rejection data was 39 nm.

The sulfonic acid functionalized silica-polysulfone membrane showed approximately 15% rejection of Na_2SO_4 indicating successful oxidation of thiol groups to

sulfonic acid groups. It was demonstrated that the membranes cab be used for ferrous ion capture from its aqueous solutions. Ferrous ions captured were converted into iron nanoparticles by reduction with sodium borohydride. This provides alternative way for preparation of membrane immobilized iron nanoparticles which can be used in many applications like catalytic dechlorination of toxic organic compounds.

Copyright © Abhay R Ladhe 2008

Chapter 5 Partitioning, adsorption and capture of ethoxylated nonionic surfactants

Ethoxylated nonionic surfactants were studied for their partitioning from D5 phase to aqueous PAA solution, for their adsorption at various solid-liquid interfaces and for surfactant capture using PAA-functionalized membranes. The results and discussed and compared in this section.

5.1 Partitioning of 15-S-5 (mixture of nonionic surfactants) from D5 to aqueous solution of polyacrylic acid (PAA)

Partitioning study of 15-S-5 between D5 and aqueous PAA solution was carried out to study the effect of partitioning on distribution of the surfactant. It was hypothesized that the ethylene oxide content of the surfactant will affect their partitioning behavior. The SCF-Mass Spectra for clear D5 phase before and after partitioning are obtained and are shown in Figure 5.1. The spectrum of D5 phase containing 15-S-5 shows numerous peaks, each peak representing individual surfactant species differing from one another either in terms of alkyl chain length or the number of ethylene oxide groups per molecules. The peak height corresponding to a particular surfactant in the spectrum obtained before partitioning was compared with that obtained after partitioning. As the peaks are sharp, the concentration of the surfactants can be approximated by the peak heights and approximate values of partition coefficient can be calculated as shown in Table 5.1.

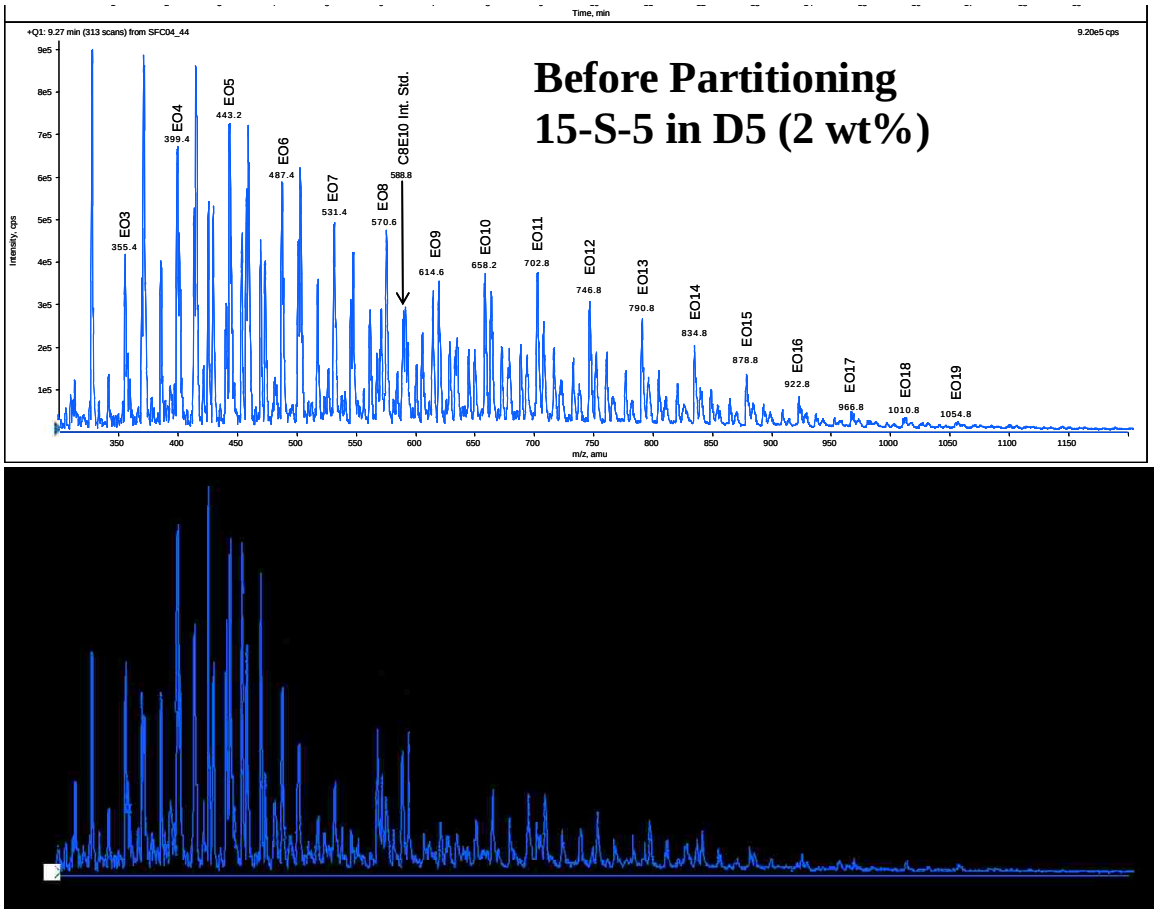

Figure 5.1 SCF-Mass spectra of solutions of 15-S-5 in D5 (2 wt%) before and after partitioning with aqueous PAA solution (3.1 mM). The spectra indicate preferential partitioning of the surfactant molecules containing higher number of ethylene oxide groups per molecule into aqueous phase. For the partitioning experiment, volume ratio of the two phases was 1:1 and pH of aqueous phase was adjusted to 3.0

Table 5.1 Partition coefficient estimation for the surfactants with varying number of ethylene oxide groups per molecule based on SCF-mass spectra

Number of ethylene oxide groups per surfactant molecule	**Peak height corresponding to the surfactant in the SCF-Mass Spectra (Unit)**		**Partition Coefficient**
	Before Partitioning (H_{BP})	**After Partitioning** (H_{AP})	$K_p = \frac{(H_{BP} - H_{AP})}{H_{AP}}$
3	4.2	4.0	0.05
5	7.2	6.2	0.16
8	4.8	2.1	0.77

It can be clearly observed that the surfactants having a higher number of ethylene oxide groups per molecule partition more favorably into the aqueous phase. This was expected because more ethylene oxide groups correspond to increased hydrophilicity, which in turn causes favorable partitioning into the aqueous phase. A few samples of the partitioned aqueous phase were analyzed by thin layer chromatography (TLC) to determine concentration of 15-S-5. It was calculated by mass balance that about 20% of the total surfactant of the system was present in the emulsion phase. The partition coefficient of 0.77 for $C_{12}E_8$ suggests that loss of surfactant from D5 was primarily due to partitioning and not just the preferential loss to emulsion phase. It was observed (Figure 5.2.) that the partition coefficient increases exponentially with increasing number of ethylene oxide groups per surfactant molecule. The slope of the graph is expected to be a strong function of solvent-surfactant hydrophobic interactions, amount of emulsion formed, temperature of the system, and pH of the aqueous phase.

In the present case, the surfactants entering the aqueous phase can form complex with PAA present in the system and this may affect equilibrium. PAA may also dissolve in the hydrophobic solvent to some extent and affect the distribution of the surfactants. To avoid these situations, PAA was immobilized in the membrane matrix. Interaction of the surfactants dissolved in the hydrophobic solvent with the immobilized PAA was studied by surfactant capture experiments which will be discussed in section 5.5

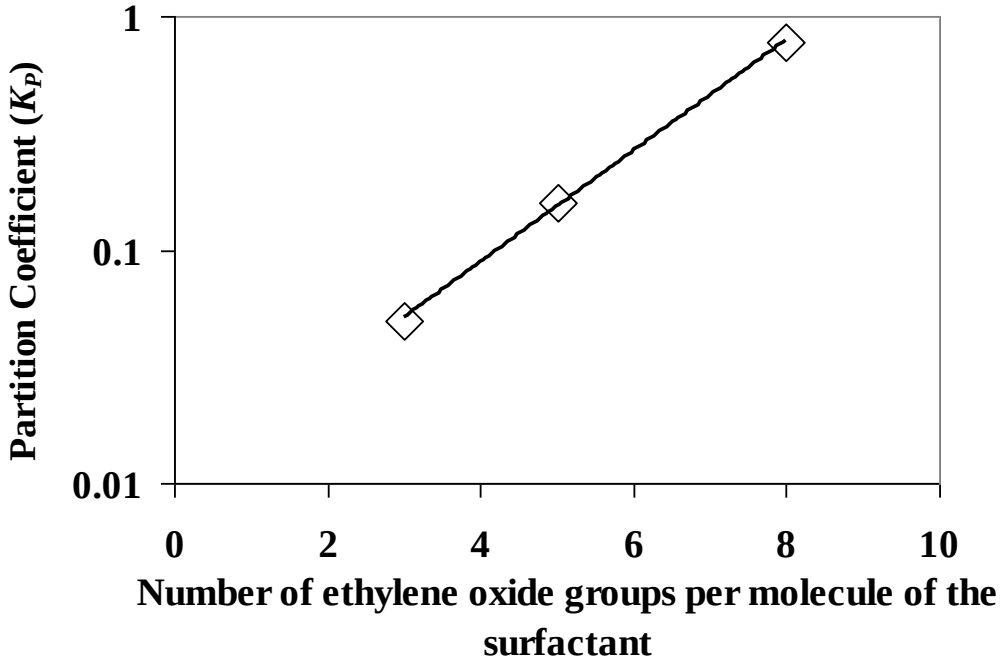

Figure 5.2 Effect of ethylene oxide group variation on partition coefficient: Solution of 15-S-5 in D5 (2 wt%) partitioned with aqueous solution of polyacrylic acid (3.1 mM) Volume ratio of the two phases = 1:1, pH of aqueous phase = 3.0 Partition coefficients calculated based on peak heights of 15-S-5 SCF-Mass Spectra before and after partitioning

5.2 Adsorption of pure ethoxylated nonionic surfactants on polymeric surfaces

Ethoxylated nonionic surfactants are used in dry cleaning operations and it is important to understand the adsorption behavior of these surfactants on different clothing materials. Cotton and polyester represent the two most commonly encountered clothing materials. Hence, adsorption behavior of the pure ethoxylated nonionic surfactants on cotton and polyester surfaces was studied. Cotton is expected to be much more hydrophilic than polyester. Cotton is composed of cellulose. Cellulose has high number of free hydroxyl groups which can readily form hydrogen bonds with water molecules and ethylene oxide groups of the surfactants. In order to get an idea of the relative hydrophilicity of the surfactants, the hydrogen bonding component (δ_H) of the Hansen solubility parameter was needed. The value of δ_H for the three surfactants can be estimated using equation (5.1) (Samaha and Naggar 1988)

$$\delta_H = (5000 \times A/V_m)^{1/2} \ (\text{cal/cm}^3)^{1/2} \qquad (5.1)$$

Where A is combined number of ethylene oxide and hydroxyl groups in the molecule and V_m is the molar volume of the surfactant. The calculated values of the δ_H parameters are 15.6, 17.27 and 18.69 $MPa^{1/2}$ for $C_{12}E_3$, $C_{12}E_5$ and $C_{12}E_8$, respectively. Higher δ_H corresponds to better hydrogen bonding ability and stronger hydrophilicity. δ_H for cellulose (cotton) is 22.3 (Matsuura et al. 1976) and for polyester is 7.8 (Deslandes et al. 1998). Hence it is expected that, in the hydrophobic D5 environment, $C_{12}E_8$ will adsorb more strongly on cotton than polyester due to stronger hydrogen bonding interaction between ethylene oxide groups of $C_{12}E_8$ and hydroxyl groups of cotton. This indeed was observed as shown in Figure 5.3. Using the values of specific surface area obtained in section 4.1, the results for surfactant adsorption using GC-FID analysis are reported in Figure 5.3 and 5.4.

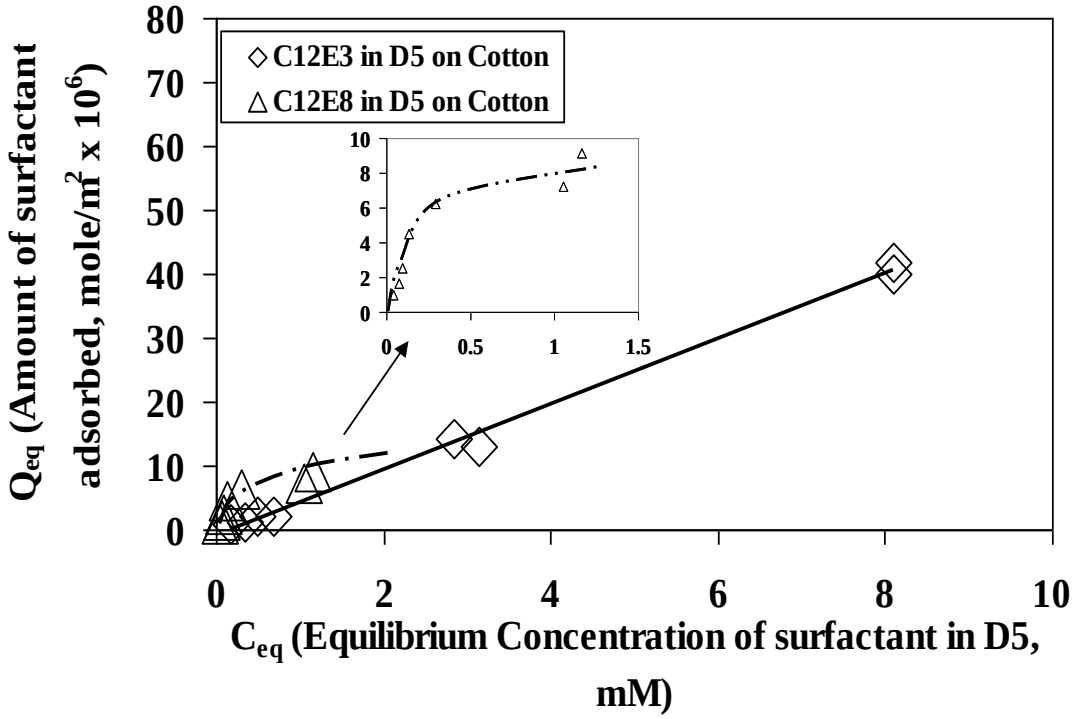

Figure 5.3 Adsorption of pure ethoxylated nonionic surfactants ($C_{12}E_3$ and $C_{12}E_8$) dissolved in D5 on cotton. Dotted curve indicates the trend line for the data. Solid line is a linear fit (R^2 = 0.996) Note: Due to solubility limitations of $C_{12}E_8$ in D5, adsorption studies were limited to 1.3 mM concentration of the surfactant

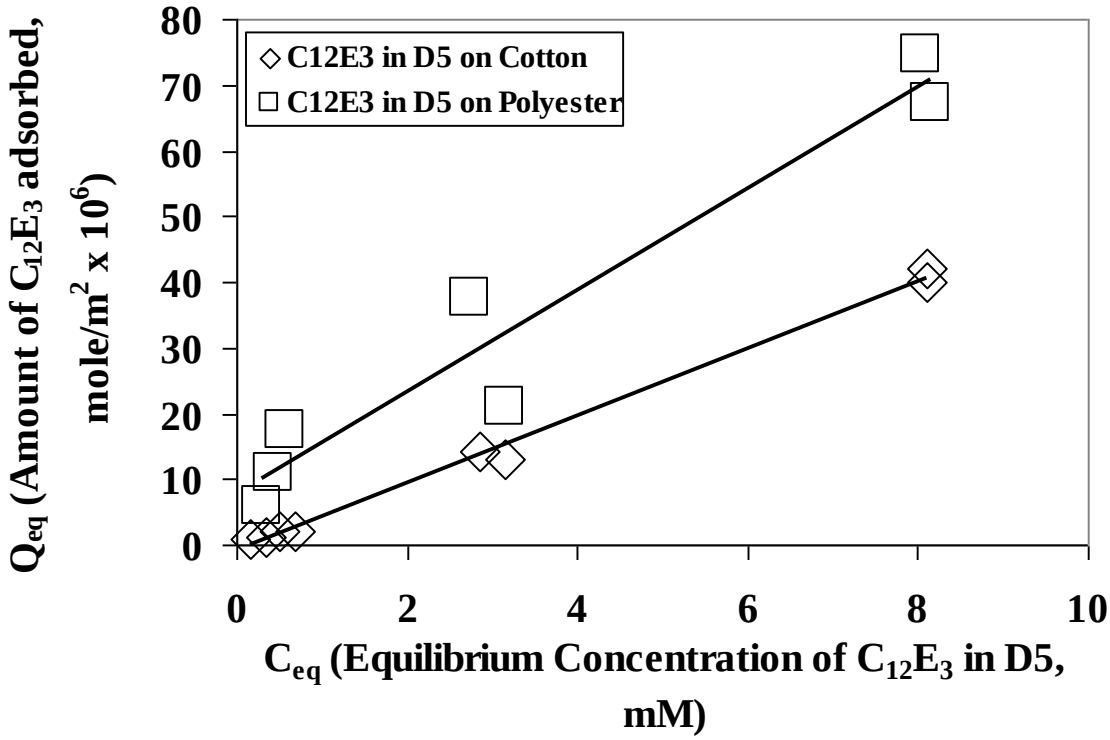

Figure 5.4 Adsorption of pure ethoxylated nonionic surfactant $C_{12}E_3$ dissolved in D5 on cotton and polyester. Solid lines indicate linear fit to the data for cotton surface (R^2 = 0.996) and for polyester surface (R^2 = 0.937) Data for adsorption of $C_{12}E_3$ in D5 on cotton is replotted for comparison

The amount of $C_{12}E_3$ adsorbed (Q_{eq}) on cotton for C_{eq} = 0.17 mM is 0.89 x 10^{-6} mole/m^2 of cotton. This lower value as compared to a Q_{eq} = 4.51 x 10^{-6} mole/m^2 at C_{eq} = 0.13 mM for $C_{12}E_8$ proves the hypothesis. In the case of $C_{12}E_8$, due to its limited solubility in D5 solvent, adsorption experiments can not be performed for concentrations greater than 1.3mM. The data for $C_{12}E_8$ adsorption within this concentration range indicates saturation behavior with a plateau value around 7 x 10^{-6} mole/m^2. In the case of $C_{12}E_3$, adsorption experiments were performed for starting concentrations as high as 8.6 mM. It is observed that equilibrium adsorption increased with increasing concentration and no saturation behavior was observed in the studied concentration range. The data can be represented by a linear relationship (R^2 = 0.996) as shown in Figure 5.3 The relatively higher saturation adsorption for $C_{12}E_3$ as compared to $C_{12}E_8$ on the cotton surface in D5 environment may be attributed to the larger hydrophilic group in the case of $C_{12}E_8$. In the case of monomeric adsorption of the surfactant molecules at the cotton-D5 surface, the ethylene oxide group steric repulsion (Claesson et al. 1999; Lomax 1996; Somasundaran and Krishnakumar 1997) is expected to be higher for $C_{12}E_8$ than that of $C_{12}E_3$, hence reaching early saturation. Critical Micelle Concentrations (CMCs) of these surfactants in D5 are not known precisely but the CMC of $C_{12}E_3$ in benzene is 4 mM (Rinia et al. 1996). It is also possible that the higher concentrations (8.6 mM) used for the adsorption of $C_{12}E_3$ are above CMC and the surfactant is adsorbing in the form of micelles (reverse micelles in this case) on the cotton surface as opposed to possible monomeric adsorption in the case of $C_{12}E_8$-cotton resulting in the large difference observed in the nature of the two adsorption isotherms. To the best of authors' knowledge, there is no literature data available to compare adsorption of ethoxylated surfactants on polymeric materials in hydrophobic environment. Torn et al. (2005) did study adsorption behavior of $C_{12}E_5$ on cellulose surface (very similar to cotton) in aqueous environment and the maximum adsorption observed was 7 x 10^{-6} mole/m^2 which is of the same order of magnitude of the results obtained for adsorption on cotton from D5 solvent.

It can also be observed from Figure 5.4, that less hydrophilic $C_{12}E_3$ adsorbs strongly on polyester (Q = 20.99 x 10^{-6} mole/m^2 for C_{eq} = 3.16 mM) as compared to its adsorption on cotton (Q = 12.97 x 10^{-6} mole/m^2 for C_{eq} = 3.14 mM). This can be attributed to favorable dispersion interaction between polyester and alkyl chain of the

surfactant. In the case of $C_{12}E_3$ adsorption on polyester, the data can be represented by a linear relationship (R^2 = 0.937) as shown in Figure 5.4. Geffroy et al. (2000) studied adsorption of $C_{12}E_5$ on polyester in aqueous environment and the equilibrium adsorption reported is 2.98 x 10^{-6} mole/m^2 which is comparable to the results obtained in this paper.

Because of the difficulty in analyzing water-based samples, the experiments with cotton and polyester were limited to D5 only. In order to demonstrate the effect of solvent on adsorption of the surfactants, adsorption experiments at QCM gold surface were carried out from both D5 and aqueous solutions. The precise nano gram level quantification of surfactant adsorption is not possible in the case of solution phase concentration difference based GC-FID analysis.

5.3 Adsorption of $C_{12}E_3$, $C_{12}E_5$ and $C_{12}E_8$ on model gold surface using QCM

The adsorption behavior for $C_{12}E_3$, $C_{12}E_5$ and $C_{12}E_8$ on gold surface from water is shown in Figure 5.5 and from D5 is shown in Figure 5.6. The adsorbed mass of surfactant was calculated using equation 2.3. The concentration range used for QCM studies does not affect bulk solution properties significantly and frequency correction was not needed. The dissipation data is also obtained for each experiment. The amount of surfactant adsorbed Q_{max}, adsorbed layer thickness, area per surfactant molecule and area per EO group are listed in Table 5.2. In order to calculate the adsorbed layer thickness, density of the adsorbed layer was assumed to be 950 kg/m^3. Unless mentioned otherwise, the 11^{th} overtone was used for all the Saurbrey mass and dissipation factor calculations. The experiments were performed under continuous peristaltic flow mode. Initially solvent (water or D5) was passed over the QCM crystal to obtain a steady baseline. After achieving a steady baseline, frequency and dissipation values are initialized to zero. Surfactant solution was introduced 10-15 minutes after zeroing baseline. Instant adsorption of the surfactants on the gold surface was observed in most of the cases represented by steep rising portions of the Saurbrey mass curves. The adsorption reached an equilibrium value represented by plateau behavior. Once the adsorption is plateau is reached, water was passed over the crystals to check for desorption behavior. Desorption

behavior is represented by steep fall in adsorption amount towards the end of the experiment. Desorption behavior was not studied for the gold-D5 interface.

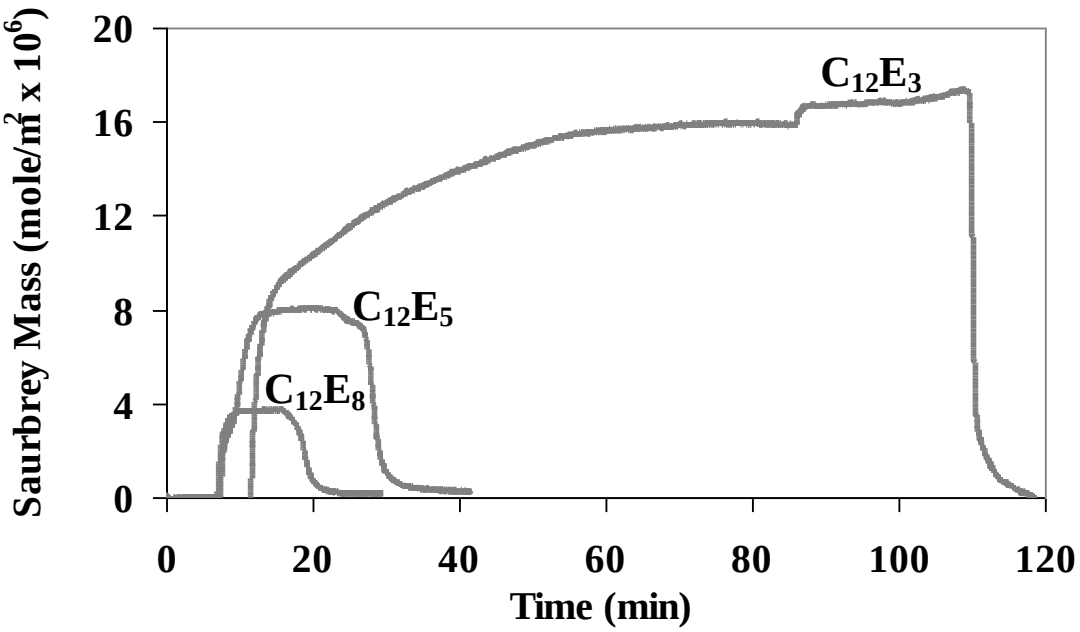

Figure 5.5 Adsorption of $C_{12}E_3$, $C_{12}E_5$ and $C_{12}E_8$ on gold surface from water using QCM-D. (Concentration of surfactant solutions = 250 mg/L i.e. 0.79 mM $C_{12}E_3$, 0.62 mM $C_{12}E_5$, and 0.46 mM $C_{12}E_8$; Surfactant solution flow rate = 0.1 mL/min)

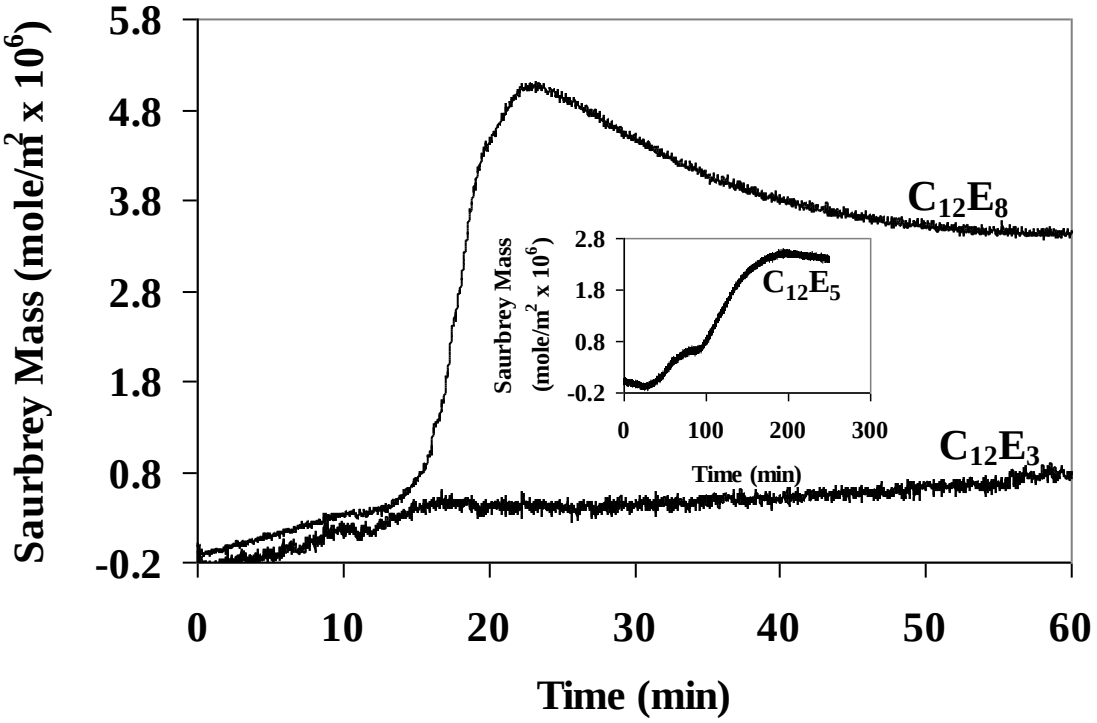

Figure 5.6 Adsorption of $C_{12}E_3$ and $C_{12}E_8$ on gold surface from D5. Inset shows adsorption of $C_{12}E_5$ on the gold surface from D5 (Concentration of surfactant solutions = 250 mg/L i.e. 0.79 mM $C_{12}E_3$, 0.62 mM for $C_{12}E_5$, and 0.46 mM $C_{12}E_8$, Surfactant solution flow rate = 0.1 mL/min)

Table 5.2 Data for adsorption of ethoxylated nonionic surfactants at various interfaces

Interface	Surfactant	Q_{max} x 10^6 mole/m^2	Adsorbed Layer Thicknes (nm)	Area per surfactant molecule (nm^2)	Area per EO group (nm^2)
Gold-Water	$C_{12}E_3$	15.9	5.3	0.10	0.034
	$C_{12}E_5$	8.00	3.4	0.21	0.041
	$C_{12}E_8$	3.70	2.1	0.45	0.056
Gold-D5	$C_{12}E_3$	Insignificant	-	-	-
	$C_{12}E_5$	2.40	1.0	0.69	0.138
	$C_{12}E_8$	3.45	1.9	0.48	0.060
cotton-D5*	$C_{12}E_3$	3.17	N/A	0.52	0.173
	$C_{12}E_8$	6.70	N/A	0.25	0.031
polyester-D5[#]	$C_{12}E_3$	13.9	N/A	0.12	0.040

The listed Q_{max} values are for 0.79, 0.62, 0.46 mM concentrations of $C_{12}E_3$, $C_{12}E_5$, and $C_{12}E_8$, respectively (250 mg/L). To calculate the adsorbed layer thickness, the adsorbed mass was divided by the surfactant layer density which was assumed to be 950 kg/m^3.

*** Data calculated using Figure 5.3**

[#] Data calculated using Figure 5.4

It can be observed from Figure 5.5 that adsorbed amount of the surfactants at gold-water interface decreased with increasing ethylene oxide (EO) groups per surfactant molecule. The trend is consistent with the literature findings in the case of silica-water interface (Desbene et al. 1997). Lower number of EO groups per surfactant molecule allows higher packing density at the interface and higher extent of chain-chain interaction (secondary mechanism of adsorption) resulting in higher adsorption. More hydrophilic $C_{12}E_8$ adsorbs to a lesser extent as compared to less hydrophilic $C_{12}E_3$ in the aqueous environment. This is due to stronger $C_{12}E_8$-water hydrogen bonding interaction compared to that of $C_{12}E_3$-water. Exactly opposite behavior is observed in the hydrophobic D5 environment. Insignificant $C_{12}E_3$ adsorption was observed at the gold-D5 interface. The discontinuity in the case of $C_{12}E_3$ (t = 85 min) is the disturbance while switching the surfactant solution with water to start the desorption experiment.

The volume of ethylene oxide group is 0.063 nm^3 (Kumar and Tilton 2004). Assuming the spherical shape, the projected area of the EO group will be 0.14 nm^2. If we assume monolayer coverage by the surfactants at the surface, the area occupied per surfactant molecule will be 0.57 nm^2, 0.95 nm^2, and 1.53 nm^2 for $C_{12}E_3$, $C_{12}E_5$, and $C_{12}E_8$, respectively. Based of these areas, the calculated adsorbed mass will be 2.9 x 10^{-6} mole/m^2, 1.7 x 10^{-6} mole/m^2, and 1.1 x 10^{-6} mole/m^2 for $C_{12}E_3$, $C_{12}E_5$, and $C_{12}E_8$, respectively. These values of the calculated adsorbed mass for monolayer coverage are in the same order of magnitude but lower than the observed values for gold water interface. This suggests the possibility of adsorption of surfactant aggregates instead of monolayer adsorption at gold-water interface.

5.3.1 Adsorbed layer morphology

In order to get an idea about the adsorbed layer morphology, the dissipation data collected during the experiment was analyzed. Figure 5.7 shows a plot of ΔD vs $-\Delta f$ for adsorption of each of the three surfactants at gold-water interface.

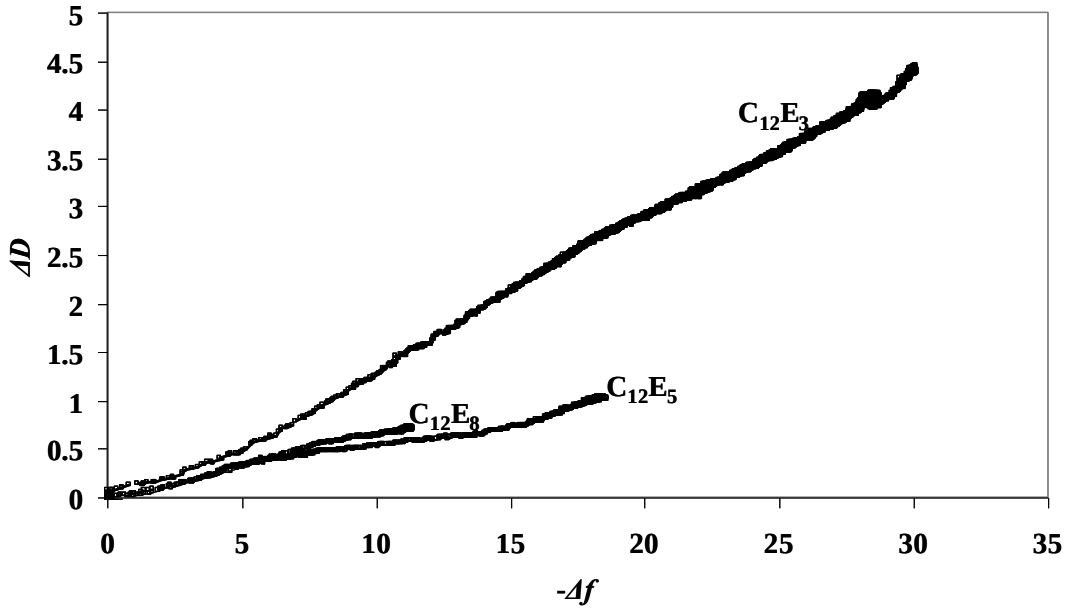

Figure 5.7 Variation of ΔD as a function of $-\Delta f$ for adsorption of $C_{12}E_3$, $C_{12}E_5$, and $C_{12}E_8$ from water on gold surface. The slope of the graph represents rigidity of the adsorbed layer (Concentration of surfactant solutions = 250 mg/L i.e. 0.79 mM $C_{12}E_3$, 0.62 mM $C_{12}E_5$ and 0.46 mM $C_{12}E_8$)

According to equation 2.2, the dissipation factor is inversely proportional to the decay time. As the fraction of the adsorbed mass dangling away from the surface increases, the crystal oscillations decay faster resulting is smaller decay time i.e. larger dissipation factor value. In Figure 5.7, it is observed that the slope of the ΔD vs $-\Delta f$ for $C_{12}E_5$ and $C_{12}E_8$ is comparable and it is lower compared to the slope for $C_{12}E_3$. The slope of the curve is the rate of increase of ΔD with respect to $-\Delta f$. Higher slope indicates that significant percentage of the adsorbed mass is dangling away from the surface.

As established in the literature, when the adsorption approaches saturation, the ethylene oxide chains stay in contact with the surface and the alkyl chains move away from the surface. In the case of $C_{12}E_n$ surfactants, for the same amount of adsorbed mass on the crystal surface (i.e. equal Δf values), the fraction of mass oriented away from the surface decreases with increasing n. This may be the reason for higher slope in the case of $C_{12}E_3$ as compared to $C_{12}E_5$ and $C_{12}E_8$. Only indirect information about adsorbed layer structure and morphology can be obtained using QCM dissipation data. Adsorbed layer structure can be studied using other techniques like AFM to get direct information. AFM has been used to study effect of surface hydrphobicity on the adsorbed layer morphology for the surfactant adsorption in aqueous environment.

5.3.2 Adsorption isotherm for $C_{12}E_3$

Adsorption of $C_{12}E_3$ at various concentrations was studied to establish adsorption isotherm. The results are shown in Figure 5.8. For concentrations below CMC (0.065 mM in water), very low adsorption was observed and a steep increase in the extent of adsorption occurred at concentrations near CMC. This is consistent with the observations reported in the literature. For concentrations above the CMC, a very slow increase in the adsorbed mass can be observed with increasing concentrations. This is not in agreement with the literature data. In the case of most of the reported studies, an adsorption plateau is observed for concentration above CMC. This may be attributed to QCM frequency drift with time.

The slope of the linear part of the adsorption isotherm obtained is 2.5×10^{-4} mole/m^2.mM. This slope is comparable to the slope of the adsorption isotherm ($2.03 \times 10^{-}$

^{4} mole/m^{2} mM) obtained by Postmus et al., (2007) in the case of $C_{12}E_5$ adsorption at silica-water interface.

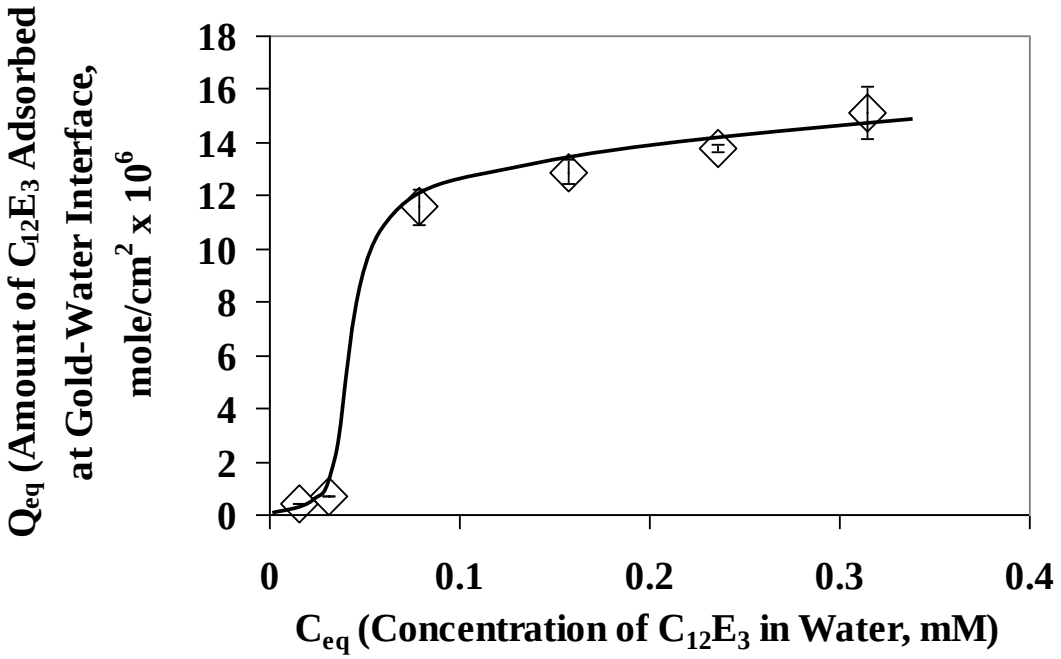

Figure 5.8 Adsorption isotherm for $C_{12}E_3$ at gold-water interface using QCM. The curve represents trend line for the data

5.4 Modeling the adsorption and desorption kinetics at gold-water interface

QCM data also provides information on adsorption/desorption kinetics. At the gold-water interface, $C_{12}E_5$ and $C_{12}E_8$ reached equilibrium within 10 minutes of introducing the surfactant solutions. In the case of $C_{12}E_3$, the equilibrium was achieved much slower (50 minutes after passing the surfactant solution). Desorption on introduction of water (pH 6) was complete in the case of $C_{12}E_3$, but in the case of $C_{12}E_5$ and $C_{12}E_8$, some residual amount remained adsorbed on the surface.

If we assume that the rate of adsorption (or desorption) is proportional to the adsorption potential then we can write,

$$dQ_s/dt = K_a(Q_{max} - Q_s) \qquad (5.2)$$

Where,

Q_s is amount of surfactant adsorbed (mole/m^2) at time t;

Q_{max} is the saturation adsorption value (mole/m^2) and

K_a is adsorption rate constant (sec^{-1}).

Integrating equation (5.2), we get

$$Q_s = Q_{max}(1-exp(-K_a t)) \qquad (5.3)$$

Equation (5.3) can be used to model the adsorption data for the ethoxylated surfactants from water and values for the adsorption rate constants can be calculated. Since the adsorption of the surfactants start at time $t = t_0 > 0$, we need to include the offset into the model equation. Hence the equation (5.3) is modified to

$$Q_s = Q_{max}(1-exp(-K_a(t-t_0)))\ldots\ldots(t>t_0) \qquad (5.4)$$

Adsorption data for $C_{12}E_3$, $C_{12}E_5$ and $C_{12}E_8$ at gold-water interface were fitted to equation (5.4) using Q-tools software provided by Q-sense and values of the adsorption rate constants are obtained as shown in Table 5.3 In order to model the desorption behavior of the surfactants, equation (5.4) is modified as follows

$$Q_s = Q_{max} - (Q_{max} - Q_{Res})(1-exp(-K_d(t-t_1)))\ldots\ldots (t>t_1) \qquad (5.5)$$

Where Q_{Res} is the residual amount of surfactant remaining on the crystal surface at the end of desorption experiment and t_1 is the time at which desorption experiment was started. The values of desorption rate constants obtained by fitting the desorption data of

the surfactant to equation (5.5) are also listed in Table 5.3 and the comparison of experimental and fitted data is shown in Figure 5.9

The adsorption rate constant value increases with increasing ethylene oxide groups per surfactant molecule. $C_{12}E_8$ has the fastest adsorption kinetics which is expected due to favorable ethylene oxide interaction of $C_{12}E_8$ with the hydrophilic gold surface. An opposite trend is observed in the case of desorption kinetics. The surfactant which adsorbs slowly is expected to desorb easily by water and vice a versa. In the case of $C_{12}E_3$ the model does not fit the experimental data and it seems that a two step adsorption model will be more appropriate. The adsorption model used was not applicable for adsorption of $C_{12}E_8$ at gold-D5 interface where adsorption amount initially increases with time and then starts decreasing and stabilizes at lower adsorption value.

Table 5.3 Adsorption and desorption rate constants for ethoxylated nonionic surfactants at gold-water interface (from QCM data) (C_{eq}= 250 mg/L i.e. 0.79 mM $C_{12}E_3$, 0.62 mM $C_{12}E_5$ and 0.46 mM $C_{12}E_8$. Flow rate was maintained at 0.1 mL/min during adsorption and desorption experiments)

Interface	Surfactant	K_a (sec^{-1}) x 10^3	K_d (sec^{-1}) x 10^3
Gold-Water	$C_{12}E_3$	1.8 (R^2 = 0.85)*	17.8 (R^2 = 0.77)
	$C_{12}E_5$	6.7 (R^2 = 0.90)	8.0 (R^2 = 0.90)
	$C_{12}E_8$	22.6 (R^2 = 0.97)	5.2 (R^2 = 0.78)

***The regression coefficients R^2 are calculated for each set containing at least 500 data points**

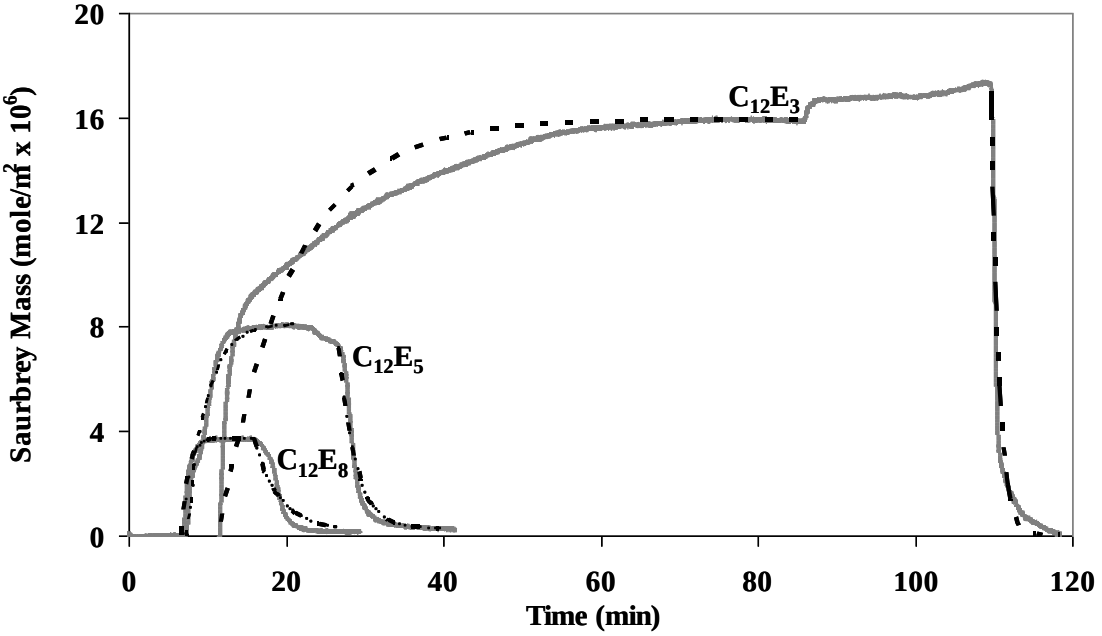

Figure 5.9 Comparison of modeled and experimental data for adsorption of $C_{12}E_3$,$C_{12}E_5$ and $C_{12}E_8$ on gold surface from water using QCM-D. (Concentration of surfactant solutions = 250 mg/L, i.e., 0.79 mM $C_{12}E_3$, 0.62 mM $C_{12}E_5$, and 0.46 mM $C_{12}E_8$). Dotted lines show fitted adsorption and desorption data using equation 5.4 and equation 5.5

5.5 Comparison of adsorption data for polymeric surfaces, QCM gold surface and literature data

At gold-water interface, Q_{max}=3.7 x 10^{-6} mole/m^2 for $C_{12}E_8$ corresponds to 0.45 nm^2 per molecule. This is comparable to 0.56 nm^2/molecule observed by Caruso et al. (1995) for the same system. The average area per ethylene oxide (EO) group is in the range of 0.034 nm^2 for $C_{12}E_3$ to 0.056 nm^2 for $C_{12}E_8$ (Refer to Table 5.2). In the case of silica-water interface, the reported literature value is 0.079 nm^2 per EO group (Desbene et al. 1997). The average area of 0.031 nm^2 per EO group for the $C_{12}E_8$ at cotton-D5 interface is of the same order of magnitude as that of gold-water and gold-D5 interface.

Although direct comparison of the data for surfactant adsorption at cotton-D5 interface with QCM data at gold-D5 interface is not possible, one should note that both cotton and gold surfaces are highly hydrophilic in nature and the ethoxylated surfactants should exhibit similar adsorption behavior on both the surfaces. In the lower concentration range surfactant adsorption is more in the case of $C_{12}E_8$ than that of $C_{12}E_3$ for both cotton-D5 and gold-D5 interface. The amount of the surfactant adsorbed for Qeq = 0.46 mM is 6 x 10^{-6} mole/m^2 in the case of cotton-D5 interface which is comparable to 4.5 x 10^{-6} mole/m^2 in the case of gold-D5 interface.

The observed $C_{12}E_8$ adsorbed layer thickness at gold-water interface is 2.1 nm. This is comparable to the adsorbed layer thickness of 3.5 nm obtained by Caruso et al (1995) in the case of adsorption of $C_{12}E_8$ at hydrophobic gold-water interface. Similarly, the maximum adsorbed amount for $C_{12}E_8$ in our case (3.7 x 10^{-6} mol/m^2) is comparable to the equilibrium adsorption (2.1 x 10^{-6} mole/m^2) reported by Kumar et al. (2004) for hydrophobic gold-water interface.

Postmus et al. (2007) studied kinetics of $C_{12}E_7$ adsorption at Silica-water interface. The slope of the adsorption curve is in the range of 5 x 10^{-7} mole/m^2 s for the particular case. The slope of the adsorption curve of $C_{12}E_8$ at gold-water interface is in the range of 3 x 10^{-8} mole/m^2 s. Tiberg et al. (1994) studied kinetics for $C_{12}E_6$ desorption at silica-water interface. The slope of the desorption curve (2 x 10^{-7} mole/m^2 s) is very much comparable to the slope of desorption curve observed in the case of $C_{12}E_5$ (1.2 x 10^{-7} mole/m^2 s) and $C_{12}E_8$ (2.04 x 10^{-8} mole/m^2 s).

5.6 Pure surfactant capture using polyacrylic acid (PAA) functionalized membranes

The PAA-functionalized membranes were studied for surfactant capture from D5 solutions. The surfactant concentrations in the feed and permeate obtained by GC-FID were used to calculate amount of surfactant captured during the permeation. To eliminate the effect of varying PAA loadings, the extent of surfactant capture was reported in terms of the moles of surfactant captured per mole of free carboxyl groups. It was assumed that ethylene glycol was completely utilized for crosslinking the PAA chains (since it was present in stoichiometrically deficient amount) and all the remaining carboxyl groups were free for interaction with the surfactants. The surfactant capture studies were carried out for the pure ethoxylated nonionic surfactants ($C_{12}E_n$) with same alkyl chain length but varying number of ethylene oxide groups per molecule.

As discussed earlier the ethylene oxide group of the surfactant actively contributes for polyelectrolyte-surfactant interaction through hydrogen bonding. Grant et al. 2000) established that hydrogen bonding between ethylene oxide groups of the surfactants and hydroxyl groups on the surface is an unlikely driving force in aqueous media, due to superior hydrogen bonding ability of water. This in turn suggests that the hydrogen bonding between the ethylene oxide and the carboxyl groups is likely to be the driving force in nonaqueous media such as D5. As all the pure surfactants used for the experiments have same alkyl chain length, there should not be much variation in the extent of dispersion interaction of these surfactants with D5 or the PAA carbon backbone. It was therefore expected that the higher ethylene oxide content per molecule should result in enhanced interactions with PAA. The amount of surfactant captured per mole of PAA indeed increased exponentially with increasing number of ethylene oxide groups per molecule (Figure 5.10). The slope of the graph will be affected by hydrophobic interaction between the surfactant and the solvent, degree of cross-linking of the PAA matrix, the extent of water present in the PAA domain and the alkyl chain length of the ethoxylated surfactants.

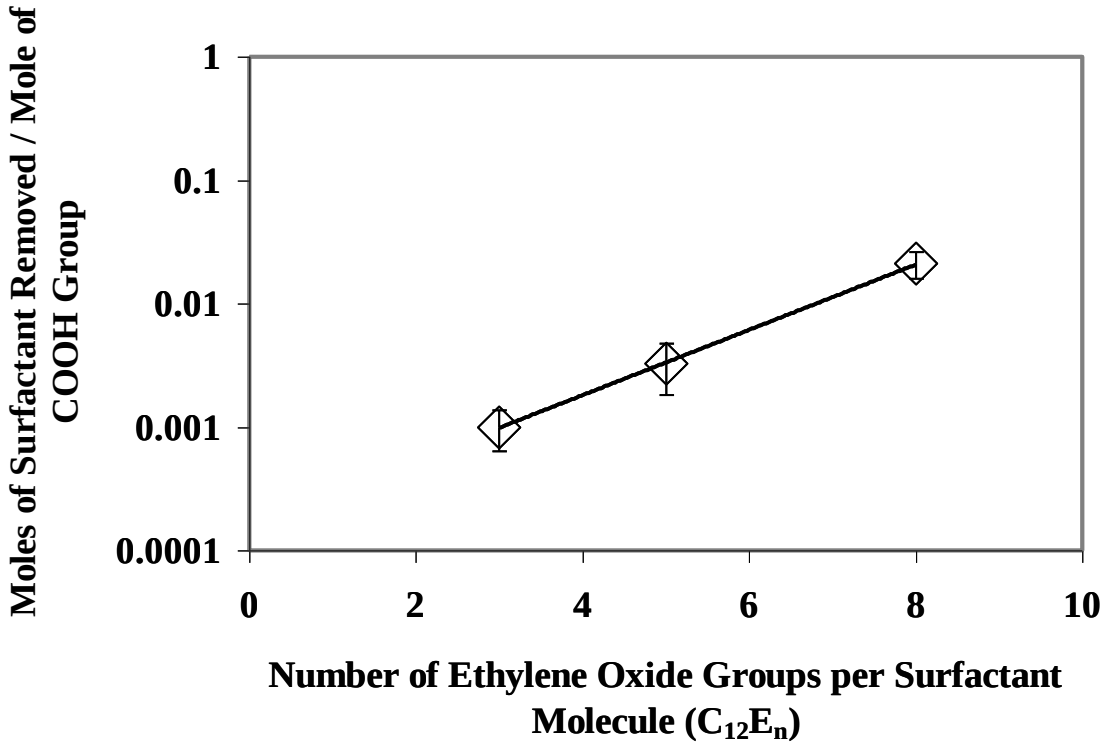

Figure 5.10 Pure surfactant ($C_{12}E_n$) capture by PAA-functionalized PVDF membrane (650 nm, 3 layer PAA coating, Transmembrane pressure = 2.04 bar) from their solution in D5 (Surfactant concentration used are 200 mg/L for $C_{12}E_8$ and 50 mg/L for $C_{12}E_5$ and $C_{12}E_3$, 0.1% water was added to the surfactant solutions before permeating through the functionalized membrane)

5.7 Calculation of surface excess concentration (Γ_{max}) for membrane surfactant capture studies and its comparison with the literature data

In order to determine the surface excess concentrations (moles of surfactant captured per m^2 of internal surface area), the effective pore radius (r_{eff}) is needed. This was obtained from the solvent permeability data as a function of pressure. The experimentally measured permeability of D5 (A_{D5}) was 1.9 x 10^{-4} cm^3/cm^2 s bar. Hagen-Poiseuille equation was used to determine r_{eff} with the assumption that the number of pores (N_p) remains approximately constant for both functionalized and bare membranes. Substituting $N_p = 8.543 \times 10^8$ and $A_m = 15 \times 10^{-4} m^2$ into equation (4.2) yields,

$$\varepsilon_m / \tau = 1.789 \times 10^{12} r_{eff}^2 \qquad (5.6)$$

Now substituting, $A_{D5} = 1.9 \times 10^{-11} m^3 / m^2 s\ Pa$, $\mu_{D5} = 3.8 \times 10^{-3} Pa\ s$ and ε_m / τ from equation (5.6) into equation (4.1) we get $r_{eff} = 80nm$.

The value of N_p used for these calculations is obtained from water permeability data. The corresponding surface excess concentration calculations are shown in Table 5.4 The literature data available for adsorption of the pure ethoxylated surfactants ($C_{12}E_n$) from their aqueous solutions onto various hydrophobic surfaces (Geffroy et al. 2000; Kumar and Tilton 2004; Gilchrist et al. 2000; Kjellin et al. 2002) is shown in Figure 5.11a. The calculated values for the membrane surfactant capture studies from hydrophobic D5 solutions are shown in Figure 5.11b. The hydrophobic attraction between alkyl chain of surfactants and the surface is the driving force in the case of the literature data for adsorption of surfactants. Similar attraction force (dispersion interaction) between alkyl chain of the surfactants and D5 solvent is the barrier for the surfactant capture experiments using hydrophilic PAA domain. Hence it was hypothesized that for the two cases, the trend with respect to number of ethylene oxide groups per surfactant molecule should be opposite which indeed is the case as shown in Figure 5.11.

Table 5.4 Surface excess concentration calculations for membrane surfactant capture experiment from D5

Internal surface area per pore = $2\pi \times r_{eff} \times L = 2\pi \times 80 \times 10^{-9} \times 1.25 \times 10^{-4} = 6.28 \times 10^{-11}\,\mathrm{m}^2$

Total surface (external + internal pore surface) area per unit external surface area of membrane

$= 6.28 \times 10^{-11} \times \frac{N_p}{A_m} = 35.8\,\mathrm{m}^2/\mathrm{m}^2$ of membrane.

From layer by layer weight gain data and degree of cross-linking for each layer,

Moles of free carboxyl groups per unit external area of membrane = 0.5 mole of COOH/m^2

Moles of free carboxyl groups per unit internal surface area = 0.5/35.8 = 0.014 moles of COOH/m^2

Number of ethylene oxide groups per surfactant molecule ($C_{12}E_n$)	**Membrane Surfactant Capture per mole of free COOH**	**Surface Excess Concentration (mole of surfactant/m^2 of total surface area)**
3	1 x 10^{-3}	14 x 10^{-6}
5	3.25 x 10^{-3}	45.5 x 10^{-6}
8	20.9 x 10^{-3}	292.6 x 10^{-6}

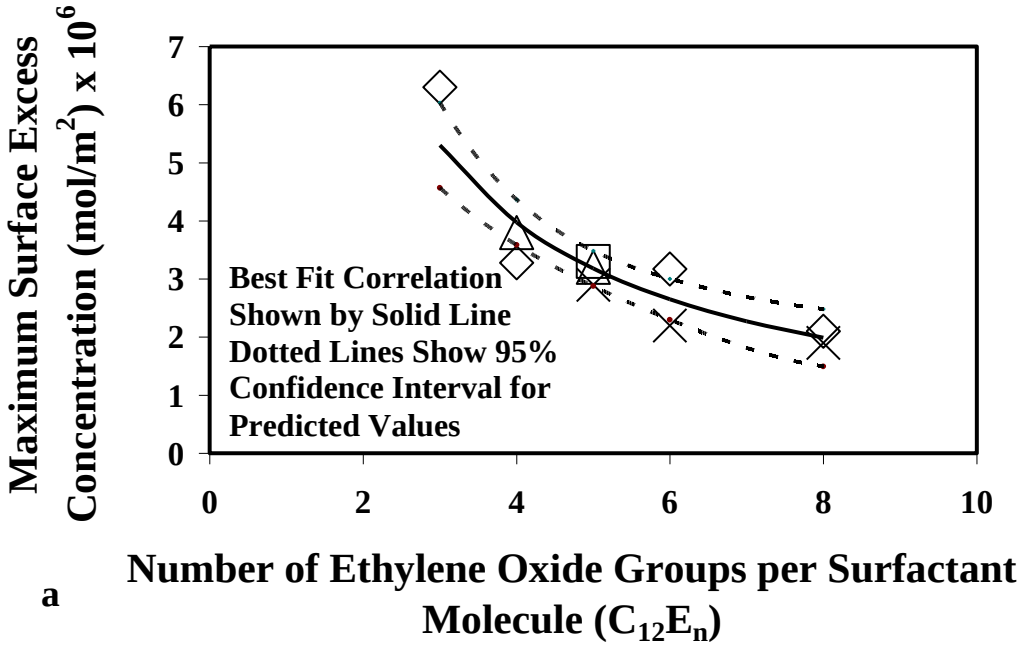

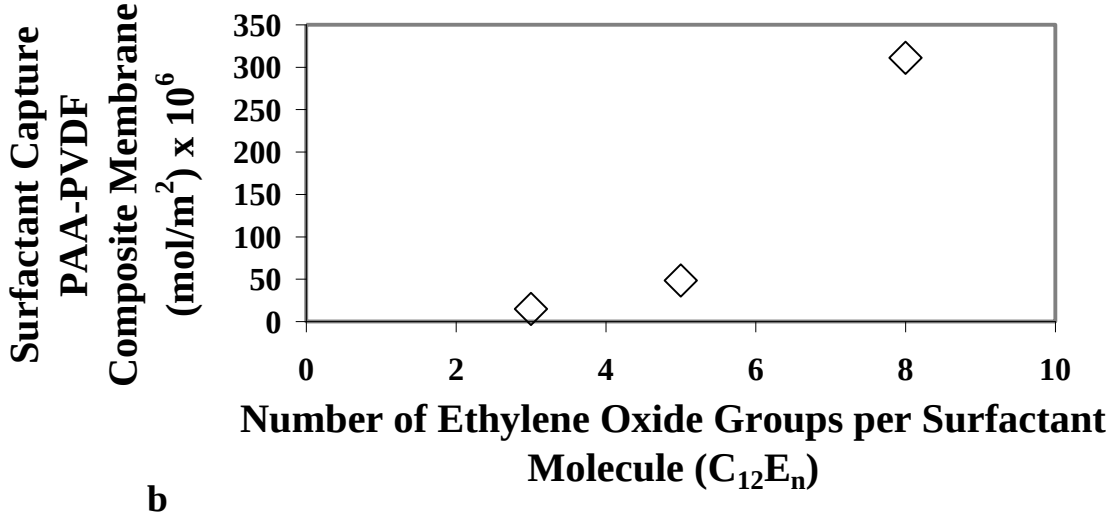

Figure 5.11 (a) Literature data for adsorption of pure ethoxylated nonionic surfactants ($C_{12}E_n$) on various hydrophobic solid-water interfaces. Best fit correlation and 95% confidence interval band for predicted values is shown (Literature data from Geffroy et al. 2000; Kumar and Tilton 2004; Gilchrist et al. 2000; Kjellin et al. 2002) (b) Experimental data for pure surfactant ($C_{12}E_n$) capture by PAA-functionalized membrane from solution in siloxane solvent (D5)

Ramaswamy et al. (2004) have done extensive membrane characterization of the Durapore PVDF membranes from Millipore. The complicated shape and highly inter-connected nature of pores was reported in the SEM images of the cross section of the membranes. The authors' data from gas-liquid porometry suggests that the calculated number average mean pore size for the Durapore membranes is about twice the nominal pore size rating provided by the manufacturer (based on model particle retention characteristics). The choice of the pore size affects the surface excess concentration calculations in the present study. N_p will be 16 times lower if the pore size value used for calculation is doubled. At the same time, curved surface area per pore ($2\pi r_p L$) will be 2 times higher. Both facts combined lead to an 8 fold decrease in the available surface area which in turn means 8 fold higher Γ_{max} values for the same experimentally measured parameters.

The maximum surface excess concentration of 6 x 10^{-6} mol/m^2 (as in the case of literature data) corresponds to a surface coverage value of about 0.28 nm^2/molecule. Volume of a CH_3 group is about 0.05 nm^3 and if we assume it to be spherical then the projected area will be 0.16 nm^2. This suggests possible monolayer adsorption in the case of the literature data. In the case of surfactant capture by membrane, the maximum surface excess concentration of 292.6 x 10^{-6} mol/m^2 corresponds to 0.005 nm^2/molecule which is very low for monolayer adsorption. This means either that the surfactant capture mechanism involves multilayer adsorption or the immobilized PAA matrix provides substantially higher extent of internal surface area than that calculated from the effective pore radius and membrane porosity.

It is also interesting to note that although different hydrophobic surfaces were used for the literature adsorption studies, the extent of maximum surface excess concentration does not vary significantly for a fixed number of ethylene oxide groups. The data can be adequately correlated (R^2 = 0.87) by the following expression:

$$\Gamma_{max} = \frac{1.59 \times 10^{-5}}{n} \qquad (5.7)$$

Where n is number of ethylene oxide groups per surfactant molecule. The 95% confidence interval for the regression coefficient is (1.47 x 10^{-5}, 1.71 x 10^{-5}) and the 95%

confidence interval for the predicted values for surface excess concentration is shown by the dotted curves.

5.8 Comparison of membrane surfactant capture in heterogeneous system with PAA-ethoxylated surfactant interaction in homogeneous aqueous system

The amount of $C_{12}E_8$ captured from D5 by the partially cross-linked PAA composite membrane is about 0.16 moles of EO per mole of COOH groups of PAA. This amount is an order of magnitude smaller when compared to 1.8 moles of EO per mole of COOH for $C_{12}E_8$-PAA system in aqueous phase as determined by Anghel et al. (1998). The comparison of extent of surfactant captured by the membrane from solution in D5 with the literature value for free PAA in aqueous solution helps to get an idea about the mechanism of PAA-surfactant interaction. The lower value for the former suggests that, there is some kind of barrier which prevents the surfactants dissolved in D5 from interacting to the fullest extent with partially cross-linked PAA. The process of surfactant capture from its solution in D5 phase using the functionalized PAA membrane requires two important steps.

1. Transport of surfactant from hydrophobic solvent domain to PAA domain
2. Interaction of ethylene oxide groups of the surfactant with carboxyl groups of PAA

The partition limitation in terms of transport of surfactant from hydrophobic solvent domain to hydrophilic PAA domain will not be present in the case of surfactant capture from its aqueous solution. In order to check the significance of this transport limitation, surfactant capture studies were carried out from aqueous and organic solutions of the surfactant. It was observed that $C_{12}E_5$ surfactant capture from D5 phase (3.25×10^{-3} mole of $C_{12}E_5$ per mole of free carboxyl group) is an order of magnitude smaller than surfactant capture from water phase (3.38×10^{-2} mole of $C_{12}E_5$ per mole of free carboxyl group). This indicates tremendous transport limitation inhibiting the surfactant in D5 phase from interacting with carboxyl groups of PAA. Since the surfactant capture experiments were performed under constant transmembrane pressure (2.04 bar), the residence time of the solutions in the membrane was constant. Considering the significant transport limitations, the results will be dependent on residence time.

The second step corresponds to the accessibility of carboxyl groups for interaction. Considering the multilayer crosslinked structure of PAA coating, it is possible that a certain fraction of free carboxyl groups may not be available for carboxyl-ethylene oxide interaction due to the diffusion limitations. It is interesting to note that adsorbed amounts from aqueous solutions were comparable for both free PAA (1.8 moles of EO per mole of COOH) and immobilized PAA (1.7 moles of EO per mole of COOH). This may indicate that there are no diffusion limitations present in the surfactant capture process by the immobilized PAA. The free PAA present in the aqueous solution is always present in helical form. In this form not all the carboxyl groups may be accessible by the surfactants for interaction. On the other hand in the case of immobilized PAA, the chains are expected to be more stretched as compared to their conformation in aqueous solution leading to higher accessibility. The diffusion limitations may still be present since there are several layers of PAA present in the pore, but the effect of diffusion limitation and increased accessibility may be comparable to lead comparable results for free PAA and immobilized PAA. To calculate the fraction of unavailable carboxyl groups due to the diffusion limitations, the PAA-functionalized membranes were studied for Ca^{2+} ion adsorption from aqueous solution, in a manner similar to surfactant adsorption studies. The concentration of Ca^{2+} ion in the feed and permeate was analyzed by atomic absorption spectroscopy. The upper limit for Ca^{2+} ion pick up was calculated by using the fact that one Ca^{2+} ion can interact with two carboxyl groups of PAA. The experimental Ca^{2+} ion capacity was found to be 40% of the theoretical maximum indicating that 60% of carboxyl groups not available for interaction due to diffusion limitations. This fraction may be higher in the case of the surfactant capture experiment as the size of the surfactant molecule is much higher as compared to a Ca^{2+} ion.

5.9 Membrane regeneration and reuse

Since the interaction between the ethylene oxide and carboxyl groups is the result of hydrogen bonding between the two groups, it is pH sensitive. The complex formation occurs only in low pH (pH 2-5) range. This fact was verified by permeating slightly alkaline water (50 mL, pH = 8) through the membrane. The surfactant was collected as its

aqueous solution on the permeate side. The aqueous phase analysis by partitioning and GC-FID showed that 70% of the captured surfactant in the membrane was collected in its aqueous permeate. The regenerated membrane was used again for the surfactant capture experiment and it picked up the surfactant to 90% of the regenerated capacity. This established the reversibility of the surfactant-PAA complex with very low capacity loss. The successful regeneration and reuse of the membranes can be exploited to develop a novel process for separation of the nonionic surfactants from organic solvents. The preferential separation of the surfactant molecules with higher number of ethylene oxide groups may be applied for purification of a surfactant mixture.

5.10 Summary of findings

The comparison of SCF-MS spectra of 15-S-5 in D5 phase before and after partitioning with aqueous PAA solution, clearly established the preferential partitioning of the higher ethoxylated nonionic surfactants into the aqueous phase from the D5 phase. The estimated partition coefficients based on peak heights showed exponential increase with increasing number of ethylene oxide groups per surfactant molecules.

Surfactant adsorption study on polymeric cotton and polyester materials proved that in the lower concentration range, $C_{12}E_8$ adsorbs strongly on the cotton surface than $C_{12}E_3$ in the hydrophobic D5 environment. $C_{12}E_8$ exhibits saturation behavior with the plateau value around 7×10^{-6} mole/m^2 as opposed to the linear behavior observed in the case of $C_{12}E_3$ under the experimental conditions. More hydrophobic $C_{12}E_3$ adsorbs strongly on polyester than cotton in the D5 environment. The reason was attributed to the favorable dispersion interaction in the case of $C_{12}E_3$-polyester.

For adsorption of the surfactants on gold-water interface, the adsorbed surfactant amount decreased with increasing ethylene oxide groups per surfactant molecule. In the case of gold-D5 interface, the adsorbed amount increased with increasing ethylene oxide content of the surfactants. The dissipation data suggested that a larger fraction of adsorbed mass is dangling away from the gold-water interface in the case of $C_{12}E_3$. Adsorption isotherm for $C_{12}E_3$ at gold-water interface was established and a steep rise in the adsorbed amount was observed at concentration in the vicinity of CMC.

The surfactant adsorption-desorption behavior at gold-water interface was modeled to determine adsorption-desorption rate constants. It was observed that adsorption rate constant increases with increasing number of ethylene oxide groups per molecule. On the other hand, the values for desorption rate constants decreased with increasing ethylene oxide content of the surfactant molecule. A two step adsorption model may be better suited for modeling $C_{12}E_3$ adsorption data.

It was demonstrated that the PAA-functionalized PVDF membranes can be successfully applied for surfactant capture from D5 solutions. The amount of surfactant captured, increased exponentially with increasing number of ethylene oxide groups in the surfactant molecule. It was also demonstrated that as expected, the trend for extent of surfactant adsorption with respect to number of ethylene oxide content is opposite for solid-water and PAA-D5 interfaces.

Accessibility studies for membrane immobilized PAA suggest that less than 40% of the carboxyl groups present in the membranes are accessible to interaction with surfactant molecules. The surfactant capture from aqueous phase was an order of magnitude more that the surfactant captures from D5 phase which indicates that significant transport limitation inhibits surfactant from D5 phase to interact with carboxyl groups in the hydrophilic PAA domain. Finally it was demonstrated that the membrane can be regenerated by permeating slightly alkaline water (pH 8) through it and the membrane can be reused for surfactant capture.

Copyright © Abhay R Ladhe 2008

Chapter 6 Functionalized mixed-matrix membranes for metal sorption

Functionalized mixed-matrix membranes were studied for metal ion sorption applications and the results are discussed in this chapter. The thiol-functionalized silica-polymer membranes were studied for Ag^{+} and Ca^{2+} sorption and the sulfonic acid functionalized silica-polymer membranes were studied for Fe^{2+} sorption behavior from aqueous solutions of the respective metal ions.

6.1 Silver ion capture using thiol-functionalized silica-polymer MMMs

Silver capture experiments were carried out to verify Ag^{+} removal from its $AgNO_3$ solution using 30% 874-85-1 thiol-functionalized silica MMM. The results are shown in Figure 6.1. The observed maximum capture was 1.5 mmole Ag/g of silica. The dotted line indicates maximum silver capture capacity. The error bars indicate analytical error of measurement for Ag^{+} concentration. In order to prove the hypothesis, that the observed silver capture is specifically due to thiol-Ag^{+} interaction, experiments were carried out for silver capture with bare polysulfone membrane and non functionalized silica-polysulfone MMM. It is clearly observed from Figure 6.1 that silver capture in both the cases is significantly less (0.45 mmole/ g of silica) than what was observed for thiol-functionalized silica (1.6 mmole/g of silica), hence proving the hypothesis. It should be noted that the non-functionalized silica membrane captured more silver (0.45 mmole/g of silica) than the pure polymer membrane (0.31 mmole/g of silica). Silica is known to have negative charge at the surface and it can attract the positively charged silver ions. This may explain the higher silver capture by non-functionalized silica membrane than the pure polymer membrane.

The concentration of silver on the retentate side was also measured to verify that the difference in feed and permeate concentration is not due to osmotic rejection or Donnan exclusion effect. In all the cases, the retentate concentration was less than feed concentration (about 90 – 95% of feed concentration) indicating successful silver capture by the membrane due to thiol-Ag^{+} interaction.

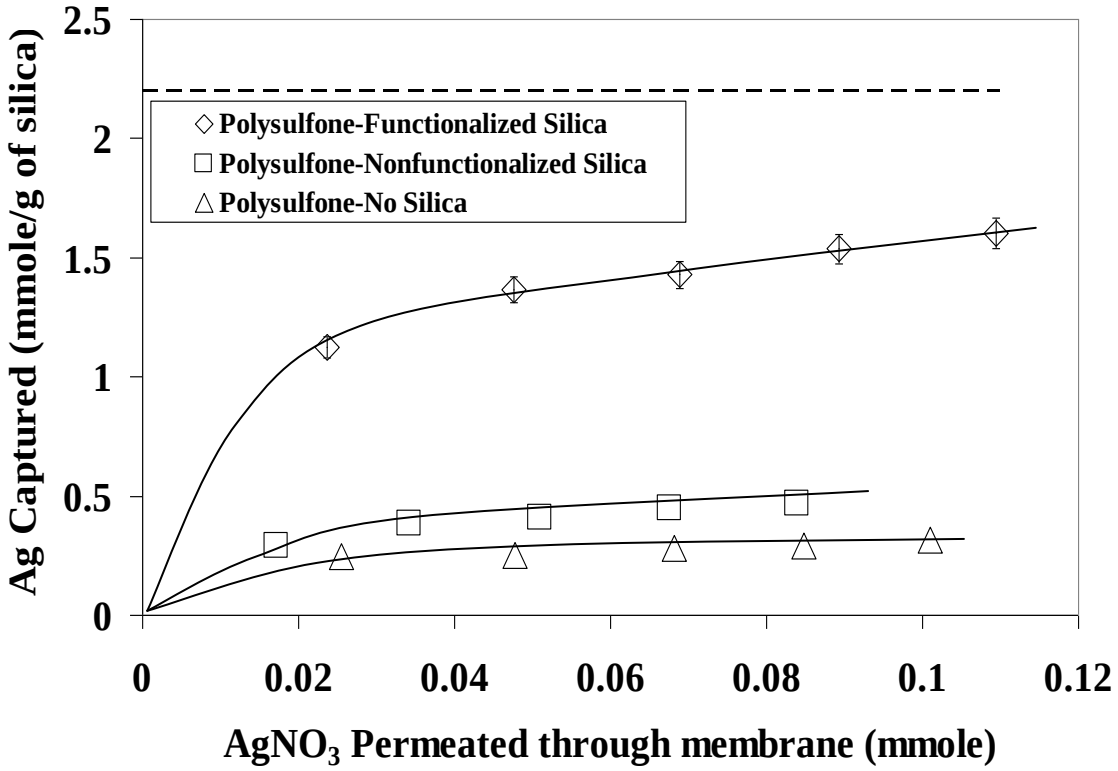

Figure 6.1 Silver capture using thiol-functionalized 30 % 874-85-1 silica-polysulfone MMM (Feed concentration 100 mg/L of Ag). Comparison with silver capture data using non-functionalized silica-MMM and bare polysulfone membrane. Horizontal dotted line at top indicates maximum silver capture capacity. Error bars indicate analytical error of measurement for Ag^+ concentration. In order to facilitate comparison, the values reported for the case of bare polysulfone membrane (mmole/g of silica), are based on amount of silica present in polysulfone-non functionalized silica case. The solid lines show trends in the data

In order to understand thiol site accessibility, silver capture experimental results with thiol-functionalized silica-MMM in convective mode were compared with soaking mode (no convective flow) results. The membrane was cut into pieces and added to the aqueous silver nitrate solution and the mixture was equilibrated for approximately 12 h. No significant silver capture was observed in the case of soaking mode as opposed to convective mode experiments. Even if the membrane is highly porous, in the soaking mode the mass transfer resistance for the silver ions to interact with thiol groups inside silica pores is expected to be high. The experimental observation clearly demonstrates the inability of the silver ions to access the thiol sites incorporated inside polysulfone matrix in absence of convective flow.

6.1.1 pH change during silver capture experiments

During silver capture with thiol-functionalized silica-MMM, it is hypothesized that the Ag^+ ion replaces hydrogen ion from the –SH (thiol) group and gets adsorbed. This should lead to higher H^+ ion concentration on the permeate side as compared to the feed solution. pH measurement on permeate side indeed showed drop in pH as compared to feed solution. The starting solution pH was 5.8-6.0, and during the initial part of silver pick up experiments (where almost complete silver capture was observed), the observed pH of permeate solution was in the range of 5.3-5.5.

6.2 Effect of silica surface area and thiol accessibility on metal ion capture

As reported in Table 3.1, the three types of silica (874-85-1, 874-86-2 and Ludox TM 50) exhibit different particle sizes, pore sizes and correspondingly different specific surface areas. 874-85-1 has higher specific surface area than 874-86-2 and Ludox TM 50. Ludox silica is nonporous as opposed to 874-85-1 and 874-86-2. Hence the entire surface area is expected to be accessible for metal ion capture in the case of Ludox. The average pore diameter values (gaps between base particles) are 11.8 nm for 874-86-2 and 3.5 nm for 874-85-1. The smaller pore diameter results in higher specific surface area but it is

possible that a portion of this surface area is unavailable for silanization and/or metal ion interaction due to transport limitations.

In order to compare the relative performances of the three types of silica, silver capture experiments were carried out with each of the functionalized silica-MMMs under same conditions. The three types of silica were functionalized with MPTMS and then used to make MMMs with cellulose acetate polymer so as to get 10 wt % silica loading in the final membrane. The choice of cellulose acetate over polysulfone for polymer phase was driven by compatibility of the acetone-water-cellulose acetate mixture with Ludox silica which was in the form of aqueous emulsion. The polysulfone-DMF solution did not form a homogeneous mixture with Ludox silica. The goal was to select one of the three silica materials based on their relative performance, and then to use that type of silica-polymer MMMs for further experiments.

It was hypothesized that the extent of metal ion capture per unit surface area should be largest for Ludox silica. This indeed was observed as shown in Figure 6.2. It was also observed that 874-86-2 has higher capture capacity per unit surface area than 874-85-1. However, this trend for silver ion capture capacity is reversed when compared in terms of silver ion capture per unit mass of silica present in the membrane as shown in the Figure 6.3. This clearly indicates that although a fraction of pore surface area of 874-85-1 was not accessible for silver ion capture, the advantage of higher specific surface area outweighs the extent of inaccessibility. 874-85-1 was used as the dispersed phase in the MMMs for all further experiments.

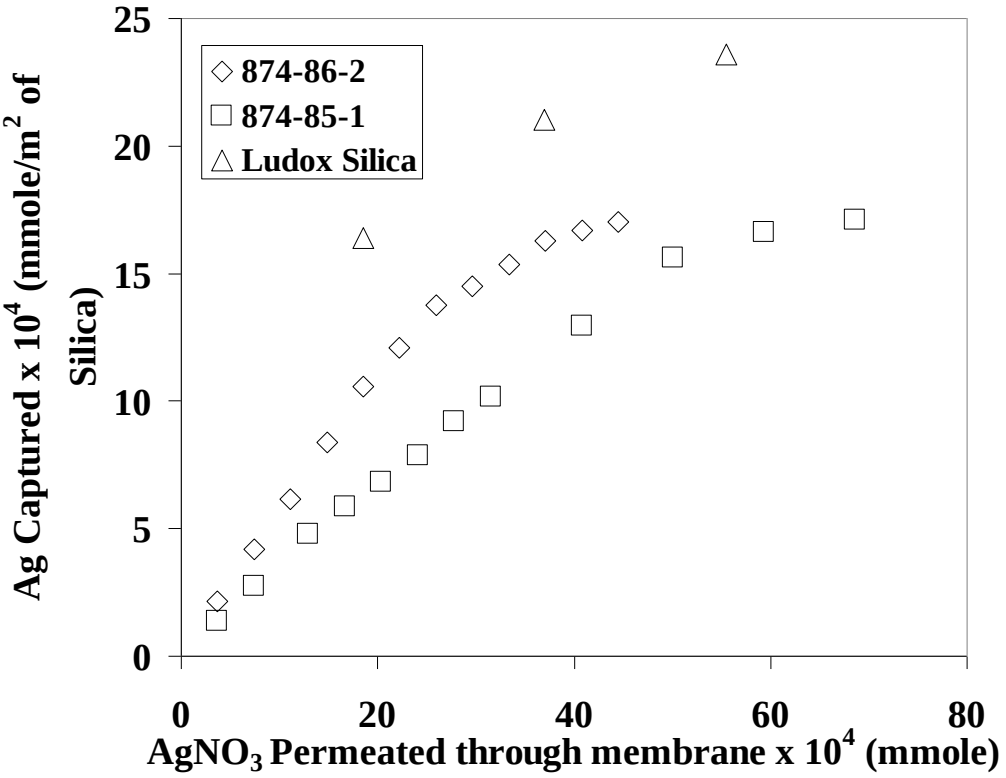

Figure 6.2 Silver capture with different functionalized silica-cellulose acetate mixed-matrix membranes (10% silica loading, Feed concentration = 17 mg/L of Ag). Effect of total surface area and accessibility of surface –SH groups on silver ion capture capacity

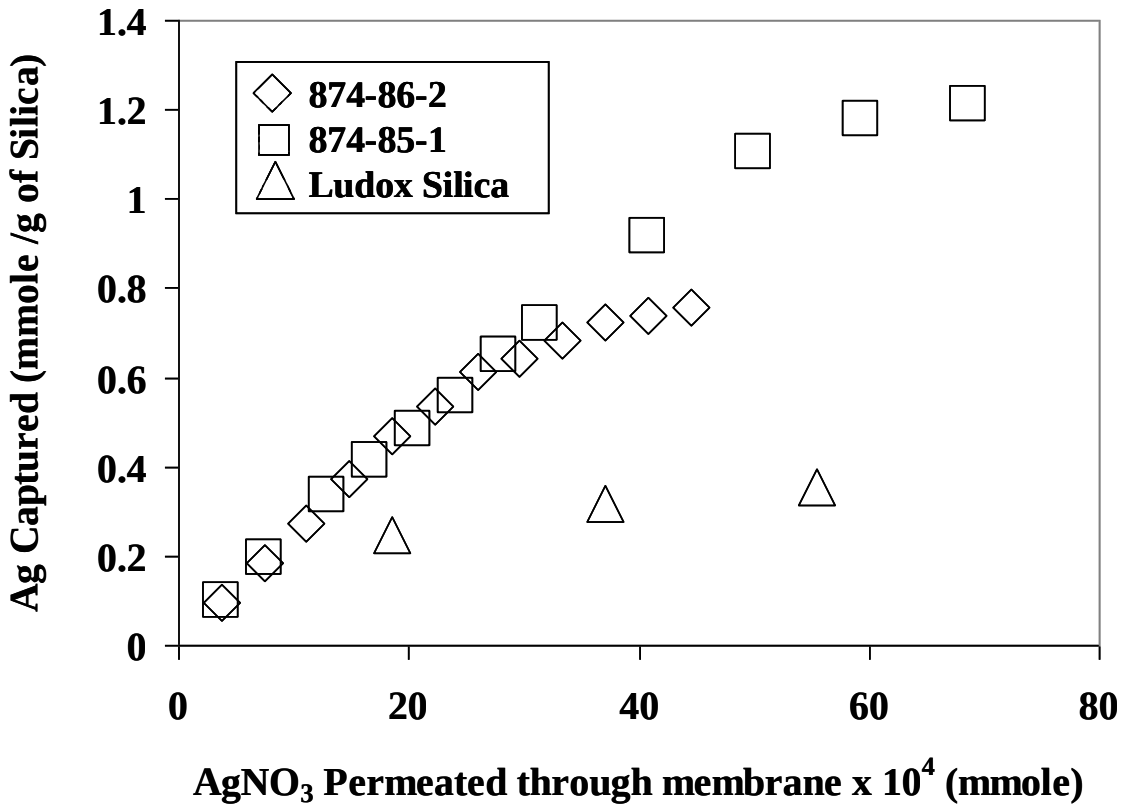

Figure 6.3 Silver capture with different functionalized silica-cellulose acetate mixed-matrix membranes (10% silica loading, Feed concentration = 17 mg/L of Ag). Data from Figure 6.2 is replotted in the form of silver capture per g of silica

This experiment also established generic applicability of MPTMS functionalized silica MMMs for silver capture using suitable polymer domains (like polysulfone, cellulose acetate, etc.). It was also observed that the silver solution permeance of the cellulose acetate membranes is significantly lower than that of the polysulfone based membranes prepared under similar conditions. For a 10% thiol-functionalized cellulose acetate membrane, the permeability was 0.2 x 10^{-4} cm/s bar as compared to 1.4 x 10^{-4} cm/s.bar in the case of polysulfone membranes. This may be attributed to better compatibility of the cellulose acetate-silica leading to formation of tight membrane matrix.

6.3 Effect of residence time (t_R) on silver capture

High permeate flux at low pressure drop is one of the advantages of membrane applications over conventional packed bed columns. High permeate flux (obtained by applying high transmembrane pressure) leads to lower residence time of the liquid inside membrane, allowing less time for Ag^+ –SH interaction to occur. At the same time high flow rates may increase the throughput of the membrane system. If the Ag^+ –SH interaction is fast (Mass transfer controlled system), higher flow rates should lead to higher rate of silver capture. Experiments were performed at various applied transmembrane pressures (ΔP = 1 to 10 bar) and silver capture was studied. The results are shown in Figure 6.4.

The residence times were calculated by dividing the water uptake of the membrane ($W_1 - W_2$) by experimental flow rates observed during the silver capture. The dotted line represents maximum silver capture capacity of the functionalized silica (2.1 mmole of Ag^+/g of silica). The solid straight line indicates the ideal case where all the silver permeated through the membrane is captured. In the initial part of the experiment all the silver was captured in all the cases indicated by the data points lying on top of the solid line. As the amount of silver permeated increased further, deviations from the ideal case were observed. In the case of lower residence times t_R = 6.5 s and t_R = 2.8 s), a plateau behavior is observed at approximately 80% capture capacity.

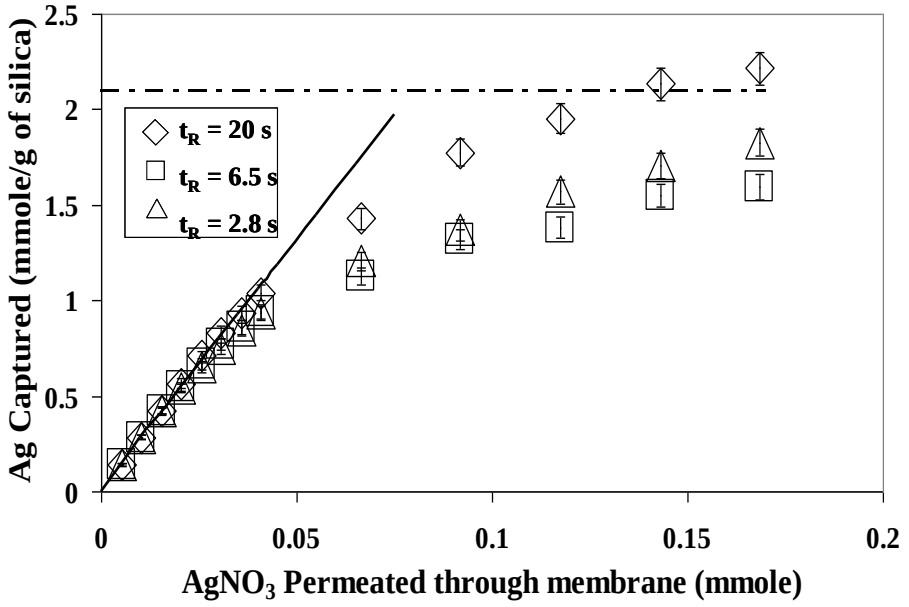

Figure 6.4 a

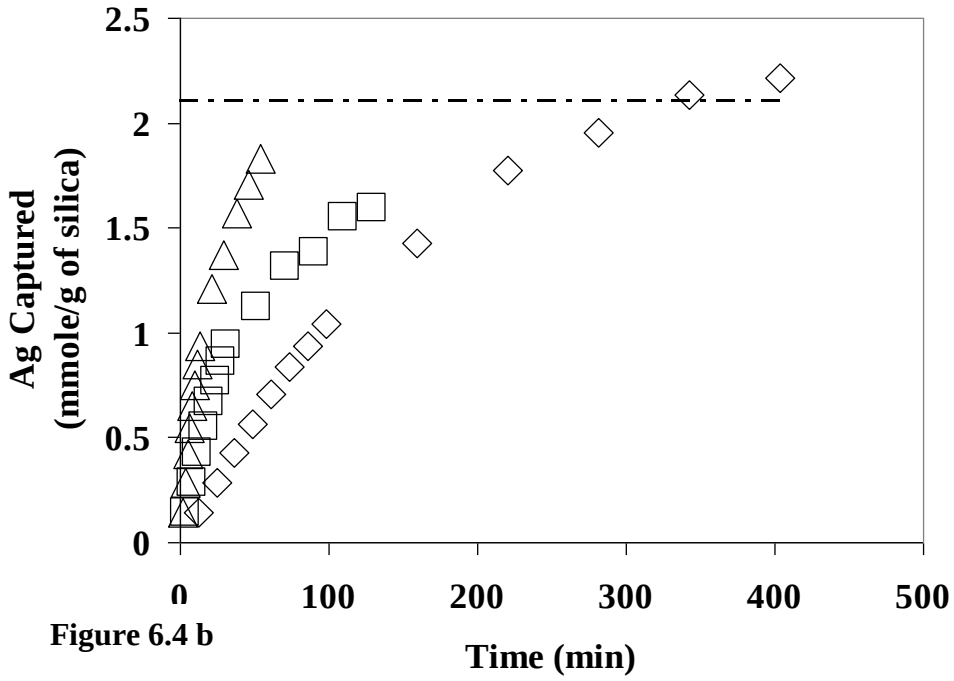

Figure 6.4 b

Figure 6.4 (a) Effect of residence time (t_R) on silver capture capacity for 40% MPTMS functionalized 874-85-1 silica - polysulfone mixed-matrix membrane (Feed concentrations ~ 100 mg/L of Ag). The error bars indicate analytical error of measurement for Ag^+ concentration. Solid line represents ideal case of silver capture. (b) Silver capture data reported as a function of time. Dotted line indicates maximum silver capture capacity

Figure 6.4 (b) represents the same data plotted in the form of amount of silver captured with respect to time. It is clearly observed that the rate of silver capture increases with increasing permeate flux within the experimental conditions studied. This indicates that under the experimental flow conditions, the Ag^{+}−SH interaction is mass transport limited.

If the sites are getting exhausted faster, then after a point a higher amount of silver ions (in the form of $AgNO_3$) will start coming out on the permeate side. This will lead to increased deviations from the ideal case. As expected, the deviations are highest for lowest residence time as observed in Figure 6.4. The maximum silver capture observed for t_R = 20 s even exceeded the maximum silver capture capacity of the silica. It is possible that while determining maximum capacity, some of the silica particles agglomerate in the process and a fraction of –SH sites become inaccessible. In the case of MMM there may be reduced agglomeration as the particles are trapped inside membrane polymer matrix resulting in better accessibility.

6.3.1 Dynamic capacity

In order to compare the relative performance of the membranes towards removal of silver ion applications, dynamic capacity was calculated in each case. The dynamic capacity was defined as amount of silver captured which was calculated by numerical integration over the filtration run until the point where the permeate concentration was approximately 10% of feed concentration. The capacity was normalized by dividing with maximum silver capture capacity (2.1 mmole/g) and results are shown in Figure 6.5. It can be observed that dynamic binding capacity initially decreases with increasing membrane flux from 70% to 45%, but remains almost constant thereafter. Figure 6.5 implies that the dynamic capacity is constant for J_W higher than 3 x 10^{-5} m/s. The constant binding capacity in the high flux regime indicates there is sufficient time for Ag^{+} –SH interaction and the process is mass transfer controlled.

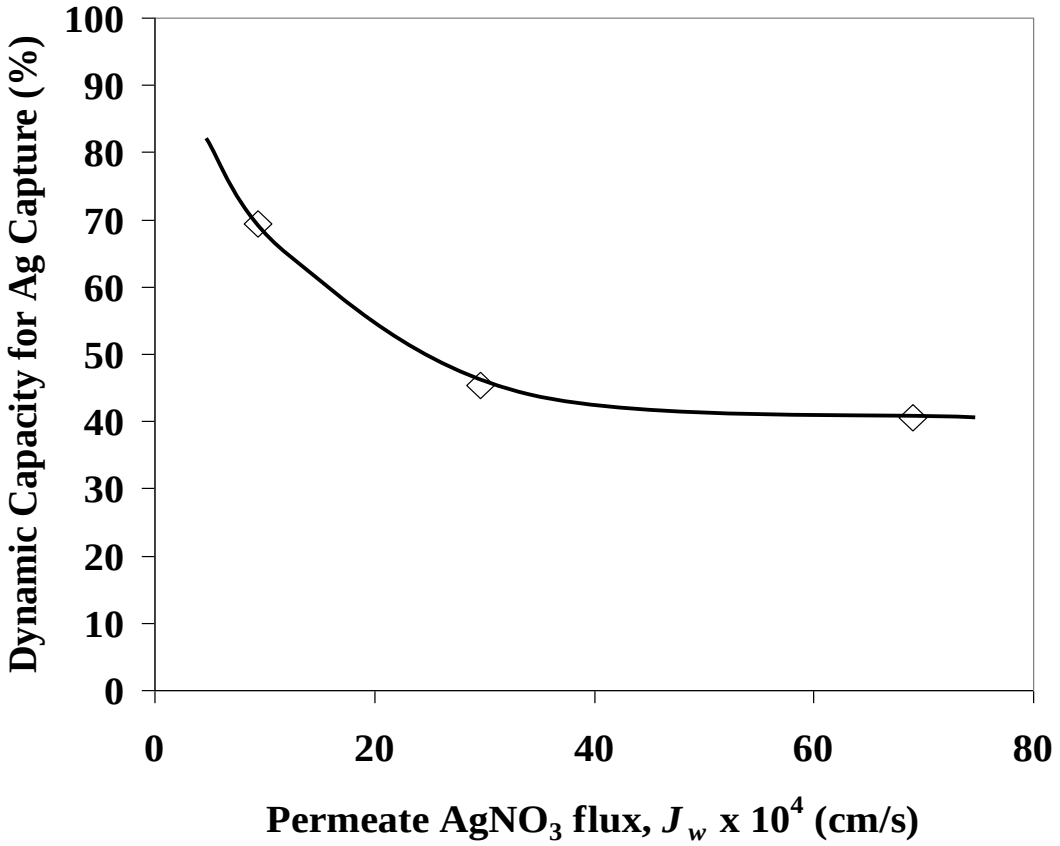

Figure 6.5 Dynamic silver capture capacity at varying $AgNO_3$ permeate flux with 40% 874-85-1 MPTMS functionalized silica polysulfone MMM (Feed concentrations ~ 100 mg/L). Solid line shows the trend in the data

6.4 Selectivity of Ag^{+}/Ca^{2+} capture

In order to verify the selectivity of the MMMs towards Ag^{+} ion, silver capture was studied from a feed containing equimolar concentration of Ag^{+} and Ca^{2+} (Metal nitrates used to prepare the solution). The results are shown in Figure 6.6. It can be clearly observed that the membrane selectively captured Ag^{+} from the metal ion mixture. The Ca^{2+} capture was negligible. Owing to the nature of the silver-thiol interaction it is expected that even in very high concentration of other metal ions like Na^{+} and Ca^{2+}, the selectivity towards silver will be high. This characteristic is important for selective capture of heavy metal ions from a metal ion mixture which usually is the case in many practical applications. Ritchie et al. (2001) have studied selectivity of thiol functional membrane systems towards target metal in very high excess of other metal ions and found that approximately 70% of the target metal is captured in the single pass.

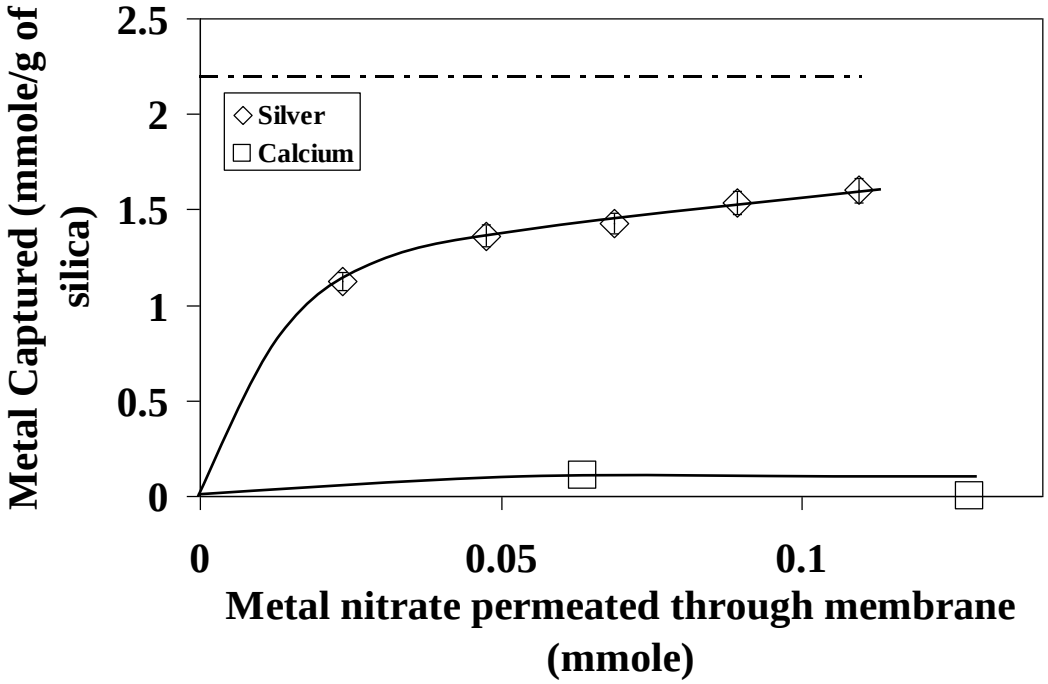

Figure 6.6 Selectivity towards metal ion capture between Ag^{+} and Ca^{2+} (Feed containing 0.89 mM concentration of each metal ion) with 30% 874-85-1 MPTMS functionalized silica-polysulfone membrane. The dotted line indicates maximum Ag^{+} capture by functionalized silica particles from Ag^{+} solution. Error bars indicate analytical error of measurement for Ag^{+} concentration. Solid lines show trends in the data

6.5 Silver capture at thiolated surface using QCM

In order to understand the Ag^+ −SH interaction, quartz crystal microbalance was used to study silver capture at model thiolated surface. This can also be used to establish sorption kinetics as the extent of sorption can be measured precisely. Figure 6.7 shows the adsorption data for the QCM experiment. The arrows indicate the time at which the feed solution is changed from water to silver solution or vice a versa. The adsorbed mass increased until 300 x 10^{-4} mmole/m^2 and reached equilibrium. The discontinuity in the increasing adsorbed mass at 230 x 10^{-4} mmole/m^2 represents water passage to check if the adsorbing mass is non-specifically adsorbed. At 300 x 10^{-4} mmole/m^2, passing of water caused some desorption and the adsorbed mass steadied at 250 x 10^{-4} mmole/m^2. On further passage of Ag^+ solution, adsorbed mass increased to 320 x 10^{-4} mmole/m^2 and stayed at that value even after repeated passing of water and Ag^+ solution alternatively. A similar experiment with non-functionalized silica crystal showed some adsorption on passage of Ag^+ solution which desorbed significantly on passage of water indicating no specific Ag^+ adsorption.

In order to convert the adsorbed mass in moles of Ag^+ adsorbed, it was assumed that the hydrogen ion of –SH group was exchanged with the Ag^+. This means that 1 mole of Ag^+ adsorption causes 106 g increase in the adsorbed mass. The calculated equilibrium adsorbed value of 320 x 10^{-4} mmole of silver/m^2 corresponds to 19 x 10^{18} thiol groups per square meter. For fully dense monolayer coverage of MPTMS on silica, Feng et al. (1997) have reported a value of 5 x 10^{18} molecules per square meter. The higher surface density of thiol groups may be attributed to adsorbed mass overestimation by QCM (Caruso et al. 1995; Rinia et al. 1996; Stalgren et al. 2002) due to coupled water of hydration with Ag^+.

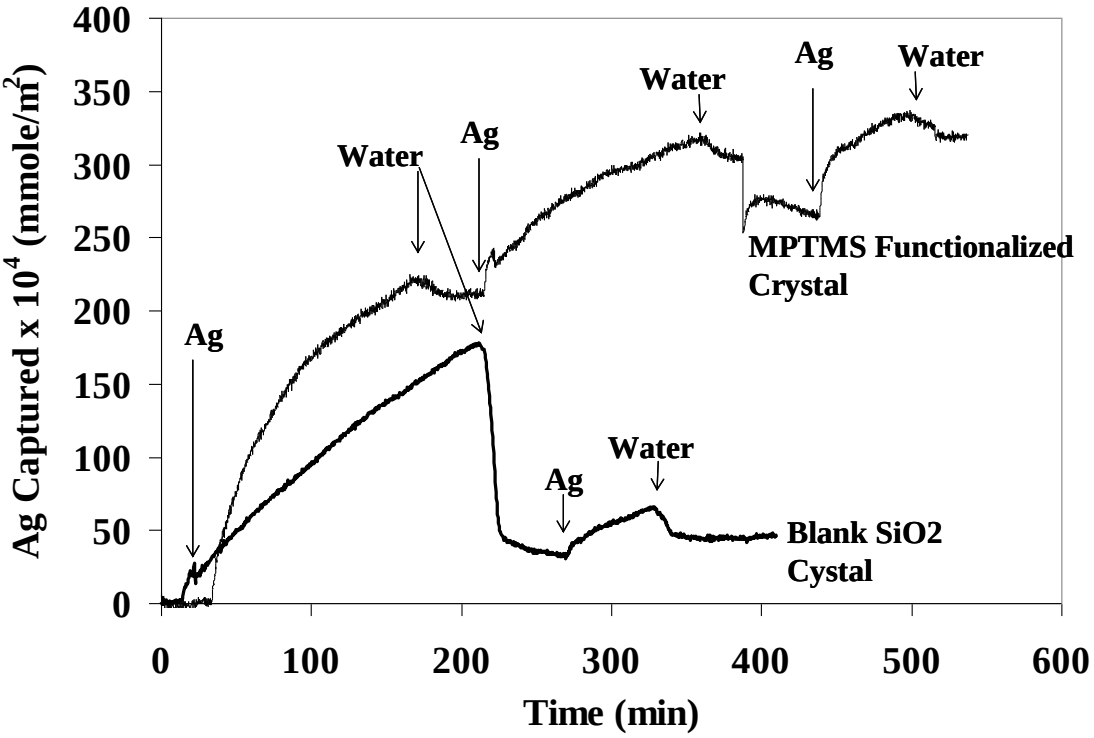

Figure 6.7 Interaction of Ag^+ with surface –SH groups of MPTMS functionalized quartz crystal by Quartz crystal microbalance. The arrows indicate the time at which the feed solution is changed from water to silver solution or vice a versa

6.6 Membrane regeneration and reuse

Several studies have been reported in the literature dealing with regeneration of thiol based sorbents and recovery of silver/mercury metals. The most common technique used is sorbent treatment with highly acidic solution like 12 M HCl (Feng et al. 1997; Walcarius and Delacote 2005). These harsh conditions can affect the sorbents and significant decrease in sorption capacity is observed in some cases.

In this study, experiments were conducted to test the membranes for silver recovery. Even after passing pH 2 aqueous solutions through the membranes, no silver recovery was observed. Highly acidic solutions (pH < 2) were thought to be detrimental to the MMMs prepared in this study. Another experiment was performed with silica functionalized with thiol as well as sulfonic acid groups. For the solution phase experiment, 25% of the silver captured was removed from this silica surface by lowering the pH of the solution to 1.8. More experiments will be required to check the regeneration, reuse, and selectivity of such silica material towards silver capture in order to optimize the conditions.

Hudson et al. (1983) employed acidic potassium cyanide solution (2M HNO_3) and reported 100% regeneration and reuse of thiol based polymeric resin for silver capture. Another approach applied for regeneration and recovery is to use mildly acidic (0.1 N HCl) thiourea solution as an eluent (Atia et al. 2005; Walcarius and Delacote 2005). Thiourea acts as a complexing legend in the eluent. 80-90% metal recovery with retained sorption capacity was obtained.

In our case, it seems that acidic thiourea treatment may be useful for regeneration. Strongly acidic conditions can damage the functionalized silica and result into loss of sorption capacity. However, due to the high market value of silver, scarifying the sorbent for silver recovery may still be economically viable.

The silver capture process using thiol-functionalized silica-polysulfone membrane was modeled to predict silver breakthrough curve. The model development, values of fitted parameters and comparison of experimental and predicted data are presented in the next chapter.

6.7 Summary of findings

In this chapter it was demonstrated that thiol-functionalized silica-polymer MMM can be successfully applied for aqueous phase silver ion capture. Significantly less silver capture by bare polysulfone membrane and nonfunctionalized-silica polysulfone membrane proved the hypothesis that the silver capture is specifically due to thiol-Ag^{+} interaction.

Three different types of silica materials were compared for silver capture and it was observed that Ludox TM 50 showed highest silver capture per unit surface area among the three materials. However in terms per unit mass of material, 874-85-1 type of silica showed highest silver capture capacity.

The MMMs were studied for silver capture at varying membrane permeance (i.e. varying residence times). The highest extent of silver capture was observed for highest residence time. It was also established that the rate of silver capture increased with increasing membrane permeance which clearly establishes that the silver capture process is mass transferred controlled under the experimental conditions studied. The calculated dynamic capacity initially decreased with increasing membrane permeance but the trend indicated that the capacity may be independent for higher membrane permeances.

It was established that the MMMs are capable of selective capture of silver ion from mixture of metal ions. The thiol-silver ion interaction was studied on thiol-functionalized gold surface using QCM.

The membrane can not be regenerated by permeating pH 2 water. Use of mildly acidic thiourea solution can be employed for regeneration. The successful regeneration will make the process economically more attractive.

Copyright © Abhay R Ladhe 2008

Chapter 7 Modeling of mixed-matrix membranes

The MMMs were modeled to predict concentration profile of metal ion along the membrane thickness at varying time. Due to the spongy morphology of the silica MMM, a membrane pore based model was deemed unsuitable in this case. The membrane pore based model incorporates core flow. In the case of adsorptive separation process like this, core flow leads to immediate appearance of the adsorbate on the permeate side. The observation of the experimental break-through curves clearly indicate that the capture efficiency is almost 100% for a substantial time in all the cases demonstrating absence of core flow. It was thought suitable to model this MMM process as a one-dimensional unsteady state problem. The MMM can be described in terms of three different phases i.e. active silica adsorbent phase, inert polymer phase and aqueous silver solution phase occupying the free volume fraction of the membrane. Figure 7.1 shows schematics of a MMM as a combination of the three phases. For the modeling purpose, the silica particles are assumed to be impermeable and non-porous. It should be noted that, throughout the model calculations, SI units were used for all the quantities but in the figures the quantities were converted to suitable units in order to aid comparison and discussion of the experimental and predicted results.

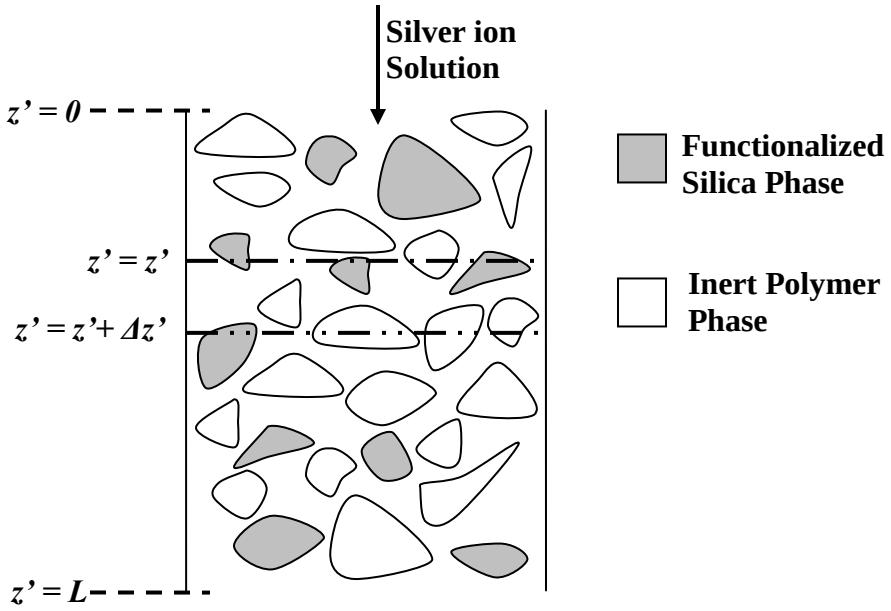

Figure 7.1 Schematic representation of mixed-matrix membrane (MMM) for modeling purpose

Following terminology was used for modeling purpose:

ϕ = Free volume fraction;

ϕ_p = Polymer volume fraction;

$(1-\phi-\phi_p)$ = Fractional volume of silica particles;

C' = Concentration of Ag^+ in bulk liquid phase (moles of Ag^+/m^3 of Liquid);

q' = Concentration of silver in silica phase (moles of Ag^+/m^3 of silica Particles);

q_{eq} = maximum concentration of silver in silica phase for C' (moles of Ag^+/m^3 of silica Particles);

J_W = Membrane Flux (m/s);

t' = time (s);

z' = Distance down the membrane thickness (m).

Taking a mass balance on the liquid phase over an element shown in Figure 7.1 we get,

$$\phi \frac{\partial C'}{\partial t'} + J_W \frac{\partial C'}{\partial z'} + (1-\phi-\phi_p)\frac{\partial q'}{\partial t'} = 0 \qquad (7.1)$$

The detailed derivation of this equation is given in Appendix C.

Similarly, taking a mass balance on the solid silica phase we get,

$$\frac{\partial q'}{\partial t'} = k(q_{eq} - q') \qquad (7.2)$$

With initial conditions as follows:

$C'(0,t') = C_0$

$q'(z,0) = 0$

$C'(z',0) = 0$

In this case, the axial diffusion is neglected as compared to axial convection.

In order to couple equations (7.1) and (7.2), following linear relationship between q_{eq} and C' was assumed.

$$q_{eq} = \gamma\, C' \qquad (7.3)$$

Where

γ = Silver – thiol affinity constant.

In this case γ will be a function of surface density of thiol groups. Substituting from equation (7.3) into equation (7.2) we get,

$$\frac{\partial q'}{\partial t'} = k(\gamma\ C' - q') \tag{7.4}$$

Similar approach has been used earlier for packed bed adsorption and the equations were solved by COMSOL (Finlayson 2005). In our case, the model was applied for metal ion sorption using mixed-matrix membranes and the breakthrough curve data was predicted for a varying membrane flux.

The equations can be made dimensionless by defining the following variables

$$C = \frac{C'}{C_0}$$

$$q = \frac{q'}{q_\infty}$$

$$z = \frac{z'}{L}$$

$$t = \frac{t'}{T_S}$$

Where,

C_0 = Inlet feed concentration of silver ion (mole/m^3);

q_∞ = maximum silver capture (moles of Ag/m^3 of silica);

L = Membrane thickness (m).

T_S = Time at which saturation of silver capture was observed and experiment was terminated (s). The saturation time varied between 60 min to 400 min for various cases studied.

The dimensionless system of PDEs is

$$\frac{\phi\ L}{J_W T_S}\frac{\partial C}{\partial t} + \frac{\partial C}{\partial z} + (1 - \phi - \phi_p)\frac{kL}{J_W}(\gamma\ C - q\frac{q_\infty}{C_0}) = 0 \tag{7.5}$$

$$\frac{\partial q}{\partial t} = \frac{kT_S C_0}{q_\infty}(\gamma\ C - q\frac{q_\infty}{C_0}) \tag{7.6}$$

With corresponding initial conditions

$C(0,t) = 1$

$q(z,0) = 0$

$C(z,0) = 0$

Femlab^{TM} (COMSOL, version 3.0a) was used to solve the set of two unsteady state partial differential equations (7.5 and 7.6). Multiphysics convection-diffusion transient state analysis was applied to the one-dimensional domain. The thickness of the membrane was partitioned into 120 elements (241 nodes). In order to get a stable solution it was required to add artificial diffusion term in the case of equation (7.5). In the absence of artificial diffusion term an unstable oscillating numerical solution is obtained. In the later part, it will also be demonstrated that addition of this term does not affect the solution of the system. The option of compensated Petrov-Galerkin method was selected in this particular case. The details required for feeding the model equations to COMSOL software and the settings used for solving the equations are explained in Appendix C. Incorporation of the artificial diffusion term and the effect of selected values of diffusivity and number of elements used for calculation on predicted data is also discussed in Appendix C.

The required values of the model parameters are obtained from the experimental conditions and are as follows:

C_0 = Feed Ag^+ concentration = 1.03 mole/m^3 (112 mg/L)

L = 150 x 10^{-6} m (Membrane thickness measured experimentally)

ϕ = 0.63 (Obtained from membrane water uptake experiment)

Volume fraction of polymer in MMM can be calculated by following expression

$$\phi_p = \frac{\rho_{Si}(1-\phi)(1-\psi)}{\rho_{Si}(1-\psi)+\psi\rho_p} \qquad (7.7)$$

Where, ρ_{Si} is density of silica (2.2 g/cm^3) and ρ_p is density of polysulfone (1.24 g/cm^3)

For a 40% Silica-Polysulfone MMM (ψ = 0.4), using equation (7.7), ϕ_p = 0.27

From silver capture experiment with functionalized silica particles only, maximum extent of silver capture was 2.1 x 10^{-3} mole/g of silica (4.62 x 10^3 mole of Ag/m^3 of silica), for a feed concentration of 100 mg/L (0.92 mole/m^3).

Using this data calculated value for γ = 5021

By applying varying transmembrane pressure, the residence time (t_R) was varied. The corresponding membrane flux (J_W , m/s) in the three cases studied are 9.4 x 10^{-6} (t_R = 20 s), 3 x 10^{-5} (t_R = 6.5 s), and 6.93 x 10^{-5} (t_R = 2.8 s).

In order to apply artificial diffusion to get a stable numerical solution, a value for silver diffusivity in the aqueous phase was required. Based on the reported data (Cussler 1996), a calculated $AgNO_3$ diffusivity value of 1.80 x 10^{-9} m^2/s was used for all the calculations. The only unknown parameter remaining was the volumetric mass transfer coefficient (k). In the case of J_W = 6.93 x 10^{-5} m/s, k was used as an adjustable parameter to match the predicted data with experimental data. The comparison of the experimental and predicted breakthrough curves is shown in Figure 7.2

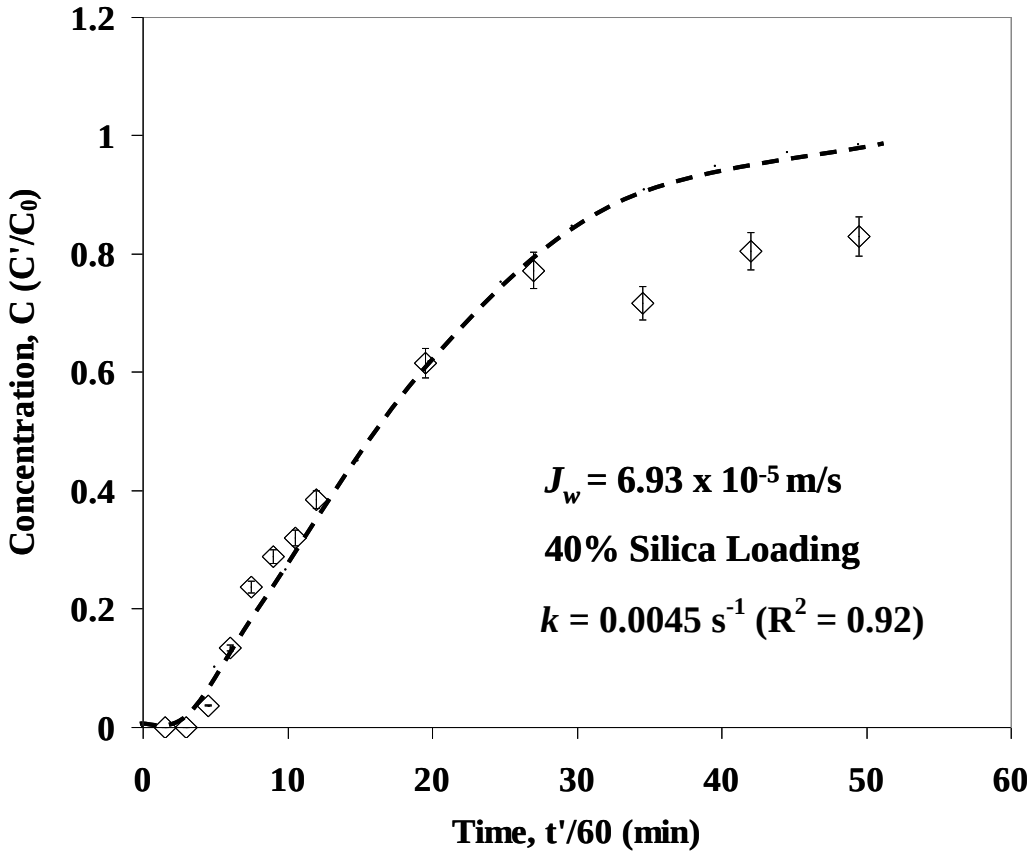

Figure 7.2 Comparison of experimental and predicted data for 874-85-1 MPTMS functionalized silica-polysulfone MMM silver breakthrough curve. Error bars indicate analytical error of measurement for Ag^+ concentration. Dotted line represents predicted data. The overall volumetric mass transfer coefficient (*k*) was used as a fitting parameter

The predicted data matches very well with the experimental data until C = 0.80. Deviations are higher beyond this point. The fitted value of the mass transfer coefficient is 0.0045 s^{-1}. The value of mass transfer coefficient for packed colums (Gas-Liquid) is generally in the range of 0.005-0.02 s^{-1} (Perry and Green 1997). In order to quantify model quality, R^2 value based on Predicted Error Sum of Squares (PRESS statistics) was calculated using following expression:

$$R^2 = 1 - \frac{\sum_{i=1}^{n}[y_i - \hat{y}_i]^2}{\sum_{i=1}^{n} y_i^2 - n\bar{y}_i^2} \qquad (7.8)$$

Where, y_i is experimental value, $\hat{y}_i$ is predicted value, $\bar{y}_i$ is mean of experimental values and *n* is number of data points used for calculation.

In this case the R^2 value for the fit is 0.92 indicating a good fit. The sensitivity of the model towards diffusivity is determined by varying it from 1 x 10^{-10} to 1 x 10^{-8} m^2/s and it was observed that the predicted outlet concentration changes by less than 1% over this range. This also indicates that the artificial diffusion term does not have any significant effect on the solution of the system. This also supports the assumption that diffusion is negligible as compared to convection in this case. The model sensitivity was also determined for 10% error in γ value (5021). Using γ = 4519 (case I) and γ = 5524 (case II), the corresponding values of mass transfer coefficients were obtained so as to fit the predicted data to the experimental data. The adjusted values are *k* = 0.0055 s^{-1} (R^2 = 0.89) and *k* = 0.0038 s^{-1} (R^2 = 0.93) for case I and case II, respectively.

7.1 Mass transfer correlation and predicting experimental breakthrough data without any adjustable parameter

It is expected that the value of *k* will vary with the permeation rate. In order to predict the breakthrough curve data for varying membrane fluxes without any adjustable parameter, a correlation between mass transfer coefficient and membrane flux was required. Based on various mass transfer correlations reported in literature, it was thought that $k \alpha J_W^{0.5}$ is a reasonable assumption. Using the value of *k* = 0.0045 s^{-1} for

corresponding J_W = 6.93 x 10^{-5} m/s, the value of the proportionality constant is estimated to be 0.541. This leads to following mass transfer correlation:

$$k = 0.541\ J_W^{0.5} \qquad (7.9)$$

Equation (7.9) was used to calculate the volumetric mass transfer coefficients for varying membrane fluxes. These values of *k* were used to predict the breakthrough curve data and the comparisons of the predicted data with the experimental data are shown in Figure 7.3 and 7.4 Figure 7.4 shows the comparison in the case of silver capture with 30% silica loading-MMM at J_W = 8.5 x 10^{-6} m/s (R^2 = 0.91). In all the cases the onset of breakthrough is predicted accurately but deviations are observed when the capture process approaches saturation. The deviations are highest in the case of J_W = 9.4 x 10^{-6} m/s (R^2 = 0.75). Considering the fact that no adjustable parameter was used, the model predictions are comparable with experimental observations. As discussed earlier, the assumption of negligible diffusion compared to convection has been verified for J_W = 6.93 x 10^{-5} m/s. It is expected that the role of diffusivity will be of greater importance for the lowest membrane flux and hence model sensitivity towards diffusivity was also determined for J_W = 9.4 x 10^{-6} m/s. It was observed that, by varying diffusivity values between 1 x 10^{-10} to 1 x 10^{-8} m^2/s, the predicted outlet concentration changes by less than 1%.

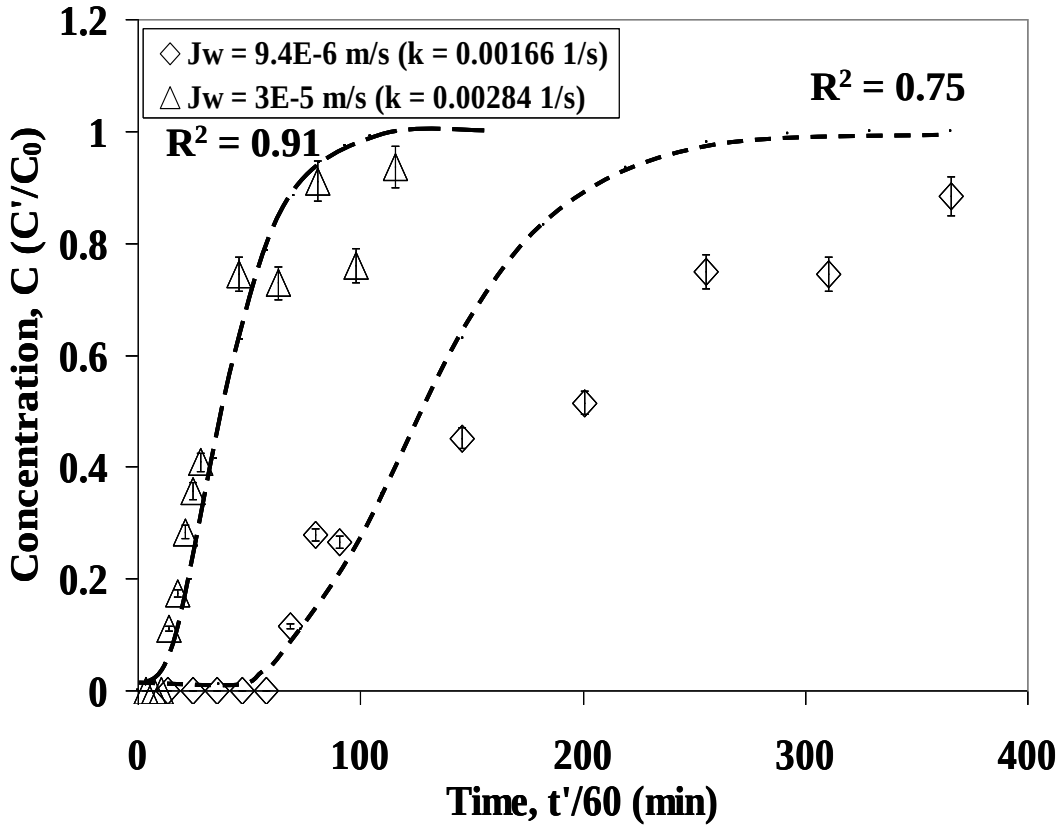

Figure 7.3 Comparison of experimental and predicted data for silver breakthrough curves using thiol-functionalized 874-85-1 silica-polysulfone MMM with 40% silica loading. The volumetric mass transfer coefficient (*k*) was obtained from correlation 7.9 Error bars indicate analytical error of measurement for Ag^{+} concentration. Dotted lines show predicted data

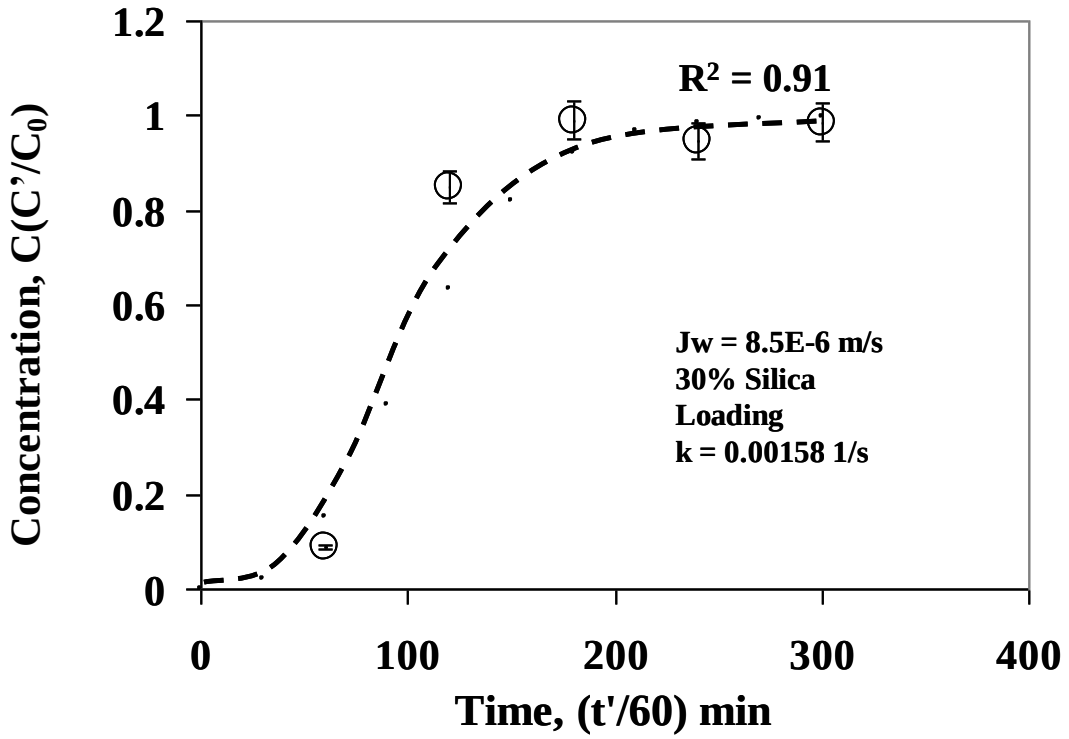

Figure 7.4 Data comparison for silver capture with 30% silica loading MMM. The volumetric mass transfer coefficient (*k*) was obtained from equation 7.9 Error bars indicate analytical error of measurement for Ag^+ concentration. Dotted line shows predicted data

In order to check the model applicability over a wide range of parameters, the model was used to predict results for silver capture experiment using a stack of two membranes. Multi stack membranes are often used to increase capacity of existing membrane processes. MPTMS functionalized 874-85-1 40% Silica-polysulfone MMM membranes were stacked together and silver solution was permeated through the stack. The silica used was deliberately functionalized under the conditions where MPTMS was the limiting reactant so as to get reduced silver capture capacity per gram of silica, thus changing one more operating condition. The corresponding parameters obtained from experimental characterization of silica and MMM are as follows: Membrane thickness = 1.1×10^{-4} m for one membrane i.e. L = 2.2×10^{-4} m for the stack; ϕ = 0.52; ϕ_p = 0.35; γ = 1880 (as compared to 5021 in previous cases). Concentration of feed solution C_0 = 0.874 mole/m^3. Using these parameters, predicted breakthrough curve was obtained (dotted line) and its comparison with experimental results is shown in Figure 7.5. The R^2 value based on PRESS statistics for this fit is 0.85. It can be observed that the model consistently overestimated exit silver ion concentration throughout this run but follows the overall trend in the data. The deviations are partially attributed to the inaccurate value of mass transfer coefficient obtained from the correlation based on single stack data.

The reasonable agreement between experimental and predicted data in above demonstrated cases proves that the model is helpful to predict experimental results over a wide range of operating conditions and parameters like silica loading, membrane flux, silver capture capacity of silica, and membrane thickness.

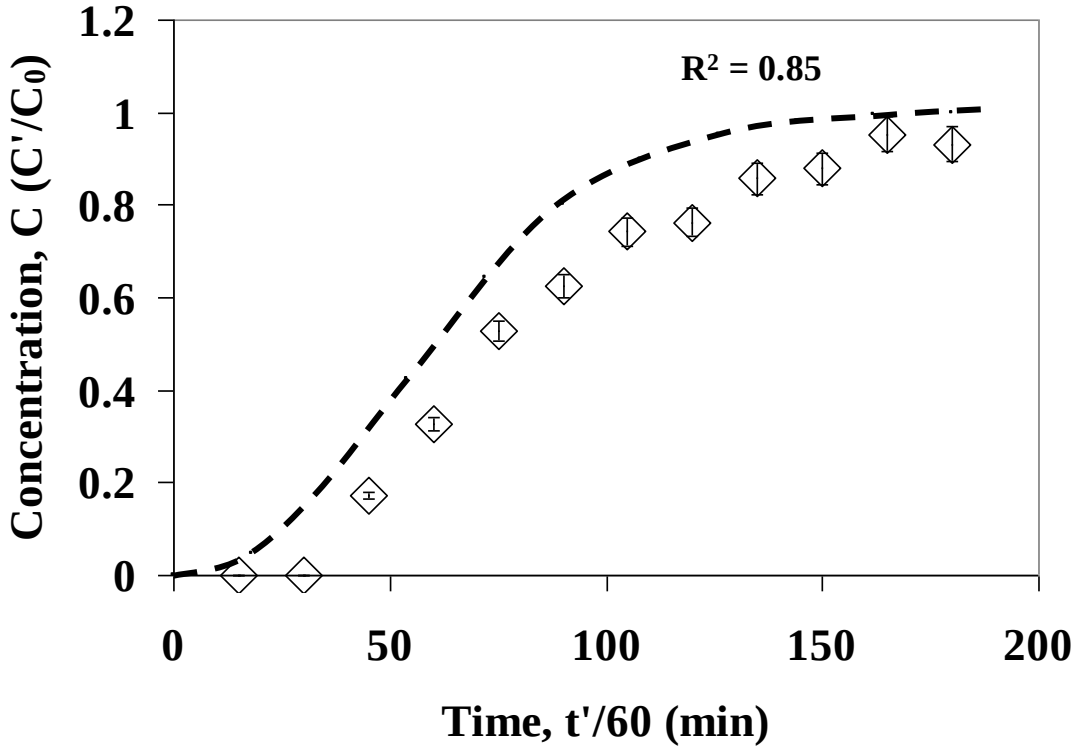

Figure 7.5 Comparison of experimental and predicted data (dotted line) for silver breakthrough curve using 40% 874-85-1 MPTMS functionalized silica-polysulfone MMMs in the case of double stack membrane experiment. The k value of 0.002 1/s is obtained using equation 7.9. The silica was functionalized under conditions where MPTMS was limiting reactant so as to deliberately achieve lower silver capture capacity (γ = 1880 as compared to 5021 in previous single stack cases) Error bars indicate analytical error of measurement for Ag^+ concentration

7.2 Effect of variation in model parameter values (*k* and γ) on model output

In the case of Figure 7.5 it was observed that the model consistently overestimated the exit concentration of the silver ions when the predicted breakthrough data was compared with the experimental data. Considering the fact that no adjustable parameter was used, the agreement is reasonable (R^2 = 0.85). In order to get an idea of effect of model parameters on model output, the predicted data was obtained for varying values of k and γ, keeping all other input variables constant. The new values of k and γ were selected in such a way that the predicted data should match more closely with the experimental data. The comparison of the experimental and predicted data for the two cases is shown in Figure 7.6 and 7.7.

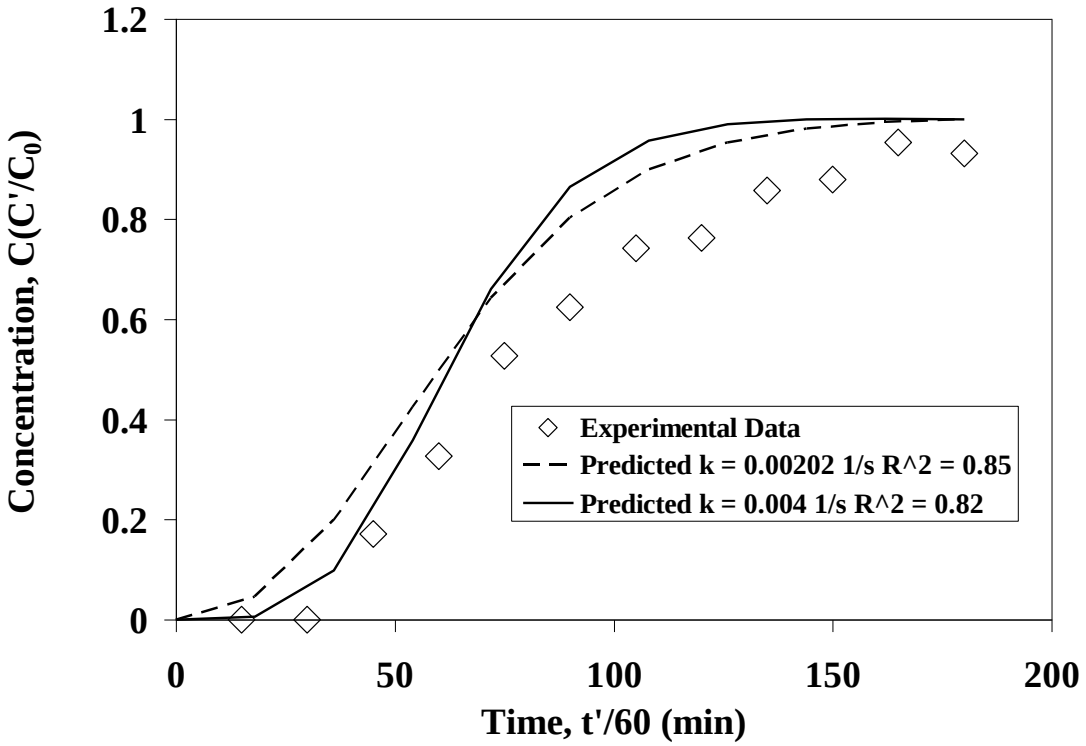

Figure 7.6 Effect of variation in mass transfer coefficient on predicted breakthrough curve for silver capture with thiol-functionalized silica polysulfone mixed-matrix membranes (γ = 1880).

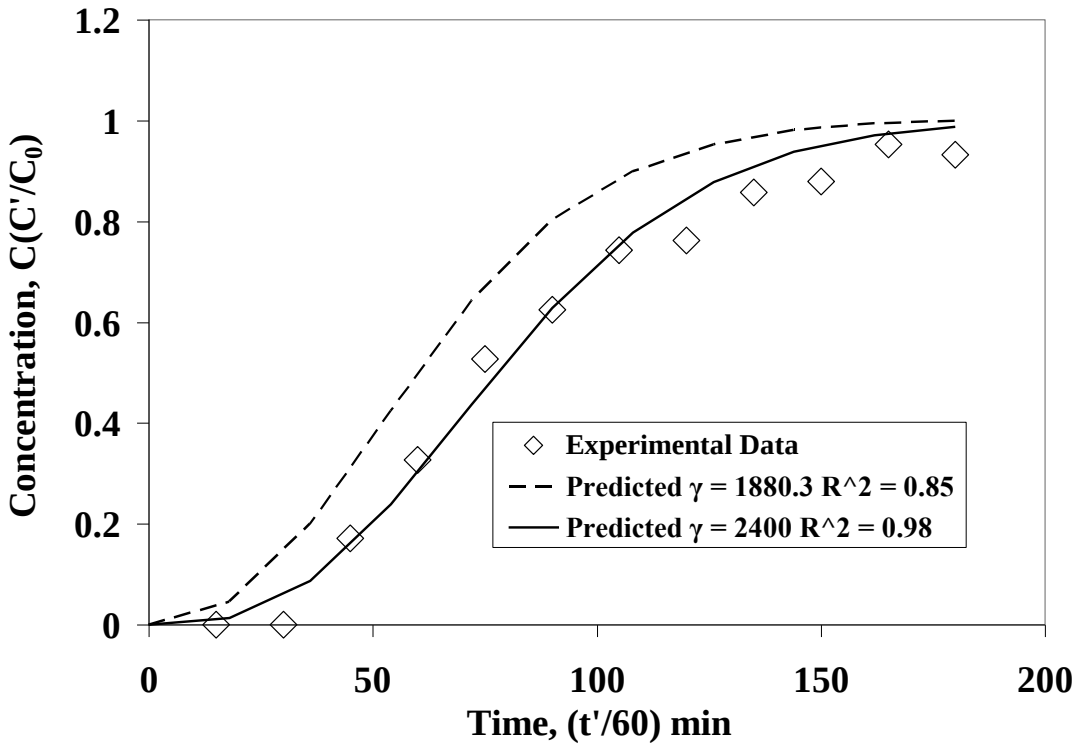

Figure 7.7 Effect of variation in silver-thiol affinity constant (γ) on predicted breakthrough curve for silver capture with thiol-functionalized silica polysulfone mixed-matrix membranes (k = 0.002 s^{-1}).

It can be observed from Figure 7.6 that increasing the mass transfer coefficient (*k*) value from 0.002 s^{-1} (obtained using equation 7.9) to 0.004 s^{-1}, lead to a better prediction of the experimental data in the region of onset of breakthrough. On the other hand, towards the saturation region, this lead to increased deviations from the experimental data. The overall effect was that the R^2 value based on PRESS statistics decreased from 0.85 to 0.82. In general, increasing the mass transfer coefficient (*k*) delays the onset of breakthrough and increases the slope of the linear part of the curve leading to early saturation.

It was also observed (Figure 7.7) that increasing the γ value from 1880 (calculated based on experimental data) to 2400 lead to extremely better match between the experimental and predicted data. The R^2 value based on PRESS statistics increased from 0.85 to 0.98. In general, the increase in γ value shifts the breakthrough curve towards right (delayed onset of breakthrough) with slight decrease in the slope of the linear part of the curve.

7.3 Prediction of silver concentration in silica phase

The model also provides information about concentration of silver in silica phase throughout the membrane as a function of time. Figure 7.8 displays the predicted silver concentration (mmole of Ag captured/g of silica) profile along the membrane thickness at varying experimental time for J_W = 6.93 x 10^{-5} m/s. As expected, the silver concentration is highest near feed side and gradually decreases along the membrane thickness. It can be also observed that the membrane is almost fully saturated with Ag in 60 minutes.

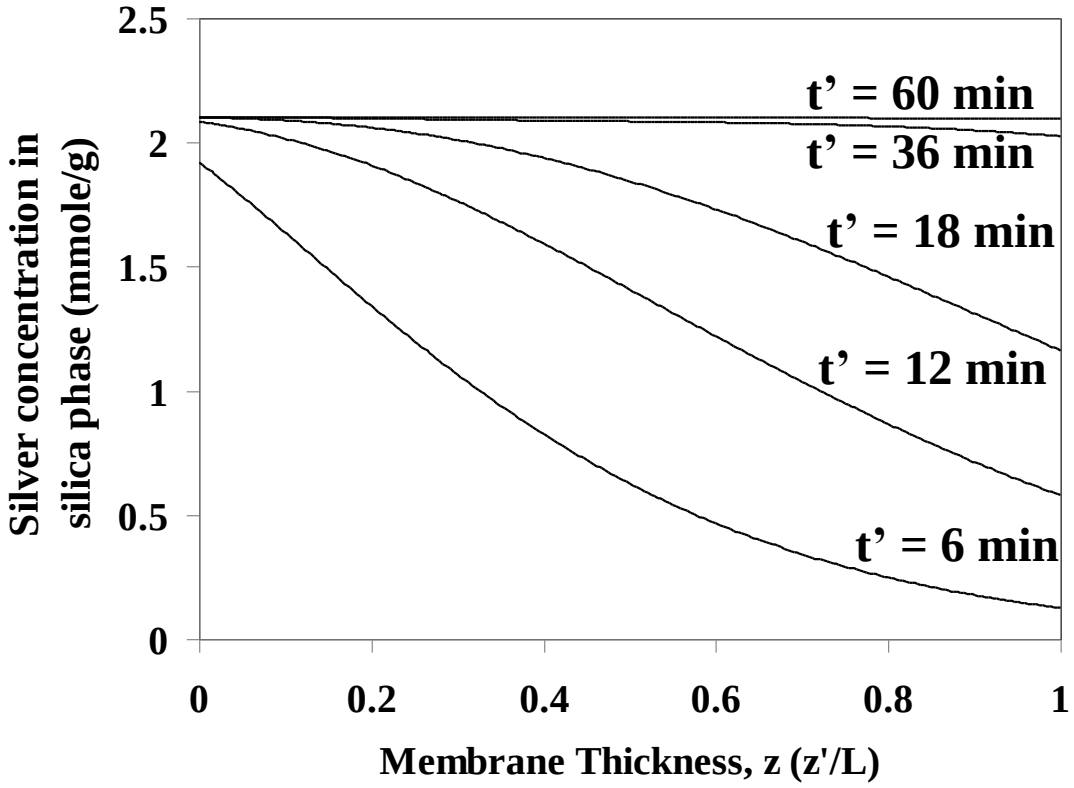

Figure 7.8 Predicted concentration of silver in silica phase along the membrane thickness at varying times. Feed is 100 mg/L aqueous silver ion solution at transmembrane pressure of 8.2 bar (Residence time, t_R = 2.8 s)

7.4 Silver concentration profile along the membrane thickness

It is also possible to predict concentration profile of silver ion at desired positions along the membrane thickness using the model. It is expected that the near the position from the membrane feed side, the earlier it will saturate. This indeed was observed as shown in Figure 7.9. The results represents silver capture using 40% silica loading silica-polysulfone membrane (ϕ = 0.63; ϕ_p = 0.27 and J_W = 6.93 x 10^{-5} m/s). A predicted result for a two stack membrane (z = 1) is also shown for comparison with single stack membrane. The model offers an efficient way to study effect of various experimental parameters on silver or other metal separation. The model is applicable for a generic case involving MMM for liquid phase applications.

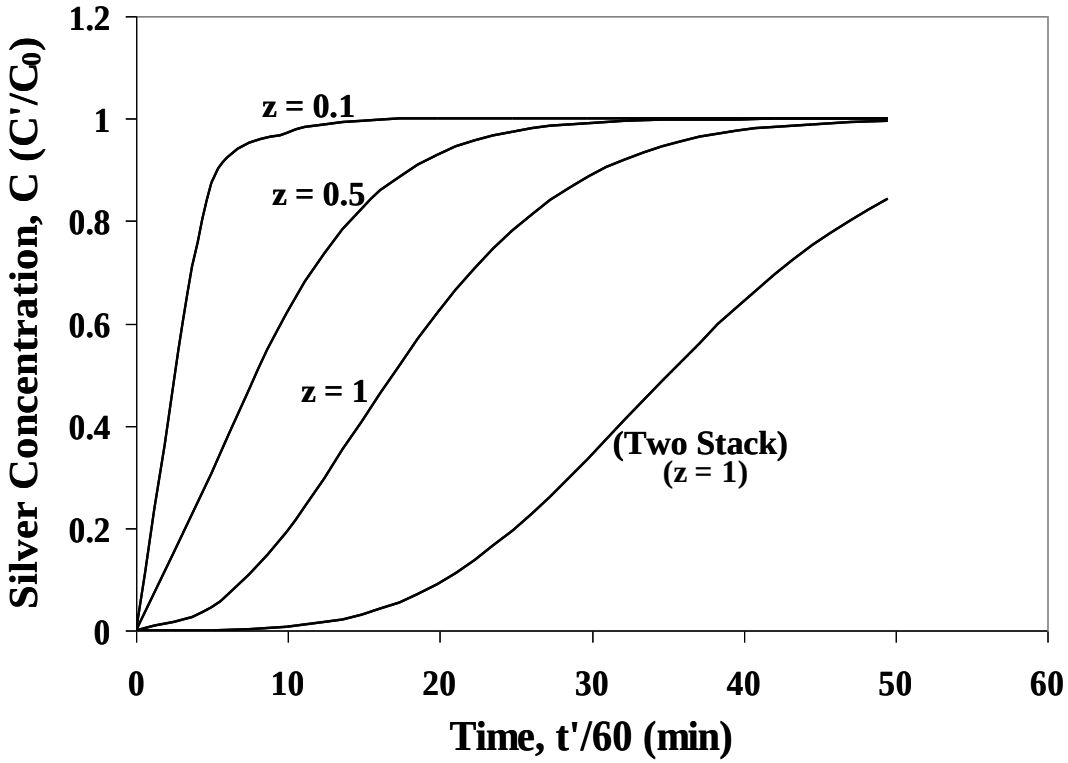

Figure 7.9 Predicted concentration profile of liquid phase silver concentration at varying membrane thickness. Two stack represents concentration profile for silver capture experiment using two membranes stacked together

7.5 Conclusive remarks

The silver capture process was successfully modeled using one-dimensional unsteady state approach. A mass transfer correlation was developed to predict dependence of the volumetric mass transfer coefficient on membrane flux. The model successfully predicted silver breakthrough curves for varying operating conditions like membrane flux, silica loading, membrane thickness, and silver capture capacity of the silica material. The applicability of the model for predicting silver concentration in the solid silica phase along the membrane thickness and at varying times is also demonstrated. The model provides an efficient way to study effect of various parameters of the silver capture process.

Copyright © Abhay R Ladhe 2008

Chapter 8 Conclusions

The research work discussed in this dissertation was directed to study application of functionalized membranes for sorption applications. For the first time, polyacrylic acid functionalized membranes were studied for ethoxylated surfactant sorptions in hydrophobic siloxane environment. Functionalized silica-polymer mixed-matrix membranes were developed and their applications for aqueous phase metal ion sorptions were demonstrated. The adsorption-desorption and partitioning behavior of ethoxylated non-ionic surfactants at various solid-liquid interfaces was also quantified. This chapter summarizes the important findings of this research work.

8.1 Overall scientific and technological advancements

The overall scientific and technological advancements achieved in this study are:

- For the first time, a functionalized membrane-based process was developed for reversible surfactant capture from hydrophobic siloxane-based solvent
- The role of ethylene oxide content in the sorption characteristics of the ethoxylated nonionic surfactants on various polymeric and model surfaces was quantified
- Development and successful application of functionalized silica-polymer mixed-matrix membranes for aqueous phase metal ion capture applications was demonstrated
- A generic model applicable for metal ion sorption applications of mixed-matrix membranes was developed and solved

8.2 Specific accomplishments

The specific accomplishments of this dissertation work are as follows:

8.2.1 Partitioning, adsorption and capture of ethoxylated nonionic surfactants

- The surfactants with higher ethylene oxide content favorably partition from hydrophobic siloxane phase into aqueous phase
- Surfactants with higher ethylene oxide content adsorb strongly on the hydrophilic cotton surface as compared to polyester surface in the hydrophobic siloxane solvent environment consistent with literature studies.
- The adsorbed surfactant amount at gold-water interface decreased with increasing ethylene oxide groups per surfactant molecule. In the case of gold-siloxane solvent interface, the adsorbed amount increased with increasing ethylene oxide content of the surfactants.
- Adsorption rate constants increased with increasing number of ethylene oxide groups per molecule. Desorption rate constants decreased with increasing ethylene oxide content of the surfactant molecule.
- Although the polyacrylic acid chains are partially cross-linked inside membrane matrix, they are capable of undergoing charge transition with changing pH of feed solution.
- In the case of surfactant capture from siloxane solvent using polyacrylic acid functionalized membranes, the amount of surfactant captured increased exponentially with increasing number of ethylene oxide groups in the surfactant molecule.
- Accessibility studies for polyacrylic acid functionalized membranes proved that more than 60% of the available carboxyl groups present in the membranes are inaccessible towards surfactant sorption
- Significant transport limitation inhibits surfactant from siloxane phase to interact with carboxyl groups in the hydrophilic polyacrylic acid domain
- The membrane can be regenerated by permeating slightly alkaline water (pH 8) through it and the membrane can be reused for surfactant capture.

8.2.2 Functionalized membranes for silver capture

- Functionalized silica materials for metal ion sorptions were successfully prepared
- Silica-polysulfone mixed-matrix membranes (MMMs) were successfully prepared with uniform distribution of the silica particles through the entire cross-section of the membrane
- Functionalized silica-polymer MMMs were successfully applied for aqueous phase metal ion capture
- The role of silica properties and membrane permeance on metal sorption behavior using mixed-matrix membranes was quantitatively established. It was observed that the silver capture process is mass transfer controlled under the experimental conditions studied
- The MMMs were successfully applied for selective capture of silver ion from solution containing mixture of silver and calcium metal ions
- The mixed-matrix membranes were successfully modeled using one-dimensional unsteady state approach. The model was verified using experimental metal ion sorption data

Copyright © Abhay R Ladhe 2008

Nomenclature

A_i Permeance of species *i*, cm^3/cm^2 s bar

A_m Area of membrane sheet, m^2

C Dimensionless concentration of silver

C' Concentration of Ag^+ in bulk liquid phase, moles of Ag^+/m^3 of liquid

C_0 Inlet feed concentration of silver ion, $mole/m^3$

C_m Mass sensitivity constant, ng cm^{-2} Hz^{-1}

D Dissipation factor

f Frequency of QCM crystal oscillation, Hz

H_{AP} Height of surfactant peak after partitioning, mm

H_{BP} Height of surfactant peak before partitioning, mm

J_i Permeate flux of species *i*, m^3/m^2 s

K_a Adsorption rate constant, s^{-1}

K_d Desorption rate constant, s^{-1}

K_p Partition coefficient

L Thickness of membrane, m

M Molecular weight of dextran, Da

N_p Number of pores in membrane sheet

q Dimensionless concentration of silver in silica phase

q' Concentration of silver in silica phase, moles of Ag^+/m^3 of silica particles

q_{eq} Maximum concentration of silver in silica phase for C', moles of Ag^+/m^3 of silica particles

q_∞ Maximum silver capture, moles of Ag/m^3 of silica

Q_{max} Saturation adsorption value, $mole/m^2$

Q_s Amount of surfactant adsorbed, $mole/m^2$

r_{eff} Effective pore radius, m

r_p Pore radius, m

r_s Hydraulic radius of the dextran molecule, nm

R Dextran rejection, %

R^2 Regression coefficient based on PRESS statistics

t Dimensionless time

t' Time, s

t_0 Clock time at which adsorption of surfactant starts, s

t_1 Clock time at which desorption of surfactant starts, s

t_R Residence time, s

T Temperature, K

T_S Time at which saturation of silver capture was observed and experiment was terminated, s

V^o Molar volumes of the organic phase, mole/m^3

V^w Molar volumes of water, mole/m^3

y_i Experimental value

$\hat{y}_i$ Predicted value

$\bar{y}_i$ Mean of experimental values

z Dimensionless distance down the membrane thickness

z' Distance down the membrane thickness, m

Greek Letters

γ Silver – thiol affinity constant

Γ_{max} Surface excess concentration, mole/m^2

δ_H Hydrogen bonding component of Hansen solubility parameter, (cal/cm^3)$^{1/2}$

ε_m Membrane porosity

μ Viscosity, Pa s

$\Delta\mu_i^0$ Standard chemical potential difference, J/mol

ρ_p Density of polysulfone, (kg/m^3)

ρ_{Si} Density of silica, (kg/m^3)

ρ_W Density of water, (kg/m^3)

ΔD	Change in dissipation factor
Δm	Mass of adsorbed layer, ng/cm^2
ΔP	Applied transmembrane pressure, bar
τ	Tortuosity of the membrane pore
τ_D	Decay time for QCM oscillations, s
ϕ	Free volume fraction
ϕ_p	Polymer volume fraction
ψ	Silica weight fraction in membrane

Material Abbreviations

15-S-5	A commercially available nonionic surfactant which is primarily a mixture of ethoxylated nonionic surfactant with variable alkyl chain length and variable number of ethylene oxide groups per molecule
C_nE_m	Ethoxylated nonionic surfactant with *n* carbon alkyl chain and *m* number of ethylene oxide groups
DIUF	Deionized ultra filtered water
DMF	Dimethylformamide
EO	Ethylene oxide
MMM	Mixed-matrix membrane
MPTMS	3-Mercaptoproptyltrimethoxysilane
PAA	Polyacrylic acid
PCTE	Polycarbonate track etched membrane
PLGA	Poly-L-glutamic acid
PMA	Polymethacrylic acid
PVDF	Polyvinylidene fluoride

Method and Technique Abbreviations

AA	Atomic absorption spectrometer
AFM	Atomic force microscope
ATR-FTIR	Attenuated total reflectance – Fourier transform infrared spectroscopy

BET	Brunauer Emmett Teller
CAC	Critical aggregation concentration
CMC	Critical micelle concentration
GC-FID	Gas chromatograpgy flame ionization detector
HPLC	High performance liquid chromatography
MF	Microfiltration
NF	Nanofiltration
QCM	Quartz crystal microbalance
QCM-D	Quartz crystal microbalance with dissipation monitoring
SCF-MS	Super critical fluid mass spectrometry
SEM	Scanning electron microscopy
SEM-EDS	Scanning electron microscopy-energy dispersive spectroscopy
TLC	Thin layer chromatography
TOC	Total organic carbon
UF	Ultrafiltration
UNIFAC	Universal functional activity coefficient

Appendix A UNIFAC Calculation details for predicting activities of the surfactant and solvent

For $C_{12}E_5$ (1) and Hexadecane (2) System, the group contribution and related parameters are tabulated in Table A.1

The equations used for calculation of activity of the surfactant and the solvent are as follows:

$$\ln \gamma_i = \ln \gamma_i^C + \ln \gamma_i^R \tag{A.1}$$

Where,

$$\ln \gamma_i^C = 1 - J_i + \ln J_i - 5q_i\left(1 - \frac{J_i}{L_i} + \ln \frac{J_i}{L_i}\right) \tag{A.2}$$

$$\ln \gamma_i^R = q_i\left[1 - \sum_k \left(\theta_k \frac{\beta_{ik}}{s_k} - e_{ik} \ln \frac{\beta_{ik}}{s_k}\right)\right] \tag{A.3}$$

$$J_i = \frac{r_i}{\sum_j r_j x_j} \tag{A.4}$$

$$L_i = \frac{q_i}{\sum_j q_j x_j} \tag{A.5}$$

$$r_i = \sum_k \nu_k^{(i)} R_k \tag{A.6}$$

$$q_i = \sum_k \nu_k^{(i)} Q_k \tag{A.7}$$

$$e_{ki} = \frac{\nu_k^{(i)} Q_k}{q_i} \tag{A.8}$$

$$\beta_{ik} = \sum_m e_{mi} \tau_{mk} \tag{A.9}$$

$$\tau_{mk} = \exp \frac{-a_{mk}}{T} \tag{A.10}$$

$$\theta_k = \frac{\sum_i x_i q_i e_{ki}}{\sum_j x_j q_j} \tag{A.11}$$

$$s_k = \sum_m \theta_m \tau_{mk} \tag{A.12}$$

Where x_i is the mole fraction of species i.

The values of interaction parameters (a_{mk}) are given in Table A.2

Table A.1 Group Contribution parameters for $C_{12}E_5$ (1) and Hexadecane (2). (Smith et al. 1996)

Group	k	R_k	Q_k	$\nu_k^{(1)}$	$\nu_k^{(2)}$
CH_3	1	0.9011	0.848	1	2
CH_2	2	0.6744	0.54	16	14
OH	15	1	1.2	1	0
CH_2O	26	0.9183	0.78	5	0

Table A.2 Interaction parameter values (Smith et al. 1996)

a(m,k)	1	2	15	26
1	0	0	986.5	251.5
2	0	0	986.5	251.5
15	156.4	156.4	0	28.06
26	83.36	83.36	237.7	0

Above equations and the group contribution data were used to estimate the activities of the surfactant ($C_{12}E_5$) and Solvent (Hexadecane) for varying mole fraction of the system. For all the calculations T = 293.16 K.

The calculated values of various parameters are shown in Table 3 for the case of $x_1 = 0.1$. The value of x_1 is varied from 0 to 1 and the calculated activity data is tabulated in Table 4. The plot of the activity coefficient is shown in Figure 2.2 The points satisfying the isoactivity criterion were determined graphically as shown in the Figure 2.2

Table A.3 Calculated values of various parameters for $x_1 = 0.1$

r1	17.283			
r2	11.2438			
q1	14.588			
q2	9.256			
e1,1	0.05813		**e1,2**	0.183232
e2,1	0.592268		**e2,2**	0.816768
e15,1	0.082259		**e15,2**	0
e26,1	0.267343		**e26,2**	0
τ (l,j)	**1**	**2**	**15**	**26**
1	1	1	0.03456	0.424054
2	1	1	0.03456	0.424054
15	0.58655	0.58655	1	0.908722
26	0.752503	0.752503	0.444493	1
β 1, 1	0.899823		**β 2, 1**	1
β 1, 2	0.899823		**β 2, 2**	1
β 1, 15	0.223569		**β 2, 15**	0.03456
β 1, 26	0.617898		**β 2, 26**	0.424054
θ 1	0.16459		**s 1**	0.985072
θ 2	0.783312		**s 2**	0.985072
θ 15	0.012258		**s 15**	0.062726
θ 26	0.03984		**s 26**	0.452941
J 1	1.458762			
J 2	0.949026			
L 1	1.490214			
L 2	0.945532			
ln r 1	2.339274		**a1**	1.03737
ln r 2	0.079693		**a2**	0.974659

Table A.4 Calculated activity data for the system $C_{12}E_5$ (1) and Hexadecane (2)

X_1	X_2	A_1	A_2
0.001	0.999	0.058	0.999
0.002	0.998	0.112	0.998
0.003	0.997	0.164	0.997
0.004	0.996	0.213	0.996
0.005	0.995	0.26	0.995
0.006	0.994	0.304	0.994
0.007	0.993	0.346	0.994
0.008	0.992	0.385	0.993
0.009	0.991	0.423	0.992
0.01	0.99	0.459	0.991
0.011	0.989	0.492	0.991
0.012	0.988	0.524	0.99
0.013	0.987	0.555	0.989
0.014	0.986	0.584	0.988
0.015	0.985	0.611	0.988
0.016	0.984	0.637	0.987
0.017	0.983	0.662	0.986
0.018	0.982	0.685	0.986
0.019	0.981	0.707	0.985
0.02	0.98	0.728	0.985
0.021	0.979	0.748	0.984
0.022	0.978	0.767	0.984
0.023	0.977	0.785	0.983
0.024	0.976	0.802	0.983
0.025	0.975	0.818	0.982
0.026	0.974	0.834	0.982
0.027	0.973	0.848	0.981
0.028	0.972	0.862	0.981
0.029	0.971	0.875	0.98
0.03	0.97	0.888	0.98
0.031	0.969	0.899	0.979
0.032	0.968	0.91	0.979
0.033	0.967	0.921	0.979
0.034	0.966	0.931	0.978
0.035	0.965	0.94	0.978
0.036	0.964	0.949	0.978
0.037	0.963	0.958	0.977
0.038	0.962	0.966	0.977
0.039	0.961	0.973	0.977
0.04	0.96	0.98	0.976
0.041	0.959	0.987	0.976
0.042	0.958	0.993	0.976

Table A.4 Continued

0.043	0.957	0.999	0.976
0.044	0.956	1.005	0.975
0.045	0.955	1.01	0.975
0.046	0.954	1.015	0.975
0.047	0.953	1.019	0.975
0.048	0.952	1.023	0.974
0.049	0.951	1.027	0.974
0.05	0.95	1.031	0.974
0.06	0.94	1.056	0.973
0.07	0.93	1.064	0.972
0.08	0.92	1.061	0.972
0.09	0.91	1.051	0.973
0.1	0.9	1.037	0.975
0.11	0.89	1.021	0.976
0.12	0.88	1.003	0.979
0.13	0.87	0.984	0.981
0.14	0.86	0.966	0.984
0.15	0.85	0.948	0.987
0.16	0.84	0.93	0.991
0.17	0.83	0.913	0.995
0.18	0.82	0.896	0.998
0.19	0.81	0.881	1.002
0.2	0.8	0.866	1.006
0.25	0.75	0.805	1.028
0.3	0.7	0.762	1.05
0.35	0.65	0.733	1.069
0.4	0.6	0.717	1.083
0.45	0.55	0.71	1.091
0.5	0.5	0.711	1.09
0.55	0.45	0.718	1.077
0.6	0.4	0.731	1.051
0.65	0.35	0.75	1.008
0.7	0.3	0.773	0.946
0.75	0.25	0.8	0.862
0.8	0.2	0.832	0.753
0.85	0.15	0.868	0.616
0.9	0.1	0.908	0.447
0.95	0.05	0.952	0.243
0.999	0.001	0.999	0.005

Copyright © Abhay R Ladhe 2008

Appendix B SEM images of silica-polysulfone mixed-matrix membranes

In order to provide more information about the morphology of the silica-polysulfone mixed-matrix membranes, additional SEM image is provided in this section.

Figure B.1 shows the SEM image for cross section of 40% 874-85-1 silica-polysulfone mixed matrix membrane. The image is obtained at higher magnification and it shows open structured porous morphology of the membrane. The porous morphology with interconnected pores is desirable for liquid phase applications.

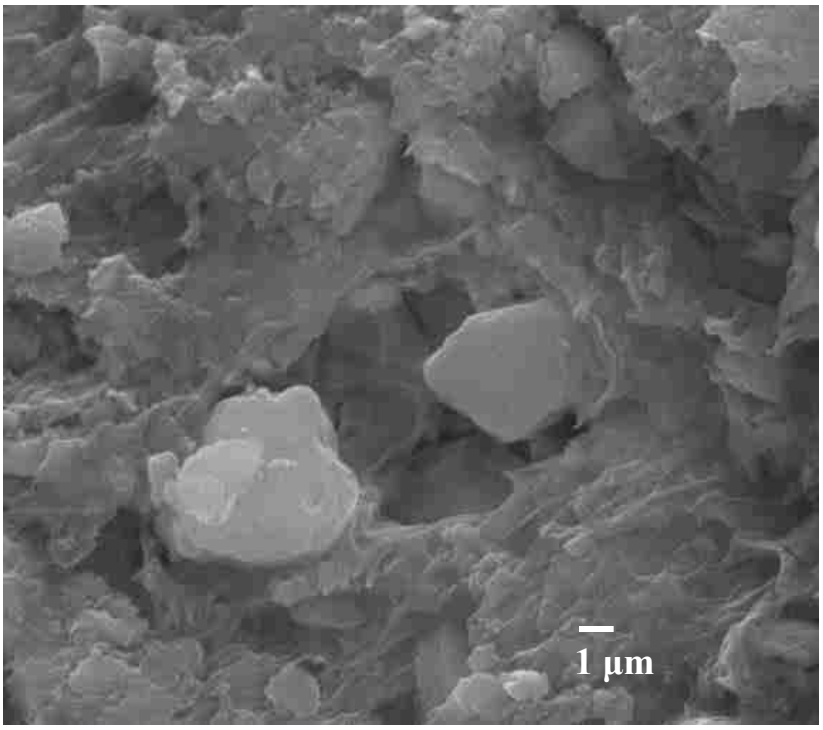

Figure B.1 SEM image of cross-section of 40% 874-85-1 silica-polysulfone mixed-matrix membrane

Copyright © Abhay R Ladhe 2008

Appendix C Details for the model and COMSOL solution for mixed-matrix membranes

This appendix contains the details for derivation of equation 7.1 and the COMSOL solution of equations 7.5 and 7.6. The effect selected diffusivity value and selected number of elements on model predictions is also discussed.

C.1 Derivation of equation 7.1 (Mass balance on the liquid phase in mixed-matrix membrane)

As shown in Figure 7.1, an element of thickness $\Delta z'$ was defined and mass balance was taken across this element for the liquid phase. Let us denote the cross sectional area of the membrane by *A*

In - Out - Captured = Accumulation

$$J_W C'\big|_{z'} - J_W C'\big|_{z'+\Delta z'} - \frac{\partial q'}{\partial t'} A\Delta z' \times \left(1-\phi-\phi_p\right) = A\Delta z' \phi \frac{\partial C'}{\partial t'} \quad \text{(C.1)}$$

Dividing both the sides by $A\Delta z'$ we get,

$$J_W\left(\frac{C'\big|_{z'} - C'\big|_{z'+\Delta z'}}{\Delta z'}\right) - (1-\phi-\phi_p)\frac{\partial q'}{\partial t'} = \phi\frac{\partial C'}{\partial t'} \quad \text{(C.2)}$$

i.e.,

$$-J_W \frac{\partial C'}{\partial z'} - (1-\phi-\phi_p)\frac{\partial q'}{\partial t'} = \phi\frac{\partial C'}{\partial t'} \quad \text{(C.3)}$$

Rearranging the terms in B.3, we get

$$\phi\frac{\partial C'}{\partial t'} + J_W \frac{\partial C'}{\partial z'} + (1-\phi-\phi_p)\frac{\partial q'}{\partial t'} = 0 \quad \text{(C.4)}$$

Equation C.4 is equivalent to equation 7.1.

COMSOL software was used to solve the system of partial differential equations in order to model the mixed-matrix membranes for sorption applications (Equation details provided in Chapter 7). A copy of the model report generated by the software is provided in this appendix to provide all the necessary details required to feed the model equations to the software and subsequent solution settings used. The specific report is

applicable for predicting the data for double stack membrane breakthrough curve as shown in Figure 7.6 For the purpose of convenience, following changes in terminologies are adopted while solving the model using COMSOL:

1. The term (J_W / ϕ) is expressed as V.

2. The term $q\frac{q_\infty}{C_0}$ is expressed as qs.

The report generated by the software is provided below.

C.2 COMSOL report for the case of double stack membrane sorption data prediction

Mixed-matrix membranes for Sorptions

1. Model Properties

Property	Value
Model name	Mixed Matrix Membranes for Sorptions
Author	Abhay Ladhe
Company	University of Kentucky
Department	Chemical and Materials Engineering
Reference	
URL	
Saved date	Feb 8, 2008 3:30:20 PM
Creation date	Jan 30, 2008 2:49:05 PM
COMSOL version	COMSOL 3.4.0.248

1.1 Application modes and modules used in this model:

Geom1 (1D)
Convection and Diffusion
Convection and Diffusion

2. Constants

Name	Expression	Value	Description
gamma	1880.2	1880.2	
C0	0.874	0.874	
V	0.2692e-4	2.692e-5	
L	2.2e-4	2.2e-4	
T	180*60	10800	
Phi	0.52	0.52	
phip	0.35	0.35	
K	0.002	0.002	
D	1.8e-9	1.8e-9	

3. Geometry

Number of geometries: 1 (Geom1)

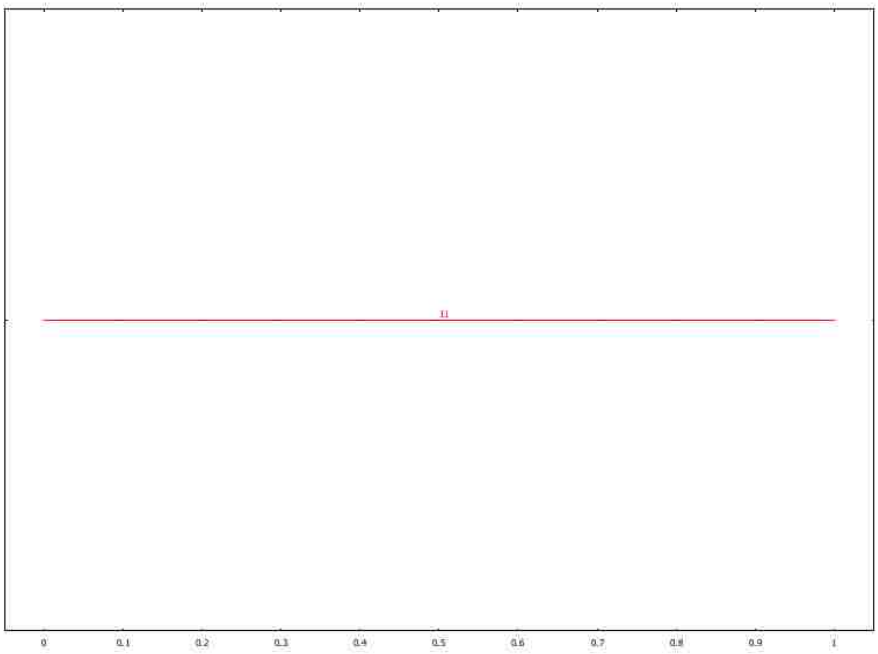

3.1 Boundary mode

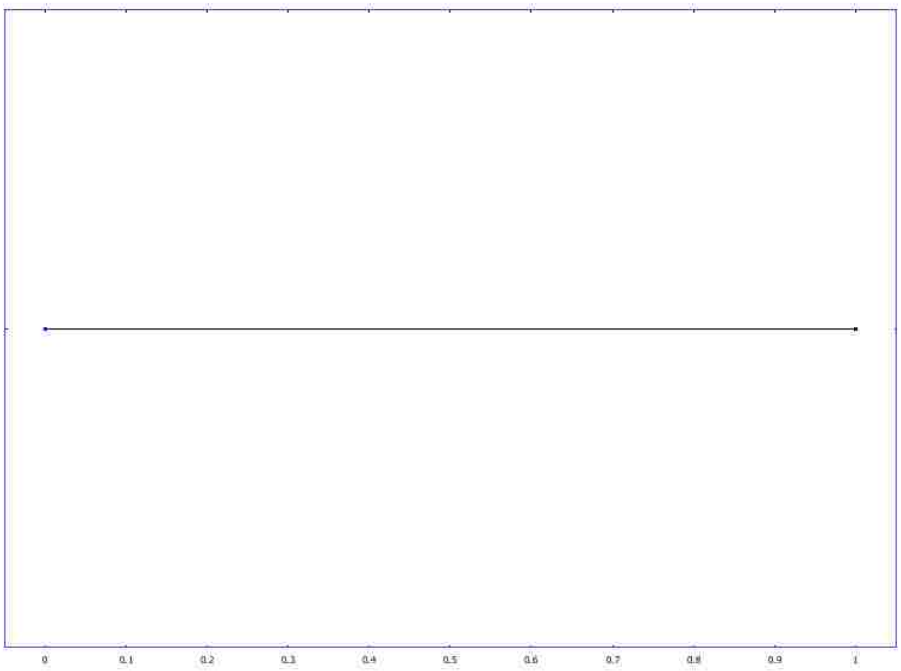

4. Geom1
Space dimensions: 1D
Independent variables: x, y, z

4.1 Expressions

4.1.1 Subdomain Expressions

Subdomain		1
Rate	mol/m^3	k*(gamma*c-qs)

4.2 Mesh

4.2.1 Mesh Statistics

Number of degrees of freedom	242
Number of mesh points	61
Number of elements	60
Number of boundary elements	2
Element length ratio	1

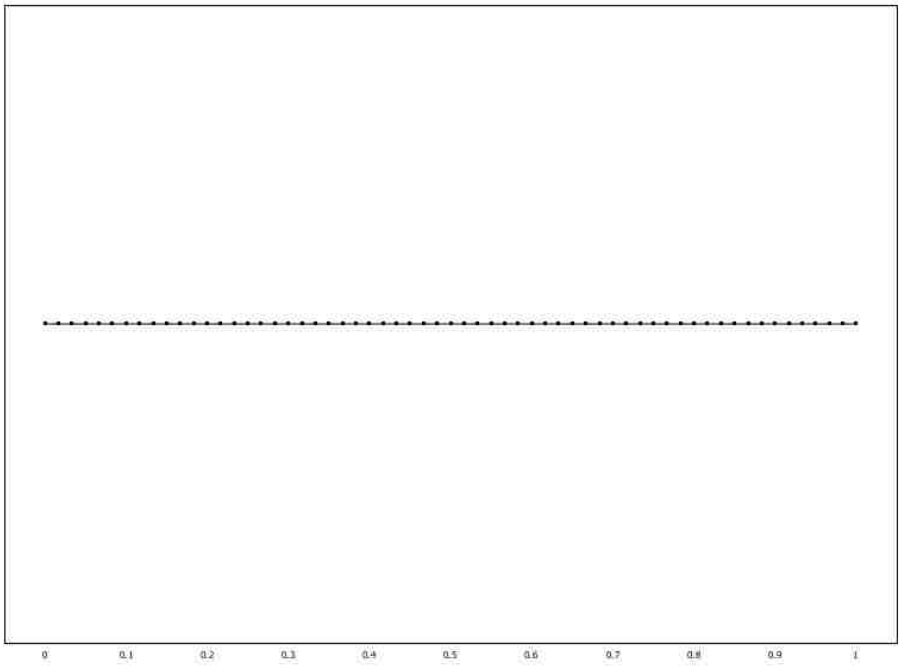

4.3 Application Mode: Convection and Diffusion (cd)
Application mode type: Convection and Diffusion
Application mode name: cd

4.3.1 Application Mode Properties

Property	Value
Default element type	Lagrange - Quadratic
Analysis type	Transient
Equation form	Non-conservative
Frame	Frame (ref)
Weak constraints	Off
Constraint type	Ideal

4.3.2 Variables
Dependent variables: c
Shape functions: shlag(2,'c')
Interior boundaries not active

4.3.3 Boundary Settings

Point		2	1
Concentration (c0)	mol/m3	0	1

4.3.4 Subdomain Settings

Subdomain		1
Diffusion coefficient (D)	m2/s	D
Reaction rate (R)	mol/(m3· s)	-((1-phi-phip)/phi)*L*rate
Time-scaling coefficient (Dts)	1	L/T
x-velocity (u)	m/s	V
Streamline diffusion switch (sdon)		1
Streamline diffusion type (sdtype)		Pg

4.4 Application Mode: Convection and Diffusion (cd2)
Application mode type: Convection and Diffusion
Application mode name: cd2

4.4.1 Application Mode Properties

Property	Value
Default element type	Lagrange - Quadratic
Analysis type	Transient
Equation form	Non-conservative
Frame	Frame (ref)
Weak constraints	Off
Constraint type	Ideal

4.4.2 Variables

Dependent variables: qs
Shape functions: shlag(2,'qs')
Interior boundaries not active

4.4.3 Subdomain Settings

Subdomain		1
Diffusion coefficient (D)	m2/s	0
Reaction rate (R)	mol/(m3· s)	T*rate

5. Solver Settings

Solve using a script: off

Analysis type	Transient
Auto select solver	On
Solver	Time dependent
Solution form	Automatic
Symmetric	Auto
Adaption	Off

5.1 Direct (UMFPACK)

Solver type: Linear system solver

Parameter	Value
Pivot threshold	0.1
Memory allocation factor	0.7

5.2 Time Stepping

Parameter	Value
Times	0:0.1:1
Relative tolerance	0.01
Absolute tolerance	0.0010
Times to store in output	Specified times
Time steps taken by solver	Free
Manual tuning of step size	Off
Initial time step	0.0010
Maximum time step	1.0
Maximum BDF order	5
Singular mass matrix	Maybe
Consistent initialization of DAE systems	Backward Euler
Error estimation strategy	Include algebraic
Allow complex numbers	Off

5.3 Advanced

Parameter	Value
Constraint handling method	Elimination
Null-space function	Automatic
Assembly block size	5000
Use Hermitian transpose of constraint matrix and in symmetry detection	Off
Use complex functions with real input	Off
Stop if error due to undefined operation	On
Store solution on file	Off
Type of scaling	Automatic
Manual scaling	
Row equilibration	On
Manual control of reassembly	Off
Load constant	On
Constraint constant	On
Mass constant	On
Damping (mass) constant	On
Jacobian constant	On
Constraint Jacobian constant	On

C.3 Output for breakthrough curve generated by postprocessing of the solution data

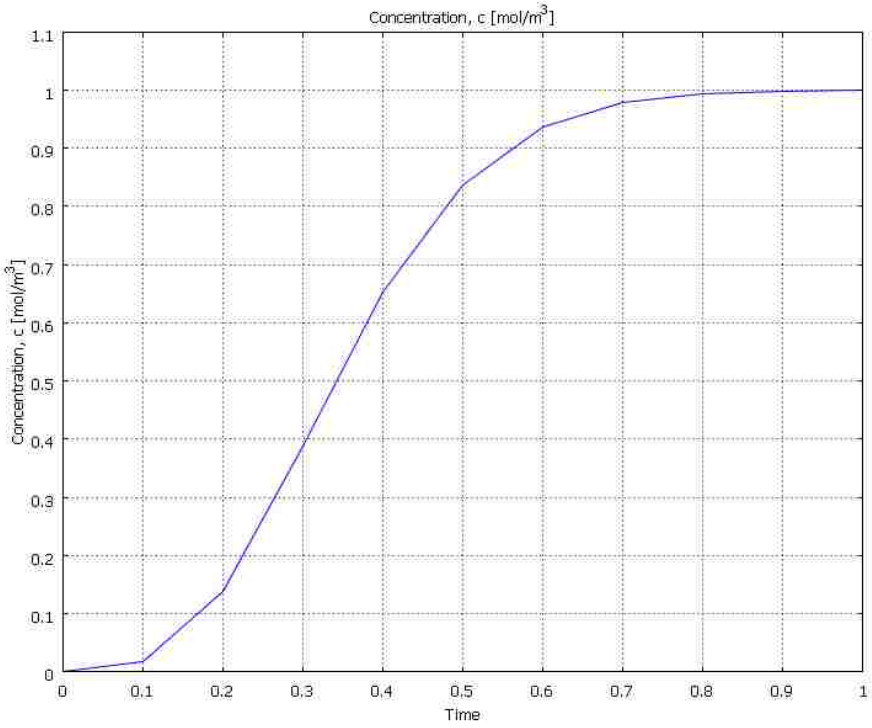

Figure C.1 Predicted breakthrough curve for silver ion in the case of silver capture with double stack thiol-functionalized silica-polysulfone membrane. (The data is also plotted in Figure 7.6 after converting the non-dimensional time to minutes)

C.4 Artificial diffusion term and effect of selected value of diffusivity on model predictions

In order to obtain a stable solution, an artificial diffusion term was added to equation 7.5 as explained in Chapter 7. The modified equation containing the artificial diffusion term is given below.

$$\frac{\phi L}{J_W T_S}\frac{\partial C}{\partial t}+\frac{\partial C}{\partial z}+(1-\phi-\phi_p)\frac{kL}{J_W}\left(\gamma\, C-q\frac{q_\infty}{C_0}\right)=\frac{D}{J_W L}\frac{\partial^2 C}{\partial z^2} \qquad \text{(C.5)}$$

The diffusivity value required for the calculation was calculated based on the reported data (Cussler 1996). The calculated diffusivity value was 1.8 x 10^{-9} m^2/s and this value was used for all the predictions. The idea of using the artificial diffusion term is to introduce enough diffusion to obtain a stable solution. In order to prove that the selected diffusivity value does not affect the model solution, the predicted data was obtained for a significantly lower diffusivity value (D = 1.8 x 10^{-15} m^2/s) and it was compared with the originally predicted data (D = 1.8 x 10^{-9} m^2/s) as shown in Figure C.2. The figure clearly shows that in both the cases, the predicted data is identical and hence the selected diffusivity value does not affect the predicted data.

It is expected that the importance of diffusion term will be pronounced at lower membrane flux values. Although, lower membrane flux may not be desirable from practical viewpoint, the data was predicted and compared for varying diffusivity values for a hypothetical case of J_W = 1.4 x 10^{-6} m/s (10 times lower flux value). The predicted data was observed to be identical (not shown in figure) indicating applicability of the model and the artificial diffusion term for this lower membrane flux region.

Figure C.2 also shows the predicted data for D = 1.8 x 10^{-5} m^2/s and J_W = 1.4 x 10^{-5} m/s. In this case, for diffusivity value higher than 1 x 10^{-6} m^2/s, the contribution of the artificial diffusion term becomes comparable to the axial convection term. As expected, this lead to a faster breakthrough as observed from Figure C.2. However, such high values of diffusivity (D > 1 x 10^{-6} m^2/s) are not realistic for metal ions in aqueous solutions (typical diffusivity value in the range of 10^{-9} m^2/s) and the model is applicable under practical conditions.

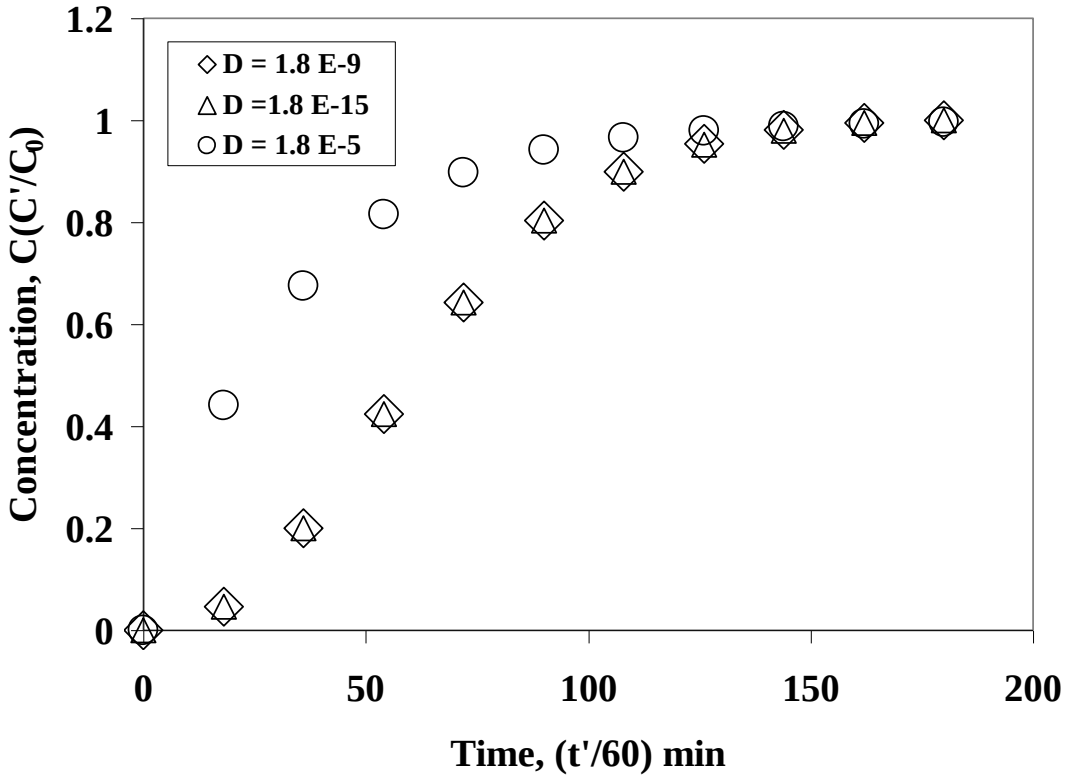

Figure C.2 Effect of selected diffusivity value on model prediction in the case of silver capture using double stack membrane. The model parameters used are: k = 0.002 s^{-1}, γ = 1880, L = 2.2 x 10^{-4} m, ϕ = 0.52, ϕ_p = 0.35, C_0 = 0.874 mole/m^3, J_W = 1.4 x 10^{-5} m/s

C.5 Effect of number of elements used for calculation on model prediction

During the solution of equations 7.5 and 7.6 using COMSOL, the membrane thickness was divided into 120 elements (N = 120) for calculation purpose. In order to prove that the number of elements selected is sufficient for accurate calculations, the model prediction was also obtained for N = 1920 in the case of silver capture using double stack membranes. The comparison of the two predicted data is shown in figure C.3 and it is clear that in both the cases the predicted data is identical and N = 120 is sufficient for calculation purpose.

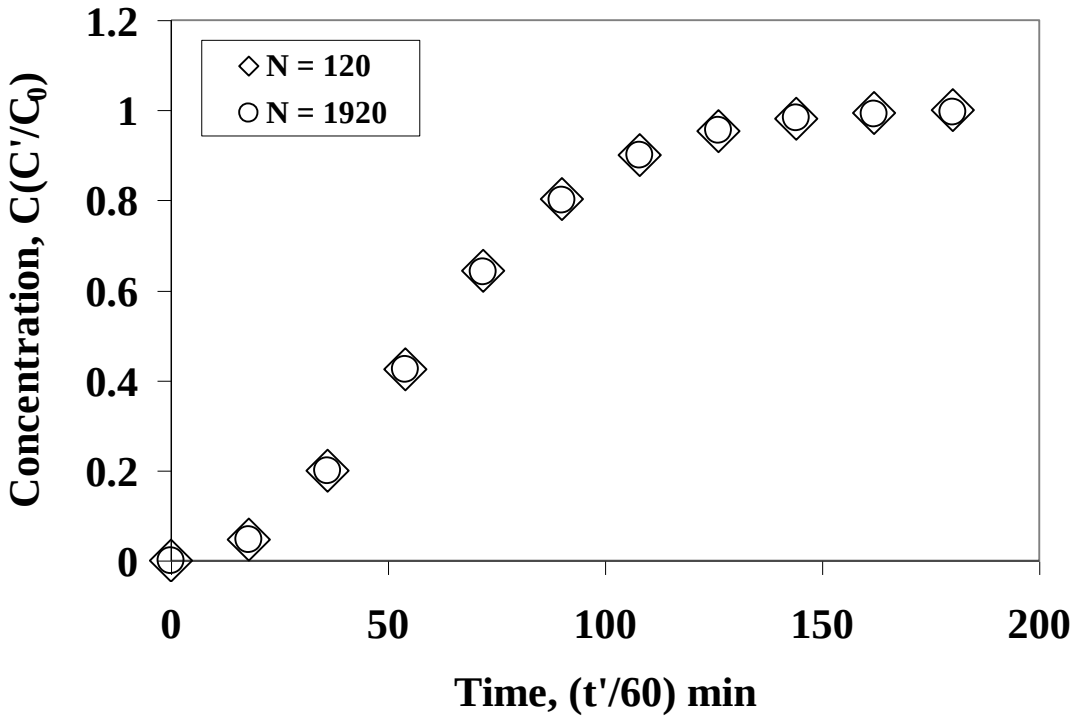

Figure C.3 Effect of selected value of number of elements used for calculation on model prediction in the case of silver capture using double stack membrane. The model parameters used are: k = 0.002 s^{-1}, γ = 1880, L = 2.2 x 10^{-4} m, ϕ = 0.52, ϕ_p = 0.35, C_0 = 0.874 mole/m^3, J_W = 1.4 x 10^{-5} m/s, D = 1.8 x 10^{-9} m^2/s

Copyright © Abhay R Ladhe 2008

References

Absalan, G. and Mehrdjardi, M.A., 2003. Separation and preconcentration of silver ion using 2-mercaptobenzothiazole immobilized on surfactant-coated alumina. Separation and Purification Technology, 33(1): 95-101.

Adoor, S.G., Sairam, M., Manjeshwar, L.S., Raju, K.V.S.N. and Aminabhavi, T.M., 2006. Sodium montmorillonite clay loaded novel mixed matrix membranes of poly(vinyl alcohol) for pervaporation dehydration of aqueous mixtures of isopropanol and 1,4-dioxane. Journal of Membrane Science, 285(1+2): 182-195.

Anghel, D.F., Saito, S., Baran, A. and Iovescu, A., 1998. Interaction between poly(acrylic acid) and nonionic surfactants with the same poly(ethylene oxide) but different hydrophobic moieties. Langmuir, 14(19): 5342-5346.

Anghel, D.F., Winnik, F.M. and Galatanu, N., 1999. Effect of the surfactant head group length on the interactions between polyethylene glycol monononylphenyl ethers and poly(acrylic acid). Colloids and Surfaces, A: Physicochemical and Engineering Aspects, 149(1-3): 339-345.

Ariga, K., Hill, J.P. and Ji, Q., 2007. Layer-by-layer assembly as a versatile bottom-up nanofabrication technique for exploratory research and realistic application. Physical Chemistry Chemical Physics, 9(19): 2319-2340.

Armistead, C.G., Tyler, A.J. and Hockey, J.A., 1971. Selective adsorption of n-fatty acids at the silica/benzene and silica/n-hexane interface. 1. Adsorption isotherms. Transactions of the Faraday Society, 67(Pt. 2): 493-9.

Asmussen, C. and Stan, H.-J., 1998. Determination of non-ionic surfactants of the alcohol polyethoxylate type by means of high temperature gas chromatography and atomic emission detection. Journal of High Resolution Chromatography, 21(11): 597-604.

Atia, A.A., Donia, A.M. and Yousif, A.M., 2005. Comparative study of the recovery of silver(I) from aqueous solutions with different chelating resins derived from glycidyl methacrylate. Journal of Applied Polymer Science, 97(3): 806-812.

Atwater, J.E. and Akse, J.R., 2007. Oxygen permeation through functionalized hydrophobic tubular ceramic membranes. Journal of Membrane Science, 301(1+2): 76-84.

Avramescu, M.-E., Girones, M., Borneman, Z. and Wessling, M., 2003. Preparation of mixed matrix adsorber membranes for protein recovery. Journal of Membrane Science, 218(1-2): 219-233.

Berglund, K.D., Timko, A.E., Przybycien, T.M. and Tilton, R.D., 2003. Use of nonionic ethylene oxide surfactants as phase-transfer catalysts for poly(acrylic acid) adsorption to silica against an electrostatic repulsion. Progress in Colloid and Polymer Science, 122: 56-66.

Bhattacharyya, D., Hestekin, J.A., Brushaber, P., Cullen, L., Bachas, L.G. and Sikdar, S.K., 1998. Novel poly-glutamic acid functionalized microfiltration membranes for sorption of heavy metals at high capacity. Journal of Membrane Science, 141(1): 121-135.

Blom, A., Warr, G.G. and Wanless, E.J., 2005. Morphology transitions in nonionic surfactant adsorbed layers near their cloud points. Langmuir, 21(25): 11850-11855.

Boccuzzi, F., Coluccia, S., Ghiotti, G., Morterra, C. and Zecchina, A., 1978. Infrared study of surface modes on silica. Journal of Physical Chemistry, 82(11): 1298-303.

Brandt, S., Goffe, R.A., Kessler, S.B., O'Connor, J.L. and Zale, S.E., 1988. Membrane-based affinity technology for commercial scale purifications. Bio/Technology, 6(7): 779-82.

Brinck, J., Joensson, B. and Tiberg, F., 1999. Influence of long-chain alcohols on the adsorption of nonionic surfactants to silica. Langmuir, 15(22): 7719-7724.

Bruening, M.L., Dotzauer, D.M., Jain, P., Lu, O. and Baker, G.L., 2008. Creation of functional membranes using polyelectrolyte multilayers and polymer brushes. Langmuir, 24(15): 7663-7673.

Butterfield, D.A. and Bhattacharyya, D., 2003. Biofunctional membranes: Site-specifically immobilized enzyme arrays. Membrane Science and Technology Series, 8(New Insights into Membrane Science and Technology: Polymeric and Biofunctional Membranes, 2003): 233-240.

Butterfield, D.A., Bhattacharyya, D., Daunert, S. and Bachas, L., 2001. Catalytic biofunctional membranes containing site-specifically immobilized enzyme arrays: a review. Journal of Membrane Science, 181(1): 29-37.

Cai, B., Zheng, Q.-K., Li, R.-X. and Wu, D.-C., 2003. Adsorption mechanism of surfactants on nonwoven fabrics. Journal of Applied Polymer Science, 89(12): 3210-3215.

Carter, T.G., Yantasee, W., Sangvanich, T., Fryxell, G.E., Johnson, D.W. and Addleman, R.S., 2008. New functional materials for heavy metal sorption: "Supramolecular" attachment of thiols to mesoporous silica substrates. Chemical Communications (Cambridge, United Kingdom)(43): 5583-5585.

Caruso, F., Serizawa, T., Furlong, D.N. and Okahata, Y., 1995. Quartz crystal microbalance and surface plasmon resonance study of surfactant adsorption onto gold and chromium oxide surfaces. Langmuir, 11(5): 1546-52.

Charcosset, C., 1998. Purification of proteins by membrane chromatography. Journal of Chemical Technology and Biotechnology, 71(2): 95-110.

Chun, K.-Y. and Stroeve, P., 2001. External control of ion transport in nanoporous membranes with surfaces modified with self-assembled monolayers. Langmuir, 17(17): 5271-5275.

Claesson, P.M. and Kjellin, U.R.M., 1999. Studies of interactions between interfaces across surfactant solutions employing various surface force techniques. Surfactant Science Series, 83(Modern Characterization Methods of Surfactant Systems): 255-333.

Conrado, R.J., Varner, J.D. and DeLisa, M.P., 2008. Engineering the spatial organization of metabolic enzymes: mimicking nature's synergy. Current Opinion in Biotechnology, 19(5): 492-499.

Crook, E.H., Fordyce, D.B. and Trebbi, G.F., 1965. Molecular-weight distribution of nonionic surfactants. II. Partition coefficients of normal distribution and homogeneous p-tert-octylphenoxyethoxyethanols (OPE's). Journal of Colloid Science, 20(3): 191-204.

Cuscito, O., Clochard, M.C., Esnouf, S., Betz, N. and Lairez, D., 2007. Nanoporous b-PVDF membranes with selectively functionalized pores. Nuclear Instruments and Methods in Physics Research, Section B: Beam Interactions with Materials and Atoms, 265(1): 309-313.

Cussler, E.L. and Editor, 1996. Diffusion: Mass Transfer in Fluid Systems, Second Edition. Cambridge University Press, 600.

Dai, Z.-W., Nie, F.-Q. and Xu, Z.-K., 2005. Acrylonitrile-based copolymer membranes containing reactive groups: Fabrication dual-layer biomimetic membranes by the immobilization of biomacromolecules. Journal of Membrane Science, 264(1-2): 20-26.

Datta, S., Bhattacharyya, D., Ray, P.D., Nath, A. and Toborek, M., 2007. Effect of pre-filtration on selective isolation of tat protein by affinity membrane separation: analysis of flux, separation efficiency, and processing time. Separation Science and Technology, 42(11): 2451-2471.

Datta, S., Ray, P.D., Nath, A. and Bhattacharyya, D., 2006. Recognition based separation of HIV-Tat protein using avidin-biotin interaction in modified microfiltration membranes. Journal of Membrane Science, 280(1+2): 298-310.

Decher, G., 1997. Fuzzy nanoassemblies: toward layered polymeric multicomposites. Science (Washington, D. C.), 277(5330): 1232-1237.

Decher, G. and Schmitt, J., 1992. Fine-tuning of the film thickness of ultrathin multilayer films composed of consecutively alternating layers of anionic and cationic polyelectrolytes. Progress in Colloid and Polymer Science, 89(Trends Colloid Interface Sci. VI): 160-4.

Denoyel, R. and Rouquerol, J., 1991. Thermodynamic (including microcalorimetry) study of the adsorption of nonionic and anionic surfactants onto silica, kaolin, and alumina. Journal of Colloid and Interface Science, 143(2): 555-72.

Desbene, P.L., Portet, F. and Treiner, C., 1997. Adsorption of pure nonionic alkylethoxylated surfactants down to low concentrations at a silica/water interface as determined using a HPLC technique. Journal of Colloid and Interface Science, 190(2): 350-356.

Deslandes, N., Bellenger, V., Jaffiol, F. and Verdu, J., 1998. Solubility parameter of a polyester composite material. Journal of Applied Polymer Science, 69(13): 2663-2671.

Feng, J. and Lim, T.-T., 2005. Pathways and kinetics of carbon tetrachloride and chloroform reductions by nano-scale Fe and Fe/Ni particles: comparison with commercial micro-scale Fe and Zn. Chemosphere, 59(9): 1267-1277.

Feng, X., Fryxell, G.E., Wang, L.Q., Kim, A.Y., Liu, J. and Kemner, K.M., 1997. Functionalized monolayers on ordered mesoporous supports. Science (Washington, D. C.), 276(5314): 923-926.

Ferry, J.D., 1936. Statistical evaluation of sieve constants in ultrafiltration. Journal of General Physiology, 20: 95-104.

Finlayson, B.A., 2005. Introduction to Chemical Engineering Computing. Wiley: 164.

Flores, M.V., Voutsas, E.C., Spiliotis, N., Eccleston, G.M., Bell, G., Tassios, D.P. and Halling, P.J., 2001. Critical micelle concentrations of nonionic surfactants in organic solvents: Approximate prediction with UNIFAC. Journal of Colloid and Interface Science, 240(1): 277-283.

Gabriel, E.M. and Gillberg, G.E., 1993. In situ modification of microporous membranes. Journal of Applied Polymer Science, 48(12): 2081-90.

Gan, Q., Allen, S.J. and Taylor, G., 2005. Analysis of process integration and intensification of enzymatic cellulose hydrolysis in a membrane bioreactor. Journal of Chemical Technology and Biotechnology, 80(6): 688-698.

Geffroy, C., Stuart, M.A.C., Wong, K., Cabane, B. and Bergeron, V., 2000. Adsorption of nonionic surfactants onto polystyrene. Kinetics and reversibility. Langmuir, 16(16): 6422-6430.

Geismann, C., Yaroshchuk, A. and Ulbricht, M., 2007. Permeability and electrokinetic characterization of poly(ethylene terephthalate) capillary pore membranes with grafted temperature-responsive polymers. Langmuir, 23(1): 76-83.

Ghoulam, M.B., Moatadid, N., Gracia, A. and Lachaise, J., 2002. Effects of oxyethylene chain length and temperature on partitioning of homogeneous polyoxyethylene nonionic surfactants between water and isooctane. Langmuir, 18(11): 4367-4371.

Giger, W., Brunner, P.H. and Schaffner, C., 1984. 4-Nonylphenol in sewage sludge: accumulation of toxic metabolites from nonionic surfactants. Science (Washington, DC, United States), 225(4662): 623-5.

Gilchrist, V.A., Lu, J.R., Keddie, J.L., Staples, E. and Garrett, P., 2000. Adsorption of penta(ethylene glycol) monododecyl ether at the solid poly(methyl methacrylate)-water interface: A spectroscopic ellipsometry study. Langmuir, 16(2): 740-748.

Giorno, L. and Drioli, E., 2000. Biocatalytic membrane reactors: applications and perspectives. Trends in Biotechnology, 18(8): 339-349.

Grant, L.M., Ederth, T. and Tiberg, F., 2000. Influence of surface hydrophobicity on the layer properties of adsorbed nonionic surfactants. Langmuir, 16(5): 2285-2291.

Gregg, S.J. and Sing, K.S.W., 1967. Adsorption, Surface Area, and Porosity. Academic, New York, 371 pp pp.

Hautojarvi, J., Kontturi, K., Nasman, J.H., Svarfvar, B.L., Viinikka, P. and Vuoristo, M., 1996. Characterization of graft-modified porous polymer membranes. Industrial and Engineering Chemistry Research, 35(2): 450-7.

Higuchi, A., Shirano, K., Harashima, M., Yoon, B.O., Hara, M., Hattori, M. and Imamura, K., 2002. Chemically modified polysulfone hollow fibers with vinylpyrrolidone having improved blood compatibility. Biomaterials, 23(13): 2659-2666.

Hilal, N., Kochkodan, V., Nigmatullin, R., Goncharuk, V. and Al-Khatib, L., 2006. Lipase-immobilized biocatalytic membranes for enzymatic esterification: Comparison of various approaches to membrane preparation. Journal of Membrane Science, 268(2): 198-207.

Ho, W. and Sirkar, K.K., 1992. Membrane Handbook, Van Nostrand Reinhold, New York.

Hollman, A.M. and Bhattacharyya, D., 2002. Controlled permeability and ion exclusion in microporous membranes functionalized with poly(L-glutamic acid). Langmuir, 18(15): 5946-5952.

Hollman, A.M. and Bhattacharyya, D., 2003. Functionalized membranes for tunable separations and toxic metal capture. Membrane Science and Technology Series, 8(New Insights into Membrane Science and Technology: Polymeric and Biofunctional Membranes, 2003): 329-352.

Hollman, A.M. and Bhattacharyya, D., 2004. Pore assembled multilayers of charged polypeptides in microporous membranes for ion separation. Langmuir, 20(13): 5418-5424.

Hollman, A.M., Christian, D.A., Ray, P.D., Galey, D., Turchan, J., Nath, A. and Bhattacharyya, D., 2005. Selective isolation and purification of tat protein via affinity membrane separation. Biotechnology Progress, 21(2): 451-459.

Hong, S.U., Miller, M.D. and Bruening, M.L., 2006. Removal of dyes, sugars, and amino acids from NaCl solutions using multilayer polyelectrolyte nanofiltration membranes. Industrial and Engineering Chemistry Research, 45(18): 6284-6288.

Huang, J., Guo, Q., Ohya, H. and Fang, J., 1998. The characteristics of crosslinked PAA composite membrane for separation of aqueous organic solutions by reverse osmosis. Journal of Membrane Science, 144(1-2): 1-11.

Hwang, J.-E. and Jegal, J., 2007. Preparation and characterization of the asymmetric microporous poly(vinylidene fluoride) (PVDF) blend membranes with hydrophilic surfaces. Korean Membrane Journal, 9(1): 1-11.

Iler, R.K., 1966. Multilayers of colloidal particles. Journal of Colloid and Interface Science, 21(6): 569-94.

Ito, Y., Park, Y.S. and Imanishi, Y., 2000. Nanometer-sized channel gating by a self-assembled polypeptide brush. Langmuir, 16(12): 5376-5381.

Jordan, J.L. and Fernandez, E.J., 2008. QCM-D sensitivity to protein adsorption reversibility. Biotechnology and Bioengineering, 101(4): 837-842.

Kang, T., Park, Y. and Yi, J., 2004. Highly selective adsorption of Pt2+ and Pd2+ using thiol-functionalized mesoporous silica. Industrial and Engineering Chemistry Research, 43(6): 1478-1484.

Kasem, K.K., Sheets, J. and Koon, N., 1998. Modified electrodes with synthetic biocatalytic membranes. Biotechnology Progress, 14(5): 791-796.

Kaur, S., Kotaki, M., Ma, Z., Gopal, R., Ramakrishna, S. and Ng, S.C., 2006. Oligosaccharide functionalized nanofibrous membrane. International Journal of Nanoscience, 5(1): 1-11.

Kesting, R.E., 1993. Synthetic Polymeric Membranes, McGraw-Hill, Inc., 300 pp pp.

Khan, A.A. and Alam, M.M., 2004. New and novel organic-inorganic type crystalline polypyrrolel/polyantimonic acid composite system: preparation, characterization and analytical applications as a cation-exchange material and Hg(II) ion-selective membrane electrode. Analytica Chimica Acta, 504(2): 253-264.

Kharitonova, T.V., Ivanova, N.I. and Summ, B.D., 2005. Adsorption of cationic and nonionic surfactants on a SiO2 surface from aqueous solutions: 1. Adsorption of dodecylpyridinium bromide and Triton X-100 from individual solutions. Colloid Journal, 67(2): 242-248.

Kim, J.-H., Tratnyek, P.G. and Chang, Y.-S., 2008. Rapid dechlorination of polychlorinated dibenzo-p-dioxins by bimetallic and nanosized zerovalent iron. Environmental Science and Technology, 42(11): 4106-4112.

Kipling, J.J. and Wright, E.H.M., 1964. The adsorption of stearic acid from solution by oxide adsorbents. Journal of the Chemical Society(Oct.): 3535-40.

Kjellin, U.R.M., Claesson, P.M. and Linse, P., 2002. Surface properties of tetra(ethylene oxide) dodecyl amide compared with poly(ethylene oxide) surfactants. 1. Effect of the headgroup on adsorption. Langmuir, 18(18): 6745-6753.

Klein, E., 1991. Affinity Membranes: Their Chemistry and Performance in Adsorptive Separation Processes, 152 pp pp.

Klein, E., 2000. Affinity membranes: a 10-year review. Journal of Membrane Science, 179(1-2): 1-27.

Knag, M., Sjoeblom, J., Oye, G. and Gulbrandsen, E., 2004. A quartz crystal microbalance study of the adsorption of quaternary ammonium derivates on iron and cementite. Colloids and Surfaces, A: Physicochemical and Engineering Aspects, 250(1-3): 269-278.

Kochkodan, V.M., Khilal, N., Goncharuk, V.V. and Nigmatullin, R., 2007. Synthesis of butyl oleate in biocatalytic membrane reactors with immobilized lipase. Ukrainskii Khimicheskii Zhurnal (Russian Edition), 73(5-6): 3-9.

Konovalova, V.V., 2000. Formation of biocatalytic membranes for ultrafiltration treatment of wastewater containing dyes. Dopovidi Natsional'noi Akademii Nauk Ukraini(12): 209-214.

Krasemann, L. and Tieke, B., 1998. Ultrathin self-assembled polyelectrolyte membranes for pervaporation. Journal of Membrane Science, 150(1): 23-30.

Krishnakumar, S. and Somasundaran, P., 1994. Role of surfactant-adsorbent acidity and solvent polarity in adsorption-desorption of surfactants from nonaqueous media. Langmuir, 10(8): 2786-9.

Kubota, N. and Shimoda, K., 2005. Cellulose in affinity membrane applications for separation and purification of proteins. Recent Developments in Carbohydrate Research, 2: 17-44.

Kugel, K., Moseley, A., Harding, G.B. and Klein, E., 1992. Microporous polycaprolactam hollow fibers for therapeutic affinity adsorption. Journal of Membrane Science, 74(1-2): 115-29.

Kulprathipanja, S., Neuzil, R.W. and Li, N.N., 1988. Gas separation by means of mixed matrix membranes. (Allied-Signal, Inc., USA). Application: US
US, pp. 7 pp Cont of U S Ser No 697,990, abandoned.

Kumar, N., Garoff, S. and Tilton, R.D., 2004. Experimental observations on the scaling of adsorption isotherms for nonionic surfactants at a hydrophobic solid-water interface. Langmuir, 20(11): 4446-4451.

Kumar, N. and Tilton, R.D., 2004. Unified model to predict self-assembly of nonionic surfactants in solution and adsorption on solid or fluid hydrophobic surfaces: Effect of molecular structure. Langmuir, 20(11): 4452-4464.

Kuraoka, K., Chujo, Y. and Yazawa, T., 2001. Hydrocarbon separation via porous glass membranes surface-modified using organosilane compounds. Journal of Membrane Science, 182(1-2): 139-149.

La Rosa, M., Uhlherr, A., Schiesser, C.H., Moody, K., Bohun, R. and Drummond, C.J., 2004. A molecular dynamics study of monolayers of nonionic poly(ethylene oxide) based surfactants. Langmuir, 20(4): 1375-1385.

Ladhe, A.R. and Bhattacharyya, D., In Press. Adsorption of ethoxylated nonionic surfactants from siloxane based solvent and aqueous systems: Use of QCM and model polymeric surfaces. Chemical Engineering Communications.

Ladhe, A.R., Radomyselski, A. and Bhattacharyya, D., 2006. Ethoxylated nonionic surfactants in hydrophobic solvent: Interaction with aqueous and membrane-immobilized poly(acrylic acid). Langmuir, 22(2): 615-621.

Ladhe, A.R., Frailie, P., Hua, D., Darsillo, M. and Bhattacharyya, D., In Press. Thiol functionalized silica-mixed matrix membranes for silver capture from aquoeus solutions: Experimental results and modeling. Journal of Membrane Science.

Lape, N.K., Yang, C. and Cussler, E.L., 2002. Flake-filled reactive membranes. Journal of Membrane Science, 209(1): 271-282.

Lee, E.M., Thomas, R.K., Cummins, P.G., Staples, E.J., Penfold, J. and Rennie, A.R., 1989. Determination of the structure of a surfactant layer adsorbed at the silica/water interface by neutron reflection. Chemical Physics Letters, 162(3): 196-202.

Lee, S.B. and Martin, C.R., 2001. Controlling the transport properties of gold nanotubule membranes using chemisorbed thiols. Chemistry of Materials, 13(10): 3236-3244.

Levitz, P. and Van Damme, H., 1986. Fluorescence decay study of the adsorption of nonionic surfactants at the solid-liquid interface. 2. Influence of polar chain length. Journal of Physical Chemistry, 90(7): 1302-10.

Li, L., Wang, B., Tan, H., Chen, T. and Xu, J., 2006. A novel nanofiltration membrane prepared with PAMAM and TMC by in situ interfacial polymerization on PEK-C ultrafiltration membrane. Journal of Membrane Science, 269(1-2): 84-93.

Lin, S.-Y., Tsay, R.-Y., Lin, L.-W. and Chen, S.-I., 1996. Adsorption kinetics of C12E8 at the air-water interface: Adsorption onto a clean interface. Langmuir, 12(26): 6530-6536.

Lin, Y.-F., Ma, C.-C.M., Lin, Y.-Y., Yen, C.-Y. and Hung, C.-H., 2007. High proton-conducting sulfonated poly(ether ether ketone)/functionalized mesoporous silica composite membranes. Key Engineering Materials, 334-335(Pt. 2, Advances in Composite Materials and Structures): 945-948.

Lindau, J., Jonsson, A.S. and Bottino, A., 1998. Flux reduction of ultrafiltration membranes with different cut-off due to adsorption of a low-molecular-weight hydrophobic solute-correlation between flux decline and pore size. Journal of Membrane Science, 149(1): 11-20.

Lindheimer, M., Keh, E., Zaini, S. and Partyka, S., 1990. Interfacial aggregation of nonionic surfactants onto silica gel: calorimetric evidence. Journal of Colloid and Interface Science, 138(1): 83-91.

Liu, C., Huang, Y., Naismith, N., Economy, J. and Talbott, J., 2003. Novel polymeric chelating fibers for selective removal of mercury and cesium from water. Environmental Science and Technology, 37(18): 4261-4268.

Liu, G., Cheng, H., Yan, L. and Zhang, G., 2005. Study of the kinetics of the pancake-to-brush transition of poly(N-isopropylacrylamide) chains. Journal of Physical Chemistry B, 109(47): 22603-22607.

Liu, Q. and Cussler, E.L., 2006. Barrier membranes made with lithographically printed flakes. Journal of Membrane Science, 285(1+2): 56-67.

Liu, X. and Bruening, M.L., 2004. Size-selective transport of uncharged solutes through multilayer polyelectrolyte membranes. Chemistry of Materials, 16(2): 351-357.
Lomax, E.G., 1996. Amphoteric Surfactants, 2 ed. Marcel Dekker, New York.

Lowry, G.V. and Johnson, K.M., 2004. Congener-specific dechlorination of dissolved PCBs by microscale and nanoscale zerovalent iron in a water/methanol solution. Environmental Science and Technology, 38(19): 5208-5216.

Mahajan, R. and Koros, W.J., 2002a. Mixed matrix membrane materials with glassy polymers. Part 1. Polymer Engineering and Science, 42(7): 1420-1431.

Mahajan, R. and Koros, W.J., 2002b. Mixed matrix membrane materials with glassy polymers. Part 2. Polymer Engineering and Science, 42(7): 1432-1441.

Majumder, M., Zhan, X., Andrews, R. and Hinds, B.J., 2007. Voltage gated carbon nanotube membranes. Langmuir, 23(16): 8624-8631.

Makkuni, A., Varma, R.S., Sikdar, S.K. and Bhattacharyya, D., 2007. Vapor phase mercury sorption by organic sulfide modified bimetallic iron-copper nanoparticle aggregates. Industrial and Engineering Chemistry Research, 46(4): 1305-1315.

Malaisamy, R. and Bruening, M.L., 2005. High-flux nanofiltration membranes prepared by adsorption of multilayer polyelectrolyte membranes on polymeric supports. Langmuir, 21(23): 10587-10592.

Marcomini, A. and Zanette, M., 1996. Chromatographic determination of non-ionic aliphatic surfactants of the alcohol polyethoxylate type in the environment. Journal of Chromatography, A, 733(1 + 2): 193-206.

Matsuura, T., Blais, P. and Sourirajan, S., 1976. Polar and nonpolar parameters for polymeric reverse osmosis membrane materials from liquid chromatographic data. Journal of Applied Polymer Science, 20(6): 1515-31.

Mauter, M.S. and Elimelech, M., 2008. Environmental applications of carbon-based nanomaterials. Environmental Science and Technology, 42(16): 5843-5859.

Mokrani, C., Fatisson, J., Guerente, L. and Labbe, P., 2005. Structural characterization of (3-Mercaptopropyl)sulfonate monolayer on gold surfaces. Langmuir, 21(10): 4400-4409.

Moseke, C., Michalek, R. and Thull, R., 2008. Physical characterization of protein adsorption: time-resolved determination of protein adsorption using quartz crystal microgravimetry. Metallic Biomaterial Interfaces: 153-161.

Mueller, M.T., Yan, X., Lee, S., Perry, S.S. and Spencer, N.D., 2005. Lubrication properties of a brushlike copolymer as a function of the amount of solvent absorbed within the brush. Macromolecules, 38(13): 5706-5713.

Nagarajan, R., 1989. Association of nonionic polymers with micelles, bilayers, and microemulsions. Journal of Chemical Physics, 90(3): 1980-94.

Nakamura, T., Yamada, Y. and Yano, K., 2007. Direct synthesis of monodispersed thiol-functionalized nanoporous silica spheres and their application to a colloidal crystal embedded with gold nanoparticles. Journal of Materials Chemistry, 17(35): 3726-3732.

Nishizawa, M., Menon, V.P. and Martin, C.R., 1995. Metal nanotubule membranes with electrochemically switchable ion-transport selectivity. Science (Washington, D. C.), 268(5211): 700-2.

Okumus, E., Gurkan, T. and Yilmaz, L., 1994. Development of a mixed-matrix membrane for pervaporation. Separation Science and Technology, 29(18): 2451-73.

Onda, M., Lvov, Y., Ariga, K. and Kunitake, T., 1996. Sequential reaction and product separation on molecular films of glucoamylase and glucose oxidase assembled on an ultrafilter. Journal of Fermentation and Bioengineering, 82(5): 502-506.

Ozyilmaz, G., Tukel, S.S. and Alptekin, O., 2005. Activity and storage stability of immobilized glucose oxidase onto magnesium silicate. Journal of Molecular Catalysis B: Enzymatic, 35(4-6): 154-160.

Paez, H.M.E., Aguilar-Arteaga, K., Galan-Vidal, C.A., Palomar-Pardave, M., Romero-Romo, M. and Ramirez-Silva, M.T., 2005. Mercury ions removal from aqueous solution using an activated composite membrane. Environmental Science and Technology, 39(19): 7667-7670.

Pan, B.C., Zhang, Q.R., Zhang, W.M., Pan, B.J., Du, W., Lv, L., Zhang, Q.J., Xu, Z.W. and Zhang, Q.X., 2007. Highly effective removal of heavy metals by polymer-based zirconium phosphate: A case study of lead ion. Journal of Colloid and Interface Science, 310(1): 99-105.

Papke, B.L., Esche, C.K. and Robinson, L.M., 1995. Ultracentrifugation sedimentation profiles: a technique for measuring colloid-surfactant interactions in non-aqueous solvents. Colloids and Surfaces, A: Physicochemical and Engineering Aspects, 95(1): 15-25.

Park, J.-H., Kim, Y.-G., Oh, C., Shin, S.-I., Kim, Y.-C., Oh, S.-G. and Kong, S.-H., 2005. Fabrication of hollow silver spheres by MPTMS-functionalized hollow silica spheres as templates. Materials Research Bulletin, 40(2): 271-280.

Pearson, R.G., 1968. Hard and soft acids and bases (HSAB). I. Fundamental principles. Journal of Chemical Education, 45(9): 581-7.

Perry, R.H., Green, D.W. and Editors, 1997. Perry's Chemical Engineers' Handbook, 7th Edition. McGraw-Hill, 2240 pp pp.

Pinto, G. and Maaroufi, A.-K., 2005. Conducting polymer composites of zinc-filled urea-formaldehyde. Journal of Applied Polymer Science, 96(6): 2011-2015.

Portet, F., Desbene, P.L. and Treiner, C., 1996. Nonideality of mixtures of pure nonionic surfactants both in solution and at silica/water interfaces. Journal of Colloid and Interface Science, 184(1): 216-226.

Postmus, B.R., Leermakers, F.A.M., Koopal, L.K. and Stuart, M.A.C., 2007. Competitive adsorption of nonionic surfactant and nonionic polymer on silica. Langmuir, 23(10): 5532-5540.

Pu, W., He, X., Wang, L., Tian, Z., Jiang, C. and Wan, C., 2006. Preparation of P(AN-MMA) microporous membrane for Li-ion batteries by phase inversion. Journal of Membrane Science, 280(1+2): 6-9.

Ramaswamy, S., Greenberg, A.R. and Peterson, M.L., 2004. Non-invasive measurement of membrane morphology via UFDR: pore-size characterization. Journal of Membrane Science, 239(1): 143-154.

Rao, G.V.R., Krug, M.E., Balamurugan, S., Xu, H., Xu, Q. and Lopez, G.P., 2002. Synthesis and characterization of silica-poly(N-isopropylacrylamide) hybrid membranes: Switchable molecular filters. Chemistry of Materials, 14(12): 5075-5080.

Rao, S. and Zydney, A.L., 2006. High resolution protein separations using affinity ultrafiltration with small charged ligands. Journal of Membrane Science, 280(1+2): 781-789.

Rauf, S., Ihsan, A., Akhtar, K., Ghauri, M.A., Rahman, M., Anwar, M.A. and Khalid, A.M., 2006. Glucose oxidase immobilization on a novel cellulose acetate-polymethylmethacrylate membrane. Journal of Biotechnology, 121(3): 351-360.

Reimhult, K., Petersson, K. and Krozer, A., 2008. QCM-D analysis of the performance of blocking agents on gold and polystyrene surfaces. Langmuir, 24(16): 8695-8700.

Rinia, H.A., Caruso, F. and Furlong, D.N., 1996. Gravimetric monitoring of nonionic surfactant adsorption from nonaqueous media onto quartz crystal microbalance electrodes and colloidal silica. Langmuir, 12(9): 2145-52.

Ritchie, S.M.C., Bachas, L.G., Olin, T., Sikdar, S.K. and Bhattacharyya, D., 1999. Surface modification of silica- and cellulose-based microfiltration membranes with functional polyamino acids for heavy metal sorption. Langmuir, 15(19): 6346-6357.

Ritchie, S.M.C. and Bhattacharyya, D., 2001. Polymeric ligand-based functionalized materials and membranes for ion exchange. Ion Exchange and Solvent Extraction: Marcel Dekker, Inc., 14: 81-118.

Ritchie, S.M.C., Kissick, K.E., Bachas, L.G., Sikdar, S.K., Parikh, C. and Bhattacharyya, D., 2001. Polycysteine and other polyamino acid functionalized microfiltration membranes for heavy metal capture. Environmental Science and Technology, 35(15): 3252-3258.

Robb, I.D. and Stevenson, P., 2000. Interaction between poly(acrylic acid) and an ethoxylated nonionic surfactant. Langmuir, 16(18): 7168-7172.

Robeson, L.M., 1991. Correlation of separation factor versus permeability for polymeric membranes. Journal of Membrane Science, 62(2): 165-85.

Roper, D.K. and Lightfoot, E.N., 1995. Separation of biomolecules using adsorptive membranes. Journal of Chromatography, A, 702(1 + 2): 3-26.

Saiful, Borneman, Z. and Wessling, M., 2006. Enzyme capturing and concentration with mixed matrix membrane adsorbers. Journal of Membrane Science, 280(1+2): 406-417.

Saito, S., 1993. Behavior of some solubilizates in nonionic surfactant-poly(acrylic acid) complexes at low temperature. Journal of Colloid and Interface Science, 158(1): 77-84.

Saito, S., 1994. Properties of nonionic surfactant-polymethacrylic acid complexes: comparison with the polyacrylic acid complexes. Journal of Colloid and Interface Science, 165(2): 505-11.

Saito, S. and Taniguchi, T., 1973. Effect of nonionic surfactants on aqueous poly(acrylic acid) solutions. Journal of Colloid and Interface Science, 44(1): 114-20.

Samaha, M.W. and Naggar, V.F., 1988. Micellar properties of non-ionic surfactants in relation to their solubility parameters. International Journal of Pharmaceutics, 42(1-3): 1-9.

Sambandam, S. and Ramani, V., 2007. SPEEK/functionalized silica composite membranes for polymer electrolyte fuel cells. Journal of Power Sources, 170(2): 259-267.

Sata, T., 1991. Ion exchange membranes and separation processes with chemical reactions. Journal of Applied Electrochemistry, 21(4): 283-94.

Sauerbrey, G., 1959. The use of quartz oscillators for weighing thin layers and for microweighing. Zeitschrift fuer Physik, 155: 206-22.

Seguin, C., Eastoe, J., Clapperton, R., Heenan, R.K. and Grillo, I., 2006. Alternative non-aqueous water-miscible solvents for surfactants. Colloids and Surfaces, A: Physicochemical and Engineering Aspects, 282+283: 134-142.

Shi, W., Shen, Y., Ge, D., Xue, M., Cao, H., Huang, S., Wang, J., Zhang, G. and Zhang, F., 2008. Functionalized anodic aluminum oxide (AAO) membranes for affinity protein separation. Journal of Membrane Science, 325(2): 801-808.

Shimotori, T., Cussler, E.L. and Arnold, W.A., 2007. Diffusion of mobile products in reactive barrier membranes. Journal of Membrane Science, 291(1+2): 111-119.

Singh, N., Chen, Z., Tomer, N., Wickramasinghe, S.R., Soice, N. and Husson, S.M., 2008. Modification of regenerated cellulose ultrafiltration membranes by surface-initiated atom transfer radical polymerization. Journal of Membrane Science, 311(1+2): 225-234.

Smith, J.M., Van Ness, H.C. and Abbott, M.M., 1996. McGraw Hill Chemical Engineering Series: Introduction to Chemical Engineering Thermodynamics. 5th Ed, 632.

Smuleac, V., Butterfield, D.A. and Bhattacharyya, D., 2004. Permeability and separation characteristics of polypeptide-functionalized polycarbonate track-etched membranes. Chemistry of Materials, 16(14): 2762-2771.

Smuleac, V., Butterfield, D.A., Sikdar, S.K., Varma, R.S. and Bhattacharyya, D., 2005. Polythiol-functionalized alumina membranes for mercury capture. Journal of Membrane Science, 251(1-2): 169-178.

Soboleva, O.A., Badun, G.A. and Summ, B.D., 2007. Adsorption of nonionic surfactant Triton X-100 on solid surfaces from aqueous and nonaqueous media. Moscow University Chemistry Bulletin, 62: 13-17.

Somasundaran, P., Snell, E.D. and Xu, Q., 1991. Adsorption behavior of alkylarylethoxylated alcohols on silica. Journal of Colloid and Interface Science, 144(1): 165-73.

Stalgren, J.J.R., Eriksson, J. and Boschkova, K., 2002. A comparative study of surfactant adsorption on model surfaces using the quartz crystal microbalance and the ellipsometer. Journal of Colloid and Interface Science, 253(1): 190-195.

Strathmann, H., 1986. Preparation of microporous membranes by phase inversion processes. Membranes and Membrane Processes, [Proc. Eur.-Jpn. Congr. Membr. Membr. Processes]: 115-35.

Tahani, A., van Damme, H., Noik, C. and Levitz, P., 1996. Adsorption of nonionic surfactants on kaolins. Journal of Colloid and Interface Science, 184(2): 469-476.

Tee, Y.-H., Grulke, E. and Bhattacharyya, D., 2005. Role of Ni/Fe nanoparticle composition on the degradation of trichloroethylene from water. Industrial and Engineering Chemistry Research, 44(18): 7062-7070.

Thirtle, P.N., Li, Z.X., Thomas, R.K., Rennie, A.R., Satija, S.K. and Sung, L.P., 1997. Structure of nonionic surfactant layers adsorbed at the solid/liquid interface on self-assembled monolayers with different surface functionality: A neutron reflection study. Langmuir, 13(20): 5451-5458.

Thoemmes, J. and Kula, M.R., 1995. Membrane chromatography - an integrative concept in the downstream processing of proteins. Biotechnology Progress, 11(4): 357-67.

Tiberg, F., Joesson, B. and Lindman, B., 1994. Ellipsometry studies of the self-assembly of nonionic surfactants at the silica-water interface: kinetic aspects. Langmuir, 10(10): 3714-22.

Torn, L.H., Koopal, L.K., de Keizer, A. and Lyklema, J., 2005. Adsorption of nonionic surfactants on cellulose surfaces: Adsorbed amounts and kinetics. Langmuir, 21(17): 7768-7775.

Tratnyek, P.G., Scherer, M.M., Deng, B. and Hu, S., 2001. Effects of natural organic matter, anthropogenic surfactants, and model quinones on the reduction of contaminants by zero-valent iron. Water Research, 35(18): 4435-4443.

Trochimczuk, A.W. and Kolarz, B.N., 2000. Synthesis and chelating properties of resins with methylthiourea, guanylthiourea and dithiocarbamate groups. European Polymer Journal, 36(11): 2359-2363.

Urmenyi, A.M., Poot, A.A., Wessling, M. and Mulder, M.H.V., 2005. Affinity membranes for hormone removal from aqueous solutions. Journal of Membrane Science, 259(1-2): 91-102.

Vane, L.M., Namboodiri, V.V. and Bowen, T.C., 2008. Hydrophobic zeolite-silicone rubber mixed matrix membranes for ethanol-water separation: Effect of zeolite and silicone component selection on pervaporation performance. Journal of Membrane Science, 308(1+2): 230-241.

Vieira, E.F.S., Cestari, A.R., Simoni, J.d.A. and Airoldi, C., 1999. Use of calorimetric titration to determine thermochemical data for interaction of cations with mercapto-modified silica gel. Thermochimica Acta, 328(1-2): 247-252.

Vieira, E.F.S., De A. Simoni, J. and Airoldi, C., 1997. Interaction of cations with SH-modified silica gel: thermochemical study through calorimetric titration and direct extent of reaction determination. Journal of Materials Chemistry, 7(11): 2249-2252.

Villalonga, R., Fujii, A., Shinohara, H., Tachibana, S. and Asano, Y., 2008. Covalent immobilization of phenylalanine dehydrogenase on cellulose membrane for biosensor construction. Sensors and Actuators, B: Chemical, B129(1): 195-199.

Viswanath, S., Wang, J., Bachas, L.G., Butterfield, D.A. and Bhattacharyya, D., 1998. Site-directed and random immobilization of subtilisin on functionalized membranes: activity determination in aqueous and organic media. Biotechnology and Bioengineering, 60(5): 608-616.

Voutsas, E.C., Flores, M.V., Spiliotis, N., Bell, G., Halling, P.J. and Tassios, D.P., 2001. Prediction of critical micelle concentrations of nonionic surfactants in aqueous and nonaqueous solvents with UNIFAC. Industrial and Engineering Chemistry Research, 40(10): 2362-2366.

Walcarius, A. and Delacote, C., 2005. Mercury(II) binding to thiol-functionalized mesoporous silicas: critical effect of pH and sorbent properties on capacity and selectivity. Analytica Chimica Acta, 547(1): 3-13.

Warta, A.M., Arnold, W.A. and Cussler, E.L., 2005. Permeable membranes containing crystalline silicotitanate as model barriers for cesium ion. Environmental Science and Technology, 39(24): 9738-9743.

Wernette, D.P., Swearingen, C.B., Cropek, D.M., Lu, Y., Sweedler, J.V. and Bohn, P.W., 2006. Incorporation of a DNAzyme into Au-coated nanocapillary array membranes with an internal standard for Pb(II) sensing. Analyst (Cambridge, United Kingdom), 131(1): 41-47.

Xu, J., 2007. Synthesis and reactivity of membrane supported bimetallic nanoparticles for PCB and trichloroethylene Doctoral Disseration, University of Kentucky.

Xu, J. and Bhattacharyya, D., 2007. Fe/Pd nanoparticle immobilization in microfiltration membrane pores: Synthesis, characterization, and application in the dechlorination of polychlorinated biphenyls. Industrial and Engineering Chemistry Research, 46(8): 2348-2359.

Yamaguchi, T., Nakao, S. and Kimura, S., 1991. Plasma-graft filling polymerization: preparation of a new type of pervaporation membrane for organic liquid mixtures. Macromolecules, 24(20): 5522-7.

Yao, F., Fu, G.-D., Zhao, J., Kang, E.-T. and Neoh, K.G., 2008. Antibacterial effect of surface-functionalized polypropylene hollow fiber membrane from surface-initiated atom transfer radical polymerization. Journal of Membrane Science, 319(1+2): 149-157.

Yen, C.-Y., Lee, C.-H., Lin, Y.-F., Lin, H.-L., Hsiao, Y.-H., Liao, S.-H., Chuang, C.-Y. and Ma, C.-C.M., 2007. Sol-gel derived sulfonated-silica/Nafion composite membrane for direct methanol fuel cell. Journal of Power Sources, 173(1): 36-44.

Ying, L., Kang, E.T. and Neoh, K.G., 2002. Covalent immobilization of glucose oxidase on microporous membranes prepared from poly(vinylidene fluoride) with grafted poly(acrylic acid) side chains. Journal of Membrane Science, 208(1-2): 361-374.

Yoshimatsu, K., Wang, H., Kita, H. and Okamoto, K.-I., 1999. Preparation of plasma-grafted membranes and their pervaporation properties to aromatic/non-aromatic mixtures. Journal of Photopolymer Science and Technology, 12(1): 15-18.

Zhang, L., Zhang, W., Shi, J., Hua, Z., Li, Y. and Yan, J., 2003. A new thioether functionalized organic-inorganic mesoporous composite as a highly selective and

capacious Hg2+ adsorbent. Chemical Communications (Cambridge, United Kingdom)(2): 210-211.

Zhang, W. and Nilsson, S., 1993. Helix-coil transition of a titrating polyelectrolyte analyzed within the Poisson-Boltzmann cell model. Effects of pH and counterion valency. Macromolecules, 26(11): 2866-70.

Zhang, W.-x., Wang, C.-B. and Lien, H.-L., 1998. Treatment of chlorinated organic contaminants with nanoscale bimetallic particles. Catalysis Today, 40(4): 387-395.

Zhang, Y., Li, H., Lin, J., Li, R. and Liang, X., 2006. Preparation and characterization of zirconium oxide particles filled acrylonitrile-methyl acrylate-sodium sulfonate acrylate copolymer hybrid membranes. Desalination, 192(1-3): 198-206.

Zou, H., Luo, Q. and Zhou, D., 2001. Affinity membrane chromatography for the analysis and purification of proteins. Journal of Biochemical and Biophysical Methods, 49(1-3):199-240.

Vita

Abhay R Ladhe was born on 11th February, 1982 in Maharashtra, India. He has received his Bachelor of Chemical Engineering degree from University of Mumbai, Institute of Chemical Technology (Formerly known as UDCT), in 2003. Then, he joined Department of Chemical Engineering, University of Kentucky, for PhD curriculum.

Awards

- Elias Klien Founders' travel award recipient for International Congress on Membranes and Membrane Processes (ICOM) 2008, Honolulu, Hawaii
- Research Challenge Trust Fund (RCTF) Fellowship, July 2005 – December 2005
- 3rd Place Award for Technical Papers from *Prodigy*, a National Level Conference at Mumbai University Institute of Chemical Technology, August 2001

Publications:

Ladhe, A. R.; Xu, J.; Hollman, A.; Smuleac, V.; Bhattacharyya, D. "Functionalized Membranes for Sorption, Separation and Reaction", Book Chapter, Submitted

Ladhe, A. R.; Frailie, P.; Hua, D.; Darsillo, M.; Bhattacharyya, D. "Thiol Functionalized Silica-Mixed Matrix Membranes for Silver Capture from Aqueous Solutions: Experimental Results and Modeling", In Press, *Journal of Membrane Science*

Ladhe, A. R.; Bhattacharyya, D. "Adsorption of Ethoxylated Nonionic Surfactants from Siloxane-Base Solvent and Aqueous Systems: Use of QCM and Model Polymeric Surfaces", In Press, *Chemical Engineering Communications*

Ladhe, A. R.; Radomyselki; A.; Bhattacharyya, D. "Ethoxylated Nonionic Surfactants in Hydrophobic Solvents: Interaction with Aqueous and Membrane-Immobilized Polyacrylic acid", *Langmuir* 2006, *22*, 615

Ladhe, A. R.; Bhattacharyya, D. "Ethoxylated Nonionic Surfactants in Hydrophobic Solvents: Separation Using Membrane Immobilized Polyacrylic Acid", *Proceedings of the Annual Meeting of American Institute of Chemical Engineers, Separations (General) (2005)*

Presentations:

A. R. Ladhe, P. Frailie and D. Bhattacharyya, "PAA and Thiol Functionalized MF/UF membranes for surfactant separation and high value metal capture: Experimental results and modeling", 2008 International Congress on Membranes and Membrane Processes (ICOM), Honolulu, Hawaii

A. R. Ladhe and D. Bhattacharyya, "Adsorption of Ethoxylated Nonionic Surfactants on various Interfaces", 2007 Annual Meeting of American Institute of Chemical Engineers, Salt Lake City, UT

A. R. Ladhe, and D. Bhattacharyya, "Adsorption Behavior of Ethoxylated Nonionic Surfactants using QCM-D", 2006 Chemical Engineering Graduate Student Symposium, Lexington, KY

A. R. Ladhe, Arseni Radomyselski and D. Bhattacharyya, "Fundamental Study of Adsorption Behavior of Ethoxylated nonionic Surfactants from Organic Solvents on Various Surfaces", 2006 Annual Meeting of American Institute of Chemical Engineers, San Francisco, CA

A. R. Ladhe, D. Bhattacharyya, "Ethoxylated Nonionic Surfactants in Hydrophobic Solvents: Separation Using Membrane Immobilized Polyacrylic Acid", 2005 Annual Meeting of American Institute of Chemical Engineers, Cincinnati, OH (Poster Presentation)

A. R. Ladhe, D. Bhattacharyya, "Separation of Ethoxylated Nonionic Surfactants from Hydrophobic Solvents using Functionalized Membranes", 229th ACS National Meeting, San Diego, CA, March 2005 (Poster Presentation)